Thesis

Characterizing Uncertainties in Doppler Measurements Using a Displaced Phase Center Antenna Configuration on Spaceborne Weather Radars

Submitted by

Sergio Daniel Graniello

Department of Electrical and Computer Engineering

In partial fulfillment of the requirements

For the Degree of Master of Science

Colorado State University

Fort Collins, Colorado

Summer 2021

Master's Committee:

Advisor: V. Chandrasekar

Margaret Cheney
José Chavéz

ABSTRACT

Characterizing Uncertainties in Doppler Measurements Using a Displaced Phase Center Antenna Configuration on Spaceborne Weather Radars

The work presented in this thesis explores a new antenna configuration for accurately obtaining Doppler measurements from a spaceborne weather radar. Spaceborne weather radars have the potential to observe the dynamic process of the atmosphere at a global scale. Unlike ground and airborne radar, spaceborne radars have a unique challenge due to high orbital velocities, which result in a decorrelation of successive pulses, adversely affecting the ability to accurately measure the vertical Doppler velocity of clouds and precipitation [1]. A Displaced phase center antenna (DPCA) configuration has been proposed to mitigate the effects that high platform velocity have on single antenna system on a spaceborne weather radar. This work describes the concept of DPCA and its benefits over a single antenna system. This thesis characterizes the performance and its uncertainty for Doppler velocity estimation associated with the technique by simulating a spaceborne weather radar with DPCA. Through this process it was determined that DPCA removes the decorrelation effect that is associated with high platform velocities, resulting in a high accuracy in Doppler estimates in both homogeneous and non-homogeneous conditions.

ACKNOWLEDGEMENTS

I would like to thank my advisor Dr. Chandra and my committee members, Dr. Margaret Cheney, and Dr. Jose Chavez. Thank you Dr. Chandra for the guidance and mentorship you have provided me throughout the course of my masters. The experiences I have been able to obtain thanks to you (conferences, traveling outside of the US and getting me in contact with prestigous companies such as JPL), have been nothing short of life changing, and has provided me the skillsets neccesary to become a better person/engineer. Thank you Dr. Cheney and Dr. Chavez for the willingness to read my thesis and for the opportunity to defend it.

This research was, in part, carried out at the Jet Propulsion Laboratory, California Institute of Technology, and was sponsored by the Summer Internship Program (SIP), the JPL Visiting Student Research Program (JVSRP) (with funding by Colorado State University), and the National Aeronautics and Space Administration (80NM0018D0004).

Thank you Robert Beauchamp and Steve Durden at the Jet Propulsion Laboratory for giving me the opportunity to research DPCA for spaceborne weather radars over the past year. Your mentorship, knowledge of spaceborne weather radar and your willingness to teach me the same thing over and over is greatly appreciated. It has been a great pleasure to work with you both.

I want to thank my family. Thanks to my mom and step father for all of the love and encouragement you have provided me all my life. Without your constant support and pushing me outside of my comfort zone, I would not be the person that I am today. I am blessed to have you both by my side. Thanks to my sister, brother-in-law and brother for leading by example and giving me the constant reassurance I needed. You have taught me

so many things in life and I hope to one day be half the person that you are. I want to thank my two best friends for always being there for me during my lows and to celebrate my highs. Finally I want to thank everyone in the CSU radar lab for all their support.

Table of Contents

CHAPTER 1

Introduction

Doppler measurements are a crucial component in characterizing the dynamic process of the atmosphere. High levels of fidelity are required to allow the scientific community to formulate accurate predictions of weather events [2]. While radar techniques have been refined to accurately measure Doppler velocities of clouds and precipitation from ground and airborne radars, spaceborne Doppler radars have a unique challenge due to the introduction of high spacecraft velocities. As the antenna moves in space, the signal decorrelates as it move half the diameter of the antenna. Since the velocity of the spacecraft is a fixed value that cannot be modified once in orbit, the only free parameters left to change are the pulse repetition frequency (PRF) and the size of the antenna. The PRF can only be so high due to the unambiguous velocity, or the max range to which a transmitted pulse can travel from and back while still maintaining the integrity of the signal. This means that to minimize decorrelation due to motion between pulses, we will require a larger antenna. An infinitely large antenna could alleviate this issue, but in practicality, the antenna can only be so big before it's design implementation becomes costly and take up too much space onboard the spacecraft. But, if the radar's antenna is not made large enough, successive pulses quickly become decorrelated leading to a degradation of accuracy in the Doppler estimates [1]. Advanced signal processing may help to lessen the effects, but single antenna systems are still subject to bias resulting from reflectivity gradients within the footprint [3].

A Displaced Phase Center Antenna Configuration (DPCA) has been proposed to remove these biases. DPCA uses a dual antenna system, in which the antennas are separated by a distance D calculated from the radars Pulse Repetition Interval (PRI) and platform velocity.

The antennas transmit and receive are then configured in a way that allows for the phase center of sequential pulses to be in the same location [2]. This resulting in an apparent cancellation of the platform's velocity, which is the largest contributor of decorrelation between pulses. To estimate the vertical velocity of precipitation from space, the dual-antenna configuration (i.e., DPCA) is a superior alternative as it does not require a larger antenna or more complex post processing to remove biases resulting from the high platform velocity. This method of scanning in conjunction with ground and airborne weather radars can provide us with accurate Doppler measurements for better observations of the atmosphere.

1.1. Problem Statement

Over the years, innovative and creative methodologies have been developed to measure meteorological formations of the atmosphere. One of these methods is through the use of a spaceborne weather radar.

Spaceborne weather radars scan the atmosphere from above, in orbits at tens to hundreds of kilometers from the surface of the Earth. A common orbit used for taking measurements of cloud and precipitation is a Low Earth Orbit (LEO) (approximately located 450 km from the surface of the Earth) due to its close proximity to the Earth [4]. At these heights, the radar relative to the earth allows for higher resolution observations of the atmosphere to be made at a global scale, which in turn improves our observation capabilities of storm formations. Additionally, since spaceborne weather radars scan from above, they allow us to take measurements of the atmosphere in locations with complex terrain, such as in mountainous areas or over oceans where land is not readily available to deploy ground radars [5].

While spaceborne weather radars have the ability to provide meterological information at a global scale, they present a challenge when taking Doppler measurements due to high orbital velocity while scanning. As the platform orbits in space, the phase centers of the antenna at each point of transmit and receive is shifted, resulting in a decorrelation effect between consecutive pulses as shown in Figure 1.1. Calculating Doppler velocity requires coherent measurements, meaning that consecutive echo pulses must be correlated [5]. If they are not well correlated, the accuracy of the Doppler estimates begins to diminish.

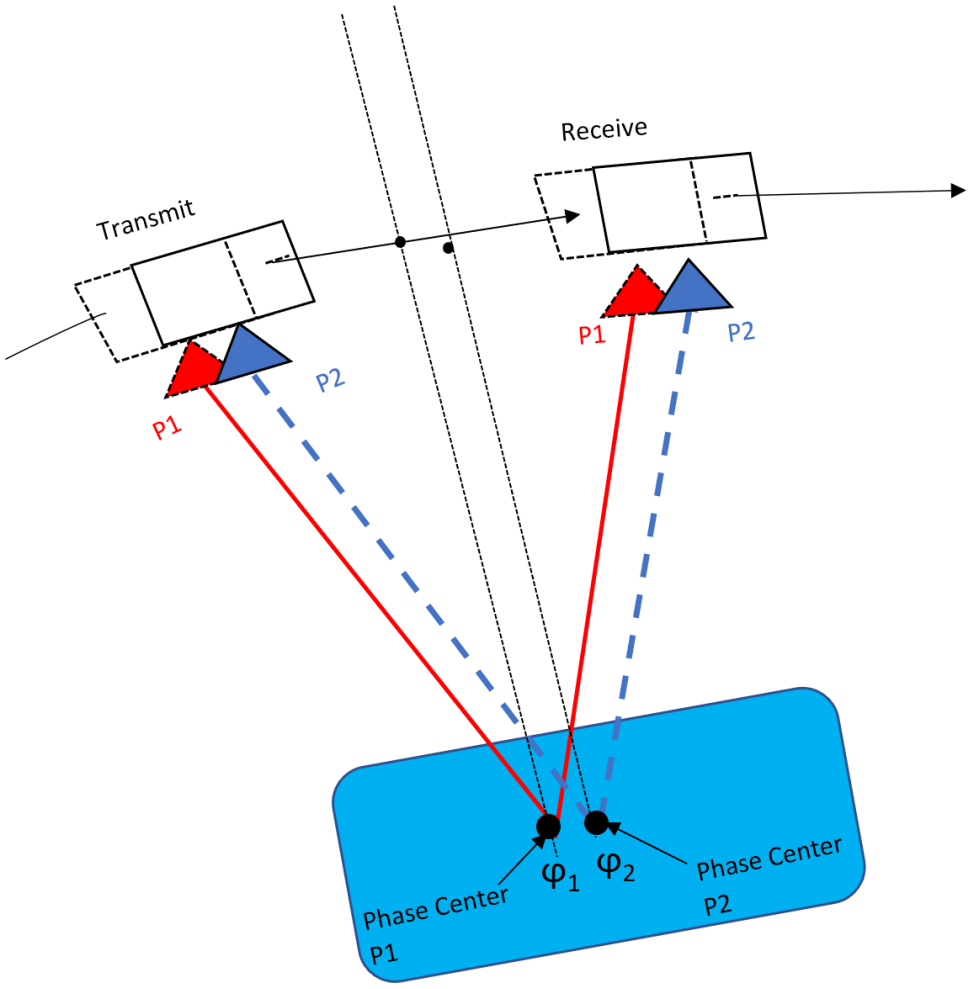

FIGURE 1.1. Example transmit and receive of a spaceborne weather radar using a single antenna. The figures shows the shifting in phase centers ϕ between consecutive transmit pulses (labeled P1 and P2).

To further explore the contribution of high platform velocity in our Doppler estimates, consider the spectrum width. In a radar bin, a dispersion of velocities occurs due to hydrological processes as well as radar system parameters. This is known as the spectrum width and is associated with a combination of factors. For ground based radars, the sources of spectrum width can be seen as [6]

- Turbulence, which is the random relative radial motion of the scatterers, denoted as σ_t
- Wind sheer, denoted as σ_s
- Difference of speed and fall of different sized hydrometeors denoted as σ_d
- The volume changing between pulses relative to the antenna motion denoted as σ_α
- Changes in orientation of the hydrometeors denoted as σ_0

Since the major sources of spectrum broadening are independent of each other, the square of the spectrum width can be calculated as

$$\sigma_v = \sigma_s^2 + \sigma_\alpha^2 + \sigma_d^2 + \sigma_0^2 + \sigma_t^2 \tag{1}$$

where σ_v is the velocity spectrum width [6].

For σ_α, the dominant motion is the scatterers moving with respect to the radar. The faster the volume changes from Pulses Repition Time (PRT) to PRT (the time between pulses), the larger the decorrelation of the signals [6]. The decorrelation between successive samples means that there is larger spectral broadening. To further understand this, if the volume where stationary, the resulting Doppler spectrum would be zero.

The spectrum width caused by this decorrelation can be seen as

$$\sigma_\alpha = \frac{\lambda}{4\pi\sigma_\tau} = \frac{\theta_1}{2\alpha cos\theta_e\sqrt{ln2}} \tag{2}$$

where θ_e is the horizontal angle of the antenna beam axis, and σ_τ is the width of the Gaussian correlation function

$$\sigma_\tau = \frac{\theta_1}{2\alpha cos\theta_e\sqrt{ln2}} \tag{3}$$

where α the rate of the antennas rotation in azimuth [6]. This is one of the main contributors to the decorrelation of the sampled signal in ground based radars.

In spaceborne weather radars, the main contributor to decorrelation between pulses, and in turn a spreading of the spectrum, is the high velocities introduced to the radar while in orbit. In this case, the Doppler spread due to motion can be defined as

$$\sigma_1 \approx 0.3\theta_1 V_s cos\beta \tag{4}$$

where θ_1 is the 3-db beamwidth of the antenna, V_s is the platform velocity and β is the nadir off-angle [5]. For our purposes, β will be close to zero as it provides better vertical resolution while minimizes clutter contamination. The equation thus reduces down to

$$\sigma_1 \approx 0.3\theta_1 V_s \tag{5}$$

As can be seen by the equation, the surface Doppler spectrum width depends on the angular spread of the antenna as well as the platform velocity. For a small antenna, the beam width

is large as can be seen by

$$\theta_1 = \frac{70\lambda}{d} \tag{6}$$

where d is the diameter of the antenna [7]. This means that there is a larger range of theta, so signals have a larger range of velocity and a wide spectrum. Taking the inverse Fourier transform of the Doppler spectrum shows a narrow autocorrelation function, meaning the signal decorrelates fast. To further this, for a wavelength of K band and an antenna size of a few meters, the spectrum width corresponds to a few tens of meters per second. The contribution from the antenna movement is then added to the other factors of spectrum width as mentioned before. This result in a broad spectrum, with most of the contribution coming from the platform velocity.

Attempts have been made to correct for this, by increasing the antenna size [8]. As the antenna size gets larger, the smaller the spectrum becomes meaning higher correlation between pulses. While this can provide moderate accuracy in most cloud conditions, the spectrum still degrades under convective clouds [3]. Additionally, increasing the antenna size may introduce other challenges such as increase in cost, additional demands on spacecraft resources and technological challenges.

Increasing the PRF can also help reduce the effects of decorrelational by reducing the amount of time it takes to transmit consecutive pulses, meaning that more of the antenna will overlap between pulses [9]. But as the PRF increase, so does the range ambiguity, which means that after a certain distance, the radar is unable to distinguish between pulses and derive information [10]. This can be expressed as

$$R_{max} = \frac{c}{2f_p} \tag{7}$$

While these methods can alleviate some of the issues associated with estimating Doppler measurements, the issue of high platform velocities will always be a major source of spectrum broadening. Instead, we propose DPCA as an alternative method for Doppler estimates.

1.2. Research Objectives

This thesis aims to present an antenna configuration known as DPCA, to remove the effects of the spacecraft's velocity from measurements of cloud and precipitation. DPCA's effectiveness comes from its two antenna configuration. By configuring the antennas to transmit and receive at different times, a common phase center is maintained between consecutive pulses leading to an apparent cancellation of the platforms velocity. The technique has not been used for weather applications from space, but was introduced by [1] as a viable alternative to the current industry standard. Additionally, DPCA has a successful history of use in improving moving target performance in airborne radars that are subject to clutter contamination, providing a strong bases to estimate the Doppler velocity of clouds and precipitation via spaceborne weather radar [11] [12].

The research will present a comprehensive analysis of DPCA in use for Doppler measurements from a spaceborne weather radar. The majority of the work will be dedicated to characterizing the uncertainty associated with having two antennas as well as provide an analytical comparison to a single antenna configuration. Lastly the thesis shows the effectiveness of DPCA under non-uniform beamfilling in contrast with a single antenna.

1.3. Thesis Organization

Chapter 2 presents a review of necessary and relevant literature for this research, with a focus on basic principles of spaceborne Doppler weather radars, single antenna systems and a comprehensive overview of DPCA.

Chapter 3 develops the model used to simulate DPCA and a single antenna case. This chapter focuses on presenting the radar system configuration and creating the scatterer plane used to simulate a spaceborne weather radar. Furthermore, the methodology used for creating a single antenna and DPCA simulation is presented. The chapter aims to provide the reader with a stronger understanding of how a spaceborne weather radar with DPCA can be implemented to provide Doppler measurements.

Chapter 4 discusses the uncertainty associated with DPCA and the methodology used to characterize it. This will entail a statistical analysis using a monte carlo like process to derive the largest sources of error resulting from a dual antenna system. The deviations resulting from the uncertainty will then be factored into the DPCA model to present a more accurate representation of Doppler estimates. Afterwards an analytical comparison of Doppler measurements between DPCA and a single antenna case will be shown.

Chapter 5 presents the concept of non-uniform beamfilling and its effects on weather radars. The chapter will then simulate a nonuniform volume to show the effects on the radar models for both DPCA and a single antenna system. Afterwards a comparison between the performance of DPCA and a single antenna system under these conditions will be shown.

Chapter 6 summarizes the research shown in this thesis. It will present the findings in a coherent manner to further prove the viability of using DPCA as an alternative to a single antenna system as well as discuss future work.

CHAPTER 2

Background

Doppler weather radars are remote sensing devices that are essential for monitoring the kinematics of storm formations. These instruments transmit pulses of microwave energy into the atmosphere which are then reflected and collected at the radar receiver. Using these returns we can computing Doppler velocity, which allows us to see and understand the motion of clouds and precipitation. This information in turn giving us better insight into the formation of weather events and can be useful in the detection of tornadoes, hurricanes, etc. Doppler spaceborne weather radars have the advantage of taking measurements from above the atmosphere. This allows the radars to profiling meteorological events in regions that are difficult for ground based weather radars to operate in. Areas such as the polar caps regions where land is sparsely separated and constantly changing as well as over oceans where land is not available to deploy stable weather radars over long periods of time [13]. Using spaceborne weather radars to measure cloud and precipitation to collected meteorological moments from space, such as reflectivity, the standard metric for return power in weather radar, has allowed for storm profiling at a global scale. Though significant advances in the field of meteorology have been made due to spaceborne weather radars, obtaining accurate Doppler measurements still remains a technical challenge due to high platform velocities introduced while the radar is in orbit.

Decades of weather research using radar systems have refined our ability to collect information on cloud formations, the effects of aerosol on the atmosphere, early detection of storm developments over the ocean and more [8]. Ground radars have been shown to produce high accuracy in returns, but are limited to regional coverage. Spaceborne weather radars

on the other hand have the potential to provide us with global coverage, but are currently limited in accuracy due to high platform velocities (7500 m/s at LEO) that produce wide Doppler spectrum. While mitigation techniques can improve the Doppler velocity estimates, the effects of the high spacecraft velocity will always be an issue single antenna systems will have to face [13].

DPCA provide a viable solution to reducing effects of high spaceborne weather radar velocities on Doppler measurements. Properly configured transmit and receive on the leading and following antenna can effectively cancel the seen platform velocity by making the phase center between concurrent pulses the same. Since the Doppler spectrum width is a factor of beamwidth and velocity, canceling out the velocity greatly reduces the spectrum width [5]. This fixes the root problem as opposed to treating the symptoms of the single antenna implementations that have been implemented to-date for spaceborne weather radar.

The goal of this chapter is to a provide a review of basic principles of spaceborne Doppler weather radars. Additionally this chapter will present the concept of DPCA on a spaceborne weather radar for taking Doppler measurements from space.

2.1. Review of Spaceborne Doppler Weather Radar

Pulse Doppler weather radar in space is a critical tool for observation and investigation of weather phenomena with near global coverage. They can be used to measure volumes of precipitation at different locations in the atmosphere by transmitting a series of microwave pulses using a directional antenna as can be seen in Figure 2.1. The pulses are generated from the radars transmitter at a pulse duration, or pulse width on the order of microseconds and are separated by a pulse repetition interval (PRI) determined by the number of pulses

transmitted in a second [6]:

$$PRI = \frac{1\ second}{\#\ of\ pulses\ per\ second} \tag{8}$$

If the radiated pulses come in contact with a surface, the transmitted signal backscatters in all direction, with the majority of the signal returning in the line of sight of the transmitter. Using the duration of time it takes for the pulse to be transmitted and received (T) as well as the constant for the speed of light (c), it is possible to determine the range at which the target can be seen The range of the particle may be determined by:

$$r = \frac{cT}{2} \tag{9}$$

The spacecraft continues to move in the along track direction at a speed of Vp. The distance the spacecraft travels in this direction during the round trip travel time of the radar's transmitted pulse, and the subsequent received echo, is:

$$D_r = V_p T \tag{10}$$

where D_r is the distance at which the radar receives the echo and V_p is the platform velocity [14].

In weather radar, the returned signals are a collection of echos from a large amount of different hydro-meteors. Since the echos cannot be collected individually by the radars receiver, the return signals are instead clustered into resolution volumes, separated by discrete range gates at a resolution sized by the radars pulse width τ

$$r_{res} = \frac{c\tau}{2} \tag{11}$$

Using this information, the radar calculates the discrete range time delays (τ_s) (the time delay of a sampling gate) to use as the sample time for a gating circuit. The received signals at each gate are then computed as the sum of all the scatterers inside the resolution volume [6]. Spaceborne weather radars observe at nadir or at off-nadir angle, depending on the

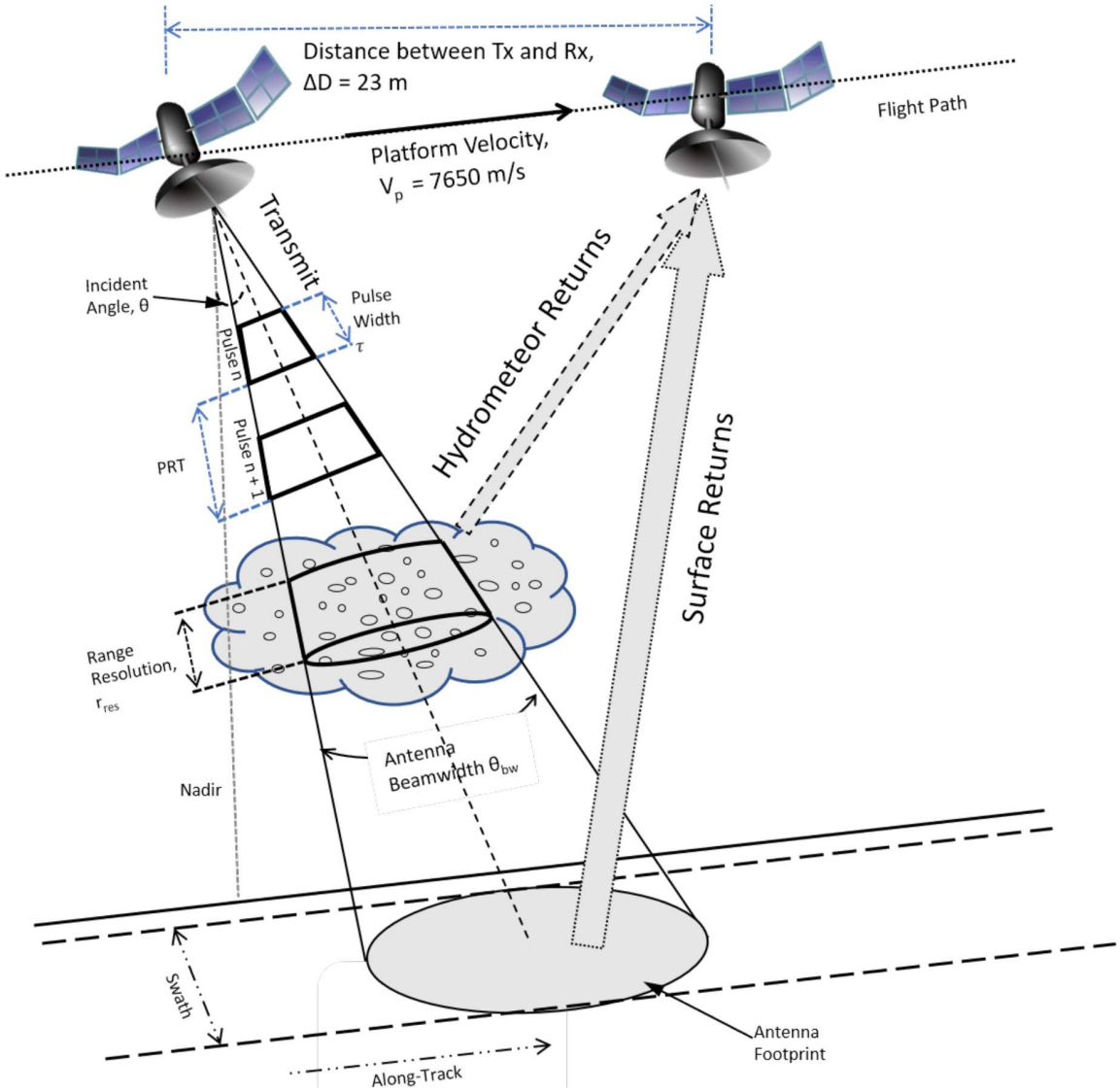

FIGURE 2.1. Visualization of basic spaceborne weather radar principles: the transmit and receive of an antenna direced at a weather target, with the added specular contributions from the surface

application. A radar pointed at geodetic nadir is pointing perpendicular to a surface defined

by a ellipsoidal model of the earth while at off-nadir the antenna is pointed at an angle away from geodetic nadir. To further this, vertical profiles of storms are taken from above the Earth. This meaning that the echos collected from the atmosphere can have contributions from the surface of the earth. The surface can contribute significant specular reflections to the backscattering echos of the precipitation if pointed at geodetic nadir. This can in turn contribute clutter to the return echo from the hydrometeors and saturate the receiver [4]. To correct this, for a single antenna system with a single footprint, the antennas are points slightly off nadir. For a scanning systems (which provide more coverage), the antennas are required to be pointed closer to nadir as it provides better vertical resolution and minimizes clutter contamination. To obtain a more accurate representation of the hydro meteors, it is necessary to have a high vertical resolution. With this in mind, a balancing act must be made to minimize the surface returns while still maintaining a high vertical resolution [4]. Usually this is done by positioning the antennas as close to nadir as possible.

The beam sent out by spaceborne weather radars is known as a footprint. This in essence is the area illuminated by the radar on the targeted object. The footprint is usually a function of the antenna size, which is related to the antennas beam width, θ_{bw}. For a system with a single footprint,the radar observes along-track, meaning in the forward direction of the flight path. Radars with multiple footprints can perform cross-track scanning, in which the scan direction goes from left and right. the size of the full scan can be seen as the antenna swath.

2.2. Calculating Mean Power of Received Signals

One of the key measurements in characterizing weather echos is reflectivity factor. This section will provide a basic background on the computation of mean power as well as show a partial derivation of the weather radar equation. The weather radar equation is the standard

equation used to describe the return power from the volumetric scatterers. The main goal of the derivation is to show all of the different components needed to characterize the returns in the radar simulator.

The signals transmitted or received by a radar are typically narrow band signals. The complex signals can expressed as

$$s(t) = [I(t) + jQ(t)]e^{j2\pi f_0 t} = a(t)e^{j\alpha(t)}e^{j2\pi f_0 t} \tag{12}$$

where I and Q are the in-phase and quadrature (or the imaginary and real) components, $a(t)$ and α(t) represent the amplitude and phase modulations and f_0 is the "carrier" frequency. If the carrier frequency term, $exp(j2\pi f_0 t)$ is suppressed, the complex envelope of the signal can be computed as:

$$V(t) = I(t) + jQ(t) = a(t)e^{j\alpha(t)} \tag{13}$$

Thus the transmit signal can be written as

$$s_t(t) = U_{tr}(t)e^{j2\pi f_0 t} \tag{14}$$

where $U_{tr}(t)$ is the transmitted waveform. The received signal can be written as

$$s_r(t) = V_r(t)e^{j2\pi f_0 t} \tag{15}$$

where $V_r(t)$ is the received voltage [15].

For a single point scatterer of a meteorological event, the received signal is a function of the transmitted waveform. For a continuous wave (CW) radar, the received voltage can be

seen as

$$V_r(t) = \frac{\lambda G\sqrt{P_t}}{4\pi r^2}(s)e^{-j2k_0 r} \tag{16}$$

where λ is the wavelength, G is the gain of the antenna, r is the range of the target with respect to the radar, P_t is the power transmitted by the transmitter, s is the scattering matrix element of a spherical particle and $2k_0 r$ is the phase shift due to the targets range from the radar. Using the equation given in (9) we can express the received signal as

$$s_r(t) = \frac{\lambda G\sqrt{P_t}}{4\pi r^2}(S)e^{-j2k_0 r}e^{j2\pi f_0 t} \tag{17a}$$

$$= Ae^{-j2\pi f_0 \tau}e^{j2\pi f_0 t} \tag{17b}$$

where A is the amplitude (denoted as the factor: $\frac{\lambda G\sqrt{P_t}}{4\pi r^2}(S)$, k_0 in the wavenumber in free space $= 2\pi/\lambda = 2\pi f_0/c$ and $\tau = 2r/c$. Since the transmitted signal is pulse continuous wave (CW) at frequency f_0, then $s_r(t) = exp(j2\pi f_0 t)$, meaning that the received signal can be represented as

$$s_r(t) = As_{tr}(t-\tau) \tag{18a}$$

$$= AU_{tr}(t-\tau)e^{j2\pi f_0(t-\tau)} \tag{18b}$$

$$= Ae^{-j2\pi f_0 \tau}U_{tr}(t-\tau)e^{j2\pi f_0 t} \tag{18c}$$

Using (9), the equation for the received voltage of a single moving particle can be seen as [15]

$$V_r(t) = Ae^{-j2\pi f_0 \tau}U_{tr}(t-\tau) \tag{19}$$

A meteorological event will have more than a single moving particle. Each of the particles or the scatterers in the volume, return a value that constructively or deconstructively interfere with each other, producing a composite phasor sample or complex voltage sample. Using (13) the value, or the received voltage, can be expressed as the discrete sum of the contributions for the individual particles or

$$V_r(t) = \sum_k A_k(\tau_k; t) e^{-j2\pi f_0 \tau_k} U_{tr}(t - \tau_k) \tag{20}$$

where A_k is the scattering amplitude of the kth particle, f_0 is the operating frequency of the radar (function of wavelength λ and c speed of light), the range time, $\tau_k = 2r_k/c$ (r_k is the instantaneous location for the kth particle) and $U_{tr}(t - \tau_k)$ is the transmit waveform shifted by the range-time delay for a particle (τ_k) [15].

A key measurements used in weather radar to classify intensity of returns is power. It corresponds to the received voltage, $V_r(t)$, which relates back to the scattering cross section per unit volume of precipitation. The received voltage $V_r(t)$ from each scatterer is a stochastic, or random process as the location and scattering amplitude is random at any given time [6]. Due to this, the covariance of power can be taken as the variance of $V_r(t)$. The equation for mean power can be shown by first using the general expression for $V_r(t_1)$ and $V_r(t_2)$ or

$$V_r(t_1) = \sum_k A_k(\tau_k; t_1) e^{-j\theta_k} U_{tr}(t_1 - \tau_k) \tag{21a}$$

$$V_r(t_2) = \sum_m A_k(\tau_m; t_2) e^{-j\theta_m} U_{tr}(t_2 - \tau_m) \tag{21b}$$

Let $t_1 = t_2 = t$ and use the lag-0 covariance to calculate mean power.

$$V_r^*(t)V_r(t) = \sum_{k=m} |A_k(\tau_k;t)|^2 |U_{tr}(t-\tau_k)|^2 + \sum\sum_{k\neq m} A_k A_m^* e^{j(\theta_m-\theta_k)} U_{tr}(t-\tau_k) U_{tr}^*(t-\tau_m) \tag{22}$$

The power is then taken as the expected value of $V_r^*(t)V_r(t)$ or

$$\bar{P}_r(t) =< |V_r(t)|^2 > \tag{23}$$

The received power in this situation is referenced to the antenna port. As mentioned previously the phase angle θ_k is uniformly distributed and independent and identically distributed (iid) random variables, meaning that the expectation of the double sum will disappear since $e^{j(\theta_m-\theta_k)} = 0$ [15]. The position and amplitude of the scatterers are independent of each other, meaning that the amplitudes A_k and phases θ_k are independent leading to $< |V_r(t)|^2 >$ being expressed as

$$\bar{P}_r(t) =< |V_r(t)|^2 >= \sum_k < \|A_k(\tau_k;t)|^2 \, |U_{tr}(t_1-\tau_k)|^2 \tag{24}$$

As mentioned previously, the amplitude of a scatterer can be expressed as $\frac{\lambda G\sqrt{P_t}}{4\pi r^2}(S)$. Replacing into (24) gives

$$\bar{P}_r(t) = \frac{\lambda^2 P_t}{(4\pi)^3} \sum_k < \frac{G_k^2 4\pi |S_k|^2}{r_k^4} > |U_{tr}(t-\tau_k)|^2 \tag{25}$$

This in turn begins to take the form of the weather radar range equation.

The weather range equation is the general equation used to relate the radars received power to the characteristics of the scatterering medium in a volume [15]. It is made up of the transmit power P_t, the gain of the antenna G_o, the beamwidth $\theta_1\phi_1$, the dielectric constant of water $|K_w|^2$, the equivalent reflectivity factor $Z_e(r_0)$, and the range to hydrometer, r_0. Using these variables we can compute an estimation of the returned power as can be seen in:

$$\bar{P}_r(r_0) = \left(\frac{cT_0}{2}\right)\left[\frac{P_t G_0^2}{\lambda^2(4\pi)^2}\right]\left(\frac{\pi\theta_1\phi_1}{8ln2}\right)\frac{\pi^5|K_w|^2 Z_e(r_0)}{r_0^2} \tag{26}$$

The mean power of a weather signal can also be estimated by averaging the instantaneous power samples, i.e

$$\hat{\bar{P}} = \frac{1}{N}\sum_{n=1}^{N} P_n \tag{27}$$

where $P_n = |V[n]|^2$ and $V[n]$ is the samples of the signal $V(t)$ In this case we are averaging in time while the previous analysis was an average over space of many hydrometeors.

2.3. Doppler overview

The majority of this thesis focuses on implementing DPCA to reduce Doppler velocity estimation uncertainty by mitigating the effects of the platform velocity. This section provides an overview of Doppler measurements and its uses in weather radar.

Doppler radars use the principles of the Doppler effect. In short, the Doppler effect is the observable frequency shift that occurs when a wave is reflected off a moving target [16]. This is proportional to the radial velocity of the object with respects to the position of the radar, i.e

$$f_d = \frac{2v_r}{\lambda} \tag{28}$$

where v_r is the radial velocity and f_d is the Doppler frequency. As mentioned previously, hydrometer volumes are a conglomeration of scatters, each with different velocity vectors. Moving particles in the volume impart different Doppler shifts based on their own radial velocities. Additionally, each moving particle backscatters energy to the receiving antenna, leading to a distribution of energy at each valid Doppler velocity bin. This is called the power spectral density (PSD) or the Doppler spectrum; a power weighted distribution of radial velocities from individual scatterers. The estimate of the mean Doppler velocity can be inferred by computing the expectation of energy in the Doppler spectrum for all velocities in [-v_a, v_a), or equivalently, from the lag-1 estimate of the autocorrelation function [6].

The spectrum of a signal is given by a Fourier transform which decomposes the signal into its frequency components. This means that the power spectral density of a stochastic signal, such as a return echo from a hydro meteor, decomposes the signal power into various frequencies. The power spectral density can be defined as

$$S(\omega) = \lim_{x\to\infty} \frac{1}{2T} E\{|\mathcal{F}[x_T(t)]|^2\} \tag{29}$$

where E is the expectation of $\mathcal{F}[x_T(t)]$, the time-limited Fourier transform shown as

$$\mathcal{F}[x_T(t)] = \int_{-T}^{T} R(t) e^{-j\omega t} dt \tag{30}$$

x(t) is the wide sense stationary random process.

The power spectral density can also be computed by taking the Fourier transform of the autocorrelation of the signal x(t).

$$S(\omega) = \int_{-\infty}^{\infty} R(t) e^{-j\omega t} dt \tag{31}$$

where $r(t)$ is the auto-correlation function.

There is a one to one correspondence between Doppler frequency and the radial velocity as shown by the equation for a doppler frequency spectrum for a single scatterer moving with a constant velocity $\vec{v}$ (velocity component parallel to the incident beam direction $(\hat{i} \cdot \vec{v})$:

$$S(f) = \sigma_b(-\hat{i}, \hat{i}) \delta(f + \frac{2\hat{i} \cdot \vec{v}}{\lambda}) \tag{32}$$

where $\sigma_b(-\hat{i}, \hat{i})$ is the bi-static scattering cross section of a particle and δ is a Dirac delta function. With this equation it is possible to see that there is a one to one correspondence between Doppler frequency and the radial velocity (velocity component parallel to the incident beam direction $(\hat{i} \cdot \vec{v})$. With this, $f = 2\hat{i} \cdot \vec{v}$ $\lambda = -2v/\lambda$ defines the radial velocity axis for the PSD, referring to the Doppler velocity spectrum.

In [6] it is shown that the shape of the Doppler spectrum is approximated by a Gaussian shape and can be defined as

$$S(f) = \frac{S_0}{\sigma_f \sqrt{2\pi}} exp \left[-\frac{(f - \bar{f})^2}{2\sigma_f^2} \right] \tag{33}$$

By using the transformation, the corresponding Doppler velocity spectrum is

$$S(v) = \frac{S_0}{\sigma_v\sqrt{2\pi}} exp\left[-\frac{(v-\bar{v})^2}{2\sigma_v^2}\right] \tag{34}$$

where $\bar{v} = -\lambda\hat{f}/2$ and $\sigma_f = (\lambda/2)\sigma_v$.

Again, assuming that the Doppler spectrum is Gaussian-shaped. the autocorrelation function can also be derived as

$$R(\tau) = S_0 exp\left(\frac{-8\pi^2\sigma_v^2\tau^2}{\lambda^2}\right) exp\left[-j\frac{4\pi\bar{v}\tau}{\lambda}\right] \tag{35}$$

Since in pulse Doppler, only samples of the signal are available, the autocorrelation function is sampled at a time T apart, given by

$$R(n) = S_0 exp\left(\frac{-8\pi^2\sigma_v^2 n^2 T_s^2}{\lambda^2}\right) exp\left[-j\frac{4\pi\bar{v}nT_s}{\lambda}\right]; \quad n = 1, 2, ..., N \tag{36}$$

where n is the lag.

Using the returns off the receiver $v[n]$, we can compute the auto correlation function at lag l, which is given by

$$\hat{R}(l) = \frac{1}{N}\sum_{n=0}^{N-l-1} V(n+l)V^*(n); 0 \leq l < N \tag{37}$$

The autocorrelation function can be used to compute the mean velocity of the sampled signal. If the Doppler spectrum is symmetric about a mean frequency $\bar{f}$, then the mean frequency can be derived from the autocorrelation. Thus the mean frequency can be computed

as

$$\bar{f} = \frac{arg[R(t)]}{2\pi t} \tag{38}$$

where arg stands for the argument of a complex number and t is time. The mean velocity can thus be computed as

$$\bar{v} = \frac{-\lambda}{4\pi t} arg[R(t)] \tag{39}$$

For pulse pair estimates, the voltages are N time samples of the received signal space T_s apart [15]. Using the lag 1, the autocorrelation function can be seen as

$$\hat{R}[1] = \frac{1}{N} \sum_{n=0}^{N-2} V(n+l)V^*(n); \tag{40}$$

The velocity can then be estimated as

$$\bar{v} = \frac{-\lambda}{4\pi t} arg[\hat{R}(1)] \tag{41}$$

The spectrum width can be computed using the magnitudes of the autocorrelation at zero lag and lag one computed as such

$$\hat{\sigma}_v = \frac{\lambda}{2\pi T_s \sqrt{2}} \left[\frac{R(0)}{R(1)}\right]^{\frac{1}{2}} \tag{42}$$

These are the fundamental equations of acquiring weather signals with pulse Doppler weather radar. In the next section, we will clarify the challenges of Doppler measurements with spaceborne weather radars.

2.4. Difficulties in Spaceborne Doppler Weather Radars

In a radar bin, a dispersion of velocities occurs due to hydrological processes as well as radar system parameters. This is known as the spectrum width and is associated with a combination of factors. In spaceborne weather radars, the main contributor to decorrelation between pulses, and in turn a spreading of the spectrum, is the high velocities introduced to the radar while in orbit. The Doppler spread due to motion can be defined as

$$\sigma_1 \approx 0.3\theta_1 V_s \tag{43}$$

where θ_1 is the 3-db beamwidth of the antenna, V_s is the platform velocity [5]. As can be seen by the equation, the surface Doppler spectrum width depends on the angular spread of the antenna as well as the platform velocity. For a small antenna, the beam width is large as can be seen by

$$\theta_1 = \frac{70\lambda}{d} \tag{44}$$

where d is the diameter of the antenna [7]. This means that there is a larger range of theta, so signals have a larger range of velocity and a wide spectrum. As the antenna size gets larger, the smaller the spectrum becomes meaning higher correlation between pulses. While this can provide moderate accuracy in most cloud conditions, the spectrum still degrades under convective clouds. Additionally having a large antenna can produce other complications on board a spacecraft, such as requiring more resources.

Another option is to increase the PRF relative to the antenna. The PRF though can only be scaled so much as it is bound by the thickness of the atmosphere layer to be monitored.

For precipitation measurements, this results in:

$$\frac{1}{PRF} = PRT > \frac{2H}{c} \tag{45}$$

where PRT is the pulse repetition time, and H is the extent of range interval with nonzero backscatter. This can be assumed to be 20 km or less for space borne measurements of clouds and precipitation. This results in a max PRF of 8000Hz (which is not practical to operate at) [3].

While these methods can alleviate some of the issues associated with collecting Doppler measurements, the issue of high platform velocities will always be a major source of spectrum broadening. Instead, we propose DPCA as an alternative method to performing Doppler measurements from a spaceborne weather radar.

2.5. Displaced Phase Center Antenna

Displaced Phase Center Antenna (DPCA) has been widely used for clutter mitigation in airborne radar . It was originally proposed by General Electric (GE) for correction of the butterfly effect, a phenomenon in which clutter leakage formed a wing-shaped pattern on a plan position indicator (PPI) display [17]. Due to the airborne radars velocity component, the clutter spectrum becomes broad when pointed abeam, leading to the effect. To correct for this, the idea was to use two beams, a leading and following beam which allowed for the signal to be received at the exact same point angle. This in turn produce an apparent cancellation of the forward velocity of the airborne radar.

Though the method had not previously been used for Doppler measurements from space, the idea was proposed by [2] as a means to remove the high platform velocities causing a degradation in returns from single antenna configurations. The concept is similar to its

use for clutter mitigation, but instead intended to remove the ambiguity between platform Doppler and target Doppler.

DPCA requires two along track antennas as opposed to the conventional single antenna configuration. By cleverly spacing your two antennas a certain distance between each other and choosing a pulse repetition time (PRT) to match the platform velocity, you are able to create a common phase center between sequential pulses, leading to a removal of the decorrelation effect seen by single antennas. From the perspective of the radar pulses, proper use of the DPCA technique will make the platform seem as if it were not moving [2].

Two DPCA implementations have been proposed. In mode 1, Figure 2.2, the leading antenna transmits a pair of pulses (separated by the PRT), hits the surface, and after a time, the leading antenna receives pulse 1 while the following antenna receiving pulse 2 a certain time later [2]. For this configuration to work, the platform must move half the distance separating the antennas during a PRI. The distance between pulses is calculated as

$$D_{p1p2} = V_s * PRT \tag{46}$$

Since the transmit between pulses is half the antenna size, the distance between antennas must be twice the size.

$$D_{sep1} = 2V_s * PRT \tag{47}$$

While this configuration is potentially less complex (only one antenna will be transmitting, resulting in less hardware needing to be implemented), it may present a design issue due to the antennas requiring a larger platform area to accommodate the separation distance. One

of the benefits we would like to include with DPCA is a smaller antenna area. Due to this, a second configuration, or mode 2 is introduced.

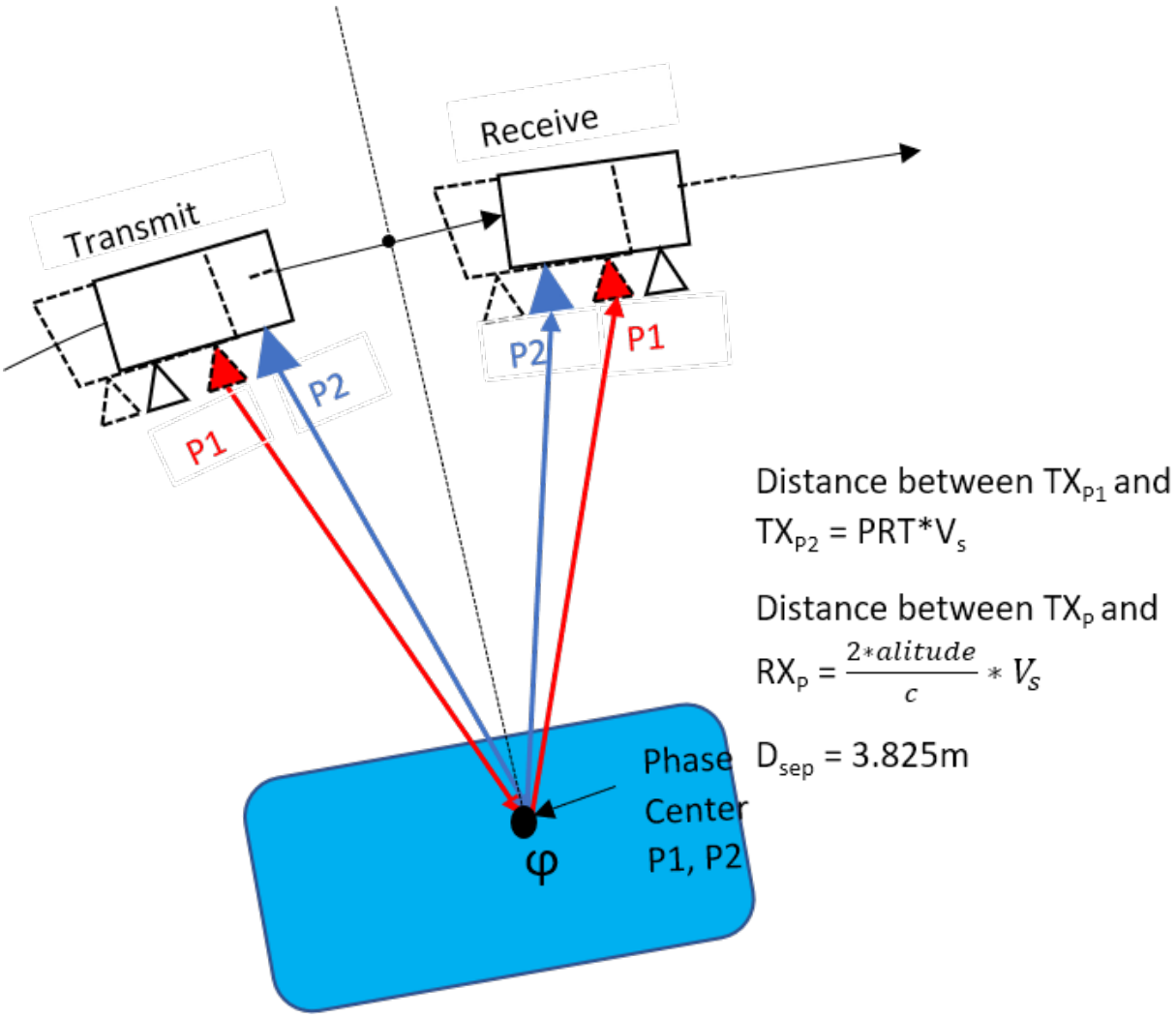

FIGURE 2.2. DPCA mode 1 scan strategy.

In mode 2, both the leading and following antennas transmit and receive as seen in Figure 2.3. This strategy requires additional hardware to implement, but has the added benefit of reducing the separation distance between antennas by a factor of two [2]. Transmit between pulses are to happen at the same position in space, meaning that the PRI can be increase

by a factor of two. The antenna separation distance for DPCA Configuration 2 is:

$$D = V_s * PRT \tag{48}$$

While both DPCA modes can provide accurate Doppler measurements from space by effectively mitigating the platform velocities, we will be focusing all of our analysis on DPCA mode 2 for practicality of use onboard a satellite in terms of size.

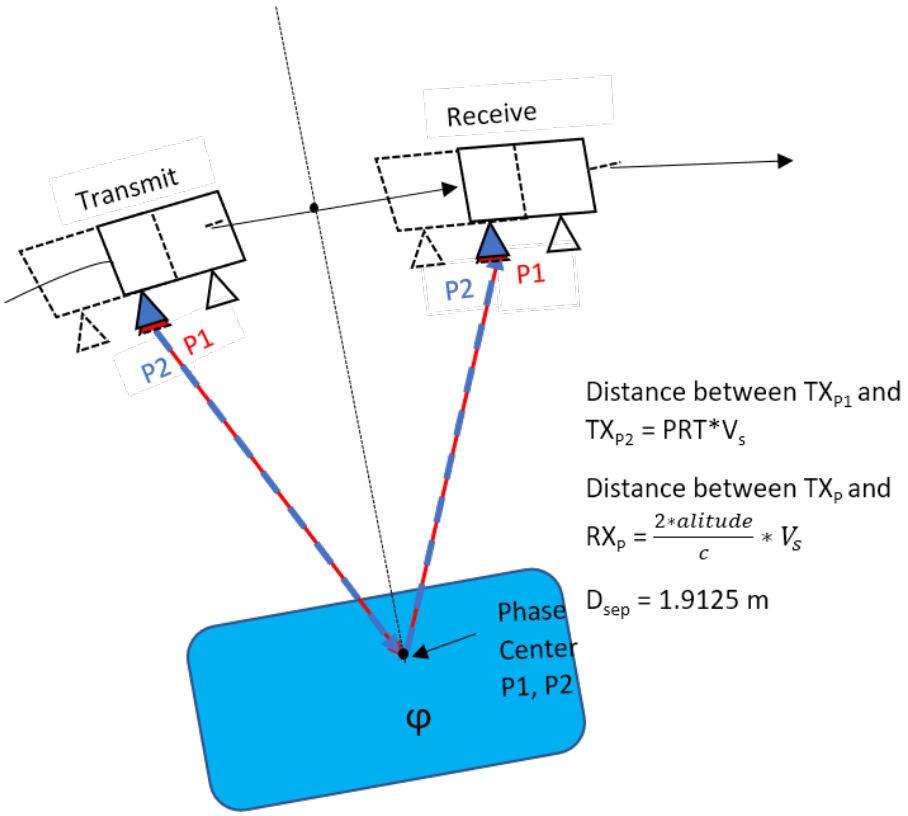

FIGURE 2.3. DPCA mode 2 scan strategy

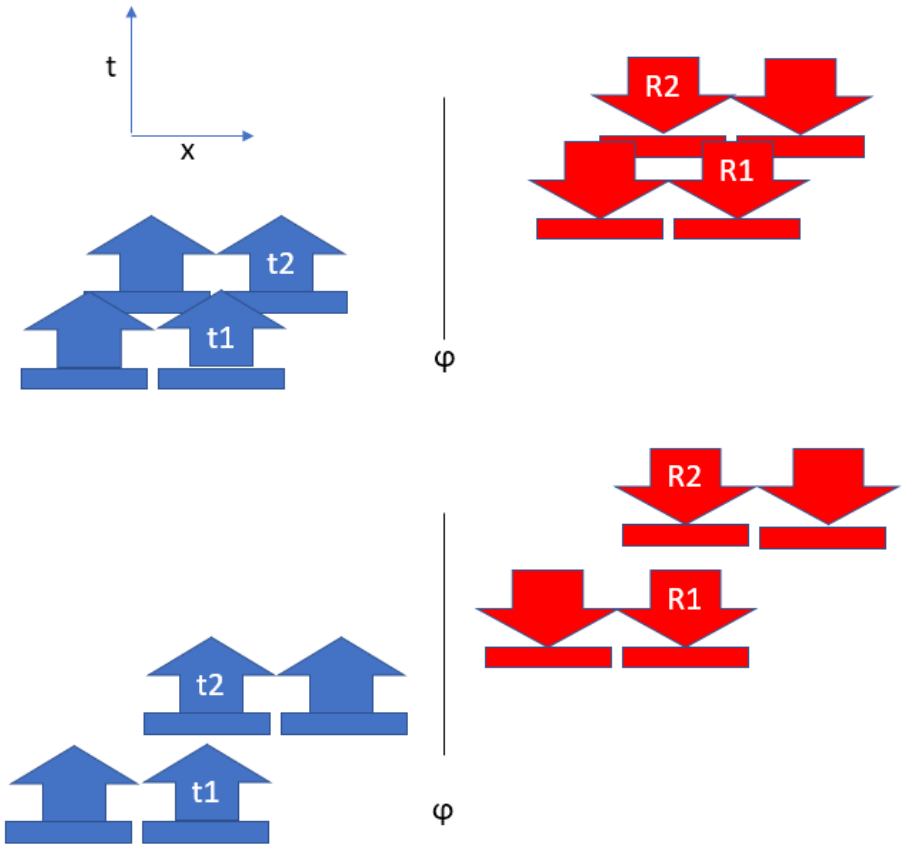

FIGURE 2.4. example of how transmit and receive of DPCA would work. The top figure shows DPCA mode 1. Here we can see that pulse one and pulse two are separated by half the distance. In DPCA mode 2, the lower figure, the transmit time is at exactly one full PRT, meaning that transmit happens at the same spot.

CHAPTER 3

DPCA Simulator

This chapter describes the model used to simulate DPCA mode 2. DPCA mode 2 alternates transmit and receive as can be seen in the discussion in Chapter 2. The goal is to create a simulator that characterizes the performance of the DPCA radar observation strategy for a system operating in LEO, while taking into account known sources of error that could arise with a two antenna configuration. The simulator will also contain a single antenna variation to provide an analytical comparison between the performance of DPCA and the current single antenna technique used in spaceborne weather radars. Additionally, to minimize biases in the comparison between the two cases, the simulation between the single antenna and DPCA will be performed under the same ideal conditions, with the only variations coming from the antenna.

The simulation will follow a typical method, in which the return signal is computed by taking the sum of the weight of each simulated scatterer that is illuminated by the radars transmitter. Some examples of these simulators can be seen in, [18], [19], [20], [21]. The idea is to create a surface with scatterers, calculate the weight of each surface scatterer illuminated by the transmitted pulse and coherently sum the received signal to get an accurate estimate of the return signal for the volume. While models may differ in the amount of detail added such as the type of antenna waveform, how the scatterers are generated, etc, they all follow the same idea. In our case, the model will consist of four different portions:

- The system parameters and characterization
- construction of the scatterer plane
- simulation of a single antenna/DPCA mode 1 or 2

- Analysis of the return voltages

The following sections contain necessary information to show how the model was constructed.

3.1. System Parameters and Characterization

This section focuses on showing the radar parameters used to simulating DPCA and a single antenna. Defining the system requires four key aspects: the positions and attitude space, transmit characteristics of the radar, the properties of the antenna, and the waveform.

Defining how the radar will act in space is crucial for correct transmit and receive of the system. It is necessary to take into account how the earths orbit affects the radar, what the orbital height is and the attitude (orientation of the platform in space) corresponding to the radar. Orbital weather radar concepts operate at LEO, or an orbital height on the order of 450km. Given the height, it is possible to calculate the forward velocity of the platform by using the orbital velocity formula. This value is necessary to choose an appropriate PRI as well as to determine the separation distance needed between the forward and following antenna for DPCA. The equation follows as:

$$v_{sc} = \frac{G_{me}}{(r_e + tx_z)}^{1/2} \tag{49}$$

with G_{me} being the gravitational constant, r_e being the radius of earth, and tx_z being the orbital height leading to an orbital velocity of 7650 m/s [7]. For this research, the attitude (yaw, pitch, roll), is assumed to always be normal to the earth or at (0,0,0). Though the attitude may change during operation, the analysis is outside of the scope of this thesis.

The transmit characteristics of the antenna are presented next. The radar operates at Ka band (35.75 GHz) using a PRI of 250 μs. The notional radar used is a monochromatic-pulse to allow for simplicity. Additionally, the antennas for DPCA will use a 1.6m dish while the

single antenna system will use a 5m dish, plausible for a single antenna configuration in space. The antenna pattern is estimated using a $sinc^2$ function with first sidelobes level at

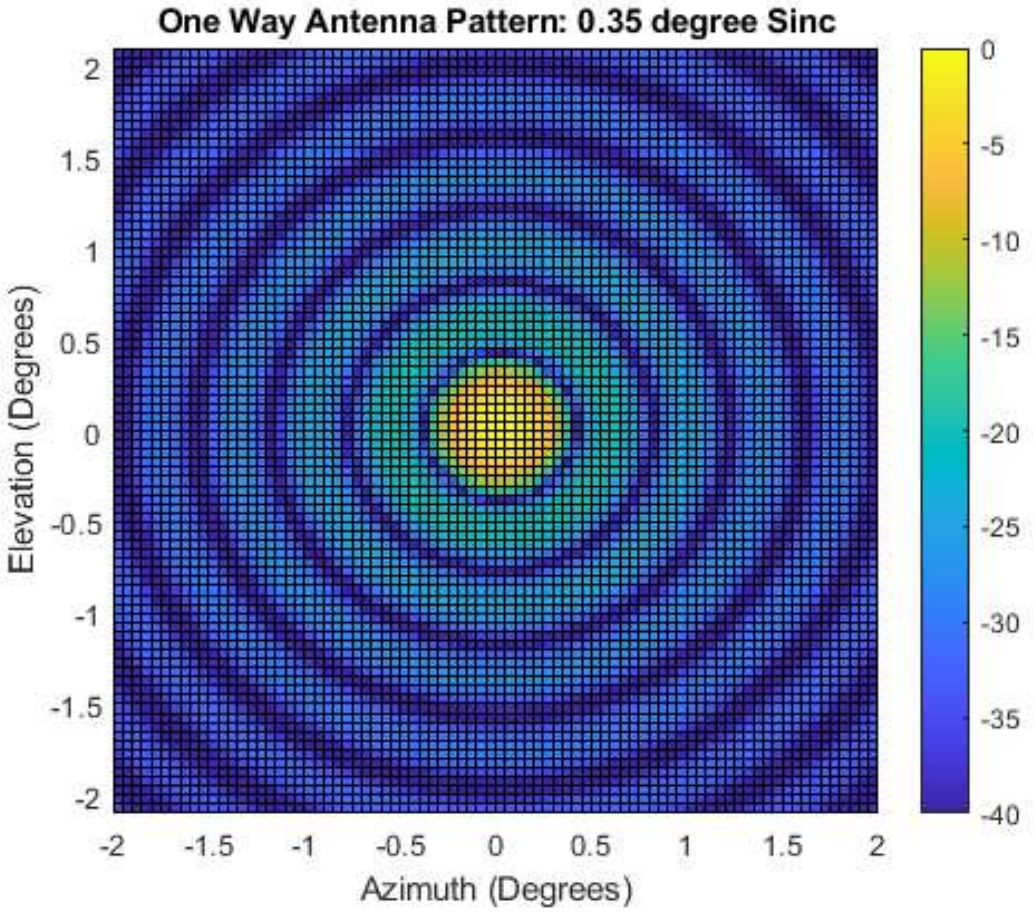

FIGURE 3.1. Estimated antenna pattern using a $sinc^2$ function.

-20db . The antenna is also made to be circularly symmetric and have a normalized boresight gain of 1 (0 dB) as can be seen in Figure 3.1.

The waveform used for our simulation is a mono-pulse waveform created from a Hanning window, a window function used to weight values in a window of time [22]. The Hanning window can be computed as

$$w(n) = 0.5(1 - cos(2\pi\frac{n}{N})), 0 \leq n \leq N \tag{50}$$

Using this equation, we compute the waveform as:

$$W_{mp} = \frac{w(n)}{\sqrt{\sum_{n=0}^{N} |w(n)|^2}} \tag{51}$$

The waveform can thus be seen in Figure 3.2

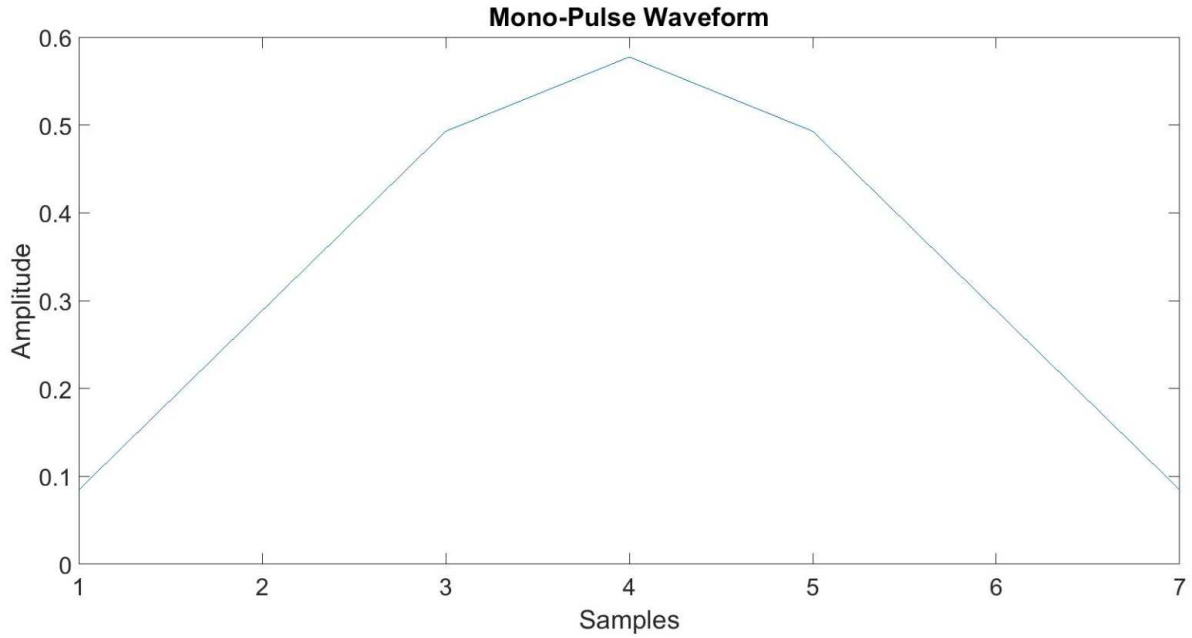

FIGURE 3.2. Mono-pulse waveform.

3.2. SCATTERER PLANE

This section focuses on building the scatterer plane for simulating a uniformly distributed volume. This can also be used to construct a non-uniform volume to characterize the effects of non-uniform beamfilling in DPCA as will be shown in Chapter 5.

The bounds of the scatterer plane are defined first. The plane must be large enough to contain the full antenna pattern (sidelobes included). As so, the bounds of the scatterer become a function of the antennas θ_{3db}. The volume can be thought of as a three dimensional object in the Cartesian plane. As shown in Figure 3.3, the z direction corresponds to the

height (h) of the volume, while x and y correspond to the length and width. The maximum

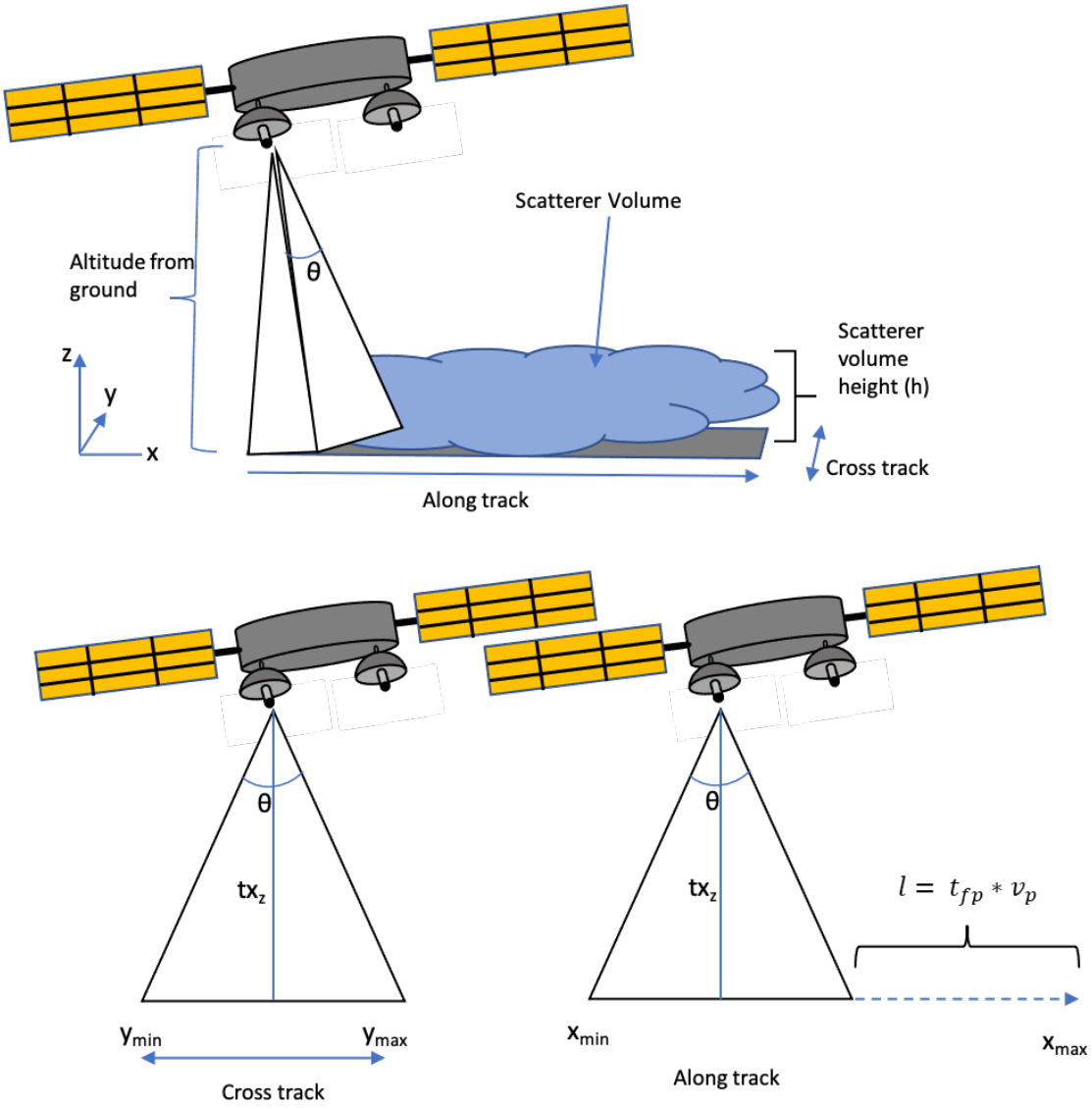

FIGURE 3.3. Diagrams showing how the scatterer plane is created.

vertical size of the plane (z directions) is chosen as an arbitrary value spanning from -1000 to 1000m to allows for a large sampling size. The width, or the y bounds are determined from calculating the width of the swath. Using the bottom left diagram in Figure 3.3, the maximum and minimum values can be calculated using simple geometry. The maximum width is calculated as

(52) $$y_{max} = 2t_{xz}tan(\theta)$$

While the minimum width is calculated as

(53) $$y_{min} = -2t_{xz}tan(\theta)$$

with t_{xz} being the altitude of the spacecraft from the surface and θ as the θ_{3db}.

The minimum length of the x bound is calculated similarly to the minimum y bound. But unlike the maximum y bound, the maximum x bound is calculated as a factor of the width of the swath as well as the platform velocity and duration of transmit time during flight. This can be seen in the bottom right graphic in Figure 3.3. the final calculation can be seen as

(54) $$x_{max} = 2t_{xz}tan(\theta) + t_{fp} * v_p$$

with t_{fp} being the total integration period for N pulses and v_p being the velocity of the platform.

Once the surface bounds are defined, we can create the scatterers for a uniform volume and for non-uniform beamfilling. For the uniform scatterer, the position of the scatterers is randomly generated via a uniform distribution as defined by

(55) $$U = \frac{1}{b-a} for\ x\ \epsilon\ [a, b]$$

Adding in the surface bounds, the equation can be seen as:

$$P_{x,y,z} = unif(b,a) * [max_{x,y,z} - min_{x,y,z}] + min_{x,y,z} \tag{56}$$

An example of the final scatterer can be seen in 3.4.

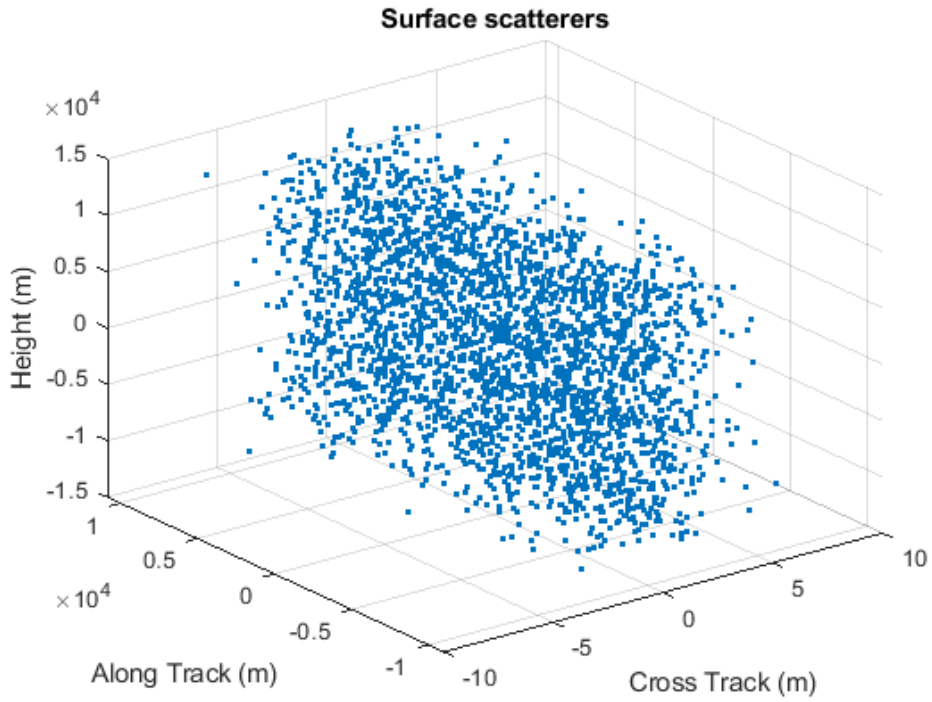

FIGURE 3.4. Uniformly distributed scatterer plane

For the non-uniform beamfilling, we are creating a line across the cross track dimension using a scatterer weight of 1. As opposed to the uniform case, the non-uniform scatterer is 2 dimensional. For simplicity, the scatterers are placed where the cross track is equal to 0 and the height is equal to 0, thus creating our scatterer planes.

3.3. SIMULATION

The simulations for a single antenna and DPCA both compute the return signal by taking the sum of the weight of each simulated scatterer that is illuminated by the radars

transmitter. First the distance of the scatterer relative to the radar is computed using:

$$R_r = \sqrt{(tx_x - x)^2 + (tx_y - y)^2 + (tx_z - z)^2} \tag{57}$$

where tx_x, tx_y and tx_z is the radars location with respect to the along track, cross track and altitude from the ground. Next we must find the portion of the antenna pattern that is radiating each point scatterer to obtain the correct gain. To do this we must calculate the ϕ and θ angle of the antenna pattern relative to the location of the scatterer. The geometry can be seen in Figure 3.5.

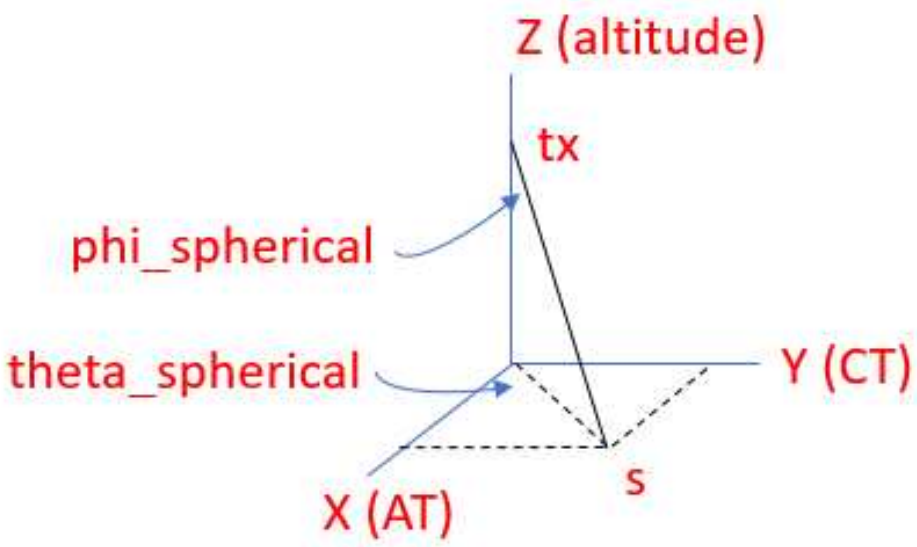

FIGURE 3.5. Diagram showing geometry of angles for the antenna pattern

For each scatterer, this can be done using:

$$phi = atan(-(tx_x - x)/(tx_z - z)) \tag{58}$$

and

$$theta = atan2((tx_y - y)/(tx_z - z)) \tag{59}$$

Next the return power of the scatterer is computed using the radar equation as shown in Chapter 2. Once the return power has been computed, the complex voltage for each is calculated using the equation:

$$Amp = Pr^{1/2} * U * e^{-2jkR_r} \tag{60}$$

where the k is the wave-number which is equal to $2 * \pi * \lambda$, P_r is the return power and U is the antenna pattern. This is then done for each scatterer and added together by range gate.

Both antenna configurations follow the same process, except for in the location at which consecutive scans happen. For a single antenna, the transmit location of each pulse happens at a distance equal to the platform velocity multiplied by the PRI, or for our simulations, at a distance of $\triangle_{ds}$ + 1.9125m, where $\triangle_{ds}$ is equal to the current position of the radar. For DPCA, the transmit locations between consecutive pulses are the same meaning that pulse 1 = pulse 2 = $\triangle_{ds}$ + 1.9125m.

3.4. Analysis

The last section of the model collects the complex voltages to compute our desired radar moments. For our analysis, the radar products that we are focused on is return power, Doppler velocity and the Doppler spectrum width using the equations provided in Chapter 2.

3.5. Summary

In this chapter, we examine how the spaceborne weather radar model is built to simulate DPCA and a single antenna system. In the single antenna case, each pulse will correspond to a different location in space, meaning that the pulses will not be well correlated when computing the Doppler moments. Using DPCA, the transmit and recieve between consecutive pulses will occur in the same place, resulting in a correlated signal. In the next chapter, we will focus on characterizing DPCA by showing how possible deviations in the configuration in a real life situation can affect the estimated Doppler moments.

CHAPTER 4

Characterization and Analysis of Uncertainty Associated with DPCA

DCPA is an effective technique for removing the high velocity contribution introduced in spaceborne weather radars. In theory, a spaceborne radar properly configured to use DPCA will results in a vertical Doppler velocity of 0 m/s. As mentioned in Chapter 2, by having a common phase centers between pulse pairs, the spacecraft will appear stationary. This feature removes the spectrum broadening due to motion, that was the largest source of velocity estimation error in a single antenna configuration. While DPCA has the potential to do this, imperfections can arise in a real implementation. Mounting the two antennas onto the platform can result in deviations in the antenna separation distance, as well a mispointing of the following antenna in relation to the leading antenna as seen by Figure 4.1. The resulting effect will lead to differences in the section of volume being illuminated between concurrent transmit pulses as seen in Figure 4.2. Factors such as thermal expansion and deviations in the platform velocity (relative to the ground) can change the points of transmit between consecutive pulses. Since all the aforementioned sources of error are a function of the separation distance between the antennas (platform velocity is function of separation distance, and the thermal expansion and the mounting imperfection can change the separation distance), and mis-pointing (mounting imperfections), we use them as a proxy to characterize the uncertainty in DPCA.

The analysis on error in DPCA followed a Monte Carlo like methodology, in which the positioning of the antennas were simulation over a large number of mis-pointing and separations distances. For a 1.6 antenna configuration at Ka-band, we used 15 different separation

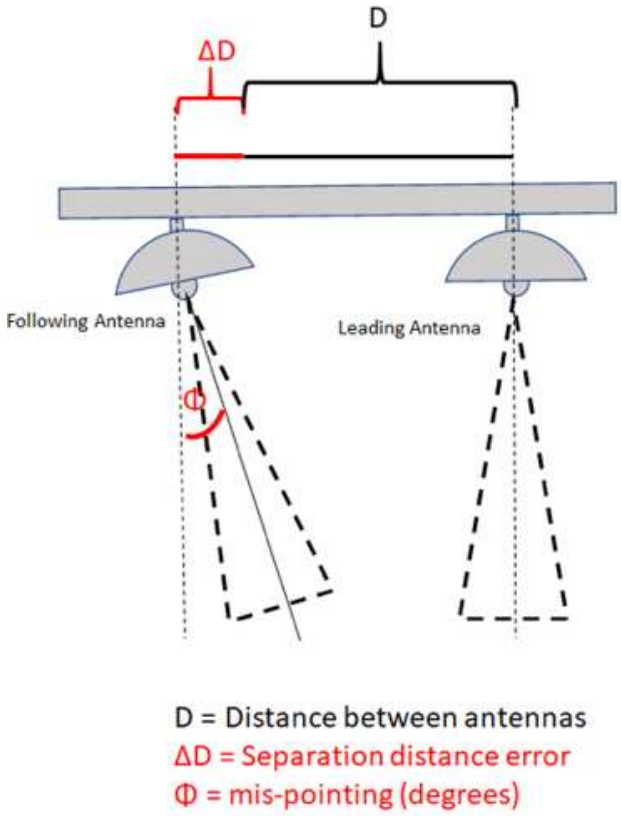

FIGURE 4.1. Diagram showing the possible error associated with DPCA.

distances varied between 1.8 - 2.0 m and 15 different pointing angles varied between -0.2deg - 0.2deg in relation to the pointing of the forward antenna (nadir). To remove any variability, the separation distance and antenna mis-pointing is simulated over one realization (a uniformly distributed volume scatterer generated by a uniform distribution). The experiment is then repeated using many different scatterer realizations to show how changing the volumes affects the Doppler returns.

This chapter will first shows the performance of DPCA under ideal conditions for the notional system design described in Chapter 3, in the hopes of validating that the simulator follows theory, as well as to provide a baseline for our future analysis. This will include a discussion of the radar moments that are used to show the performance of DPCA, as well as a statistical analysis of possible deviations from using different scatterers. Afterwards, the

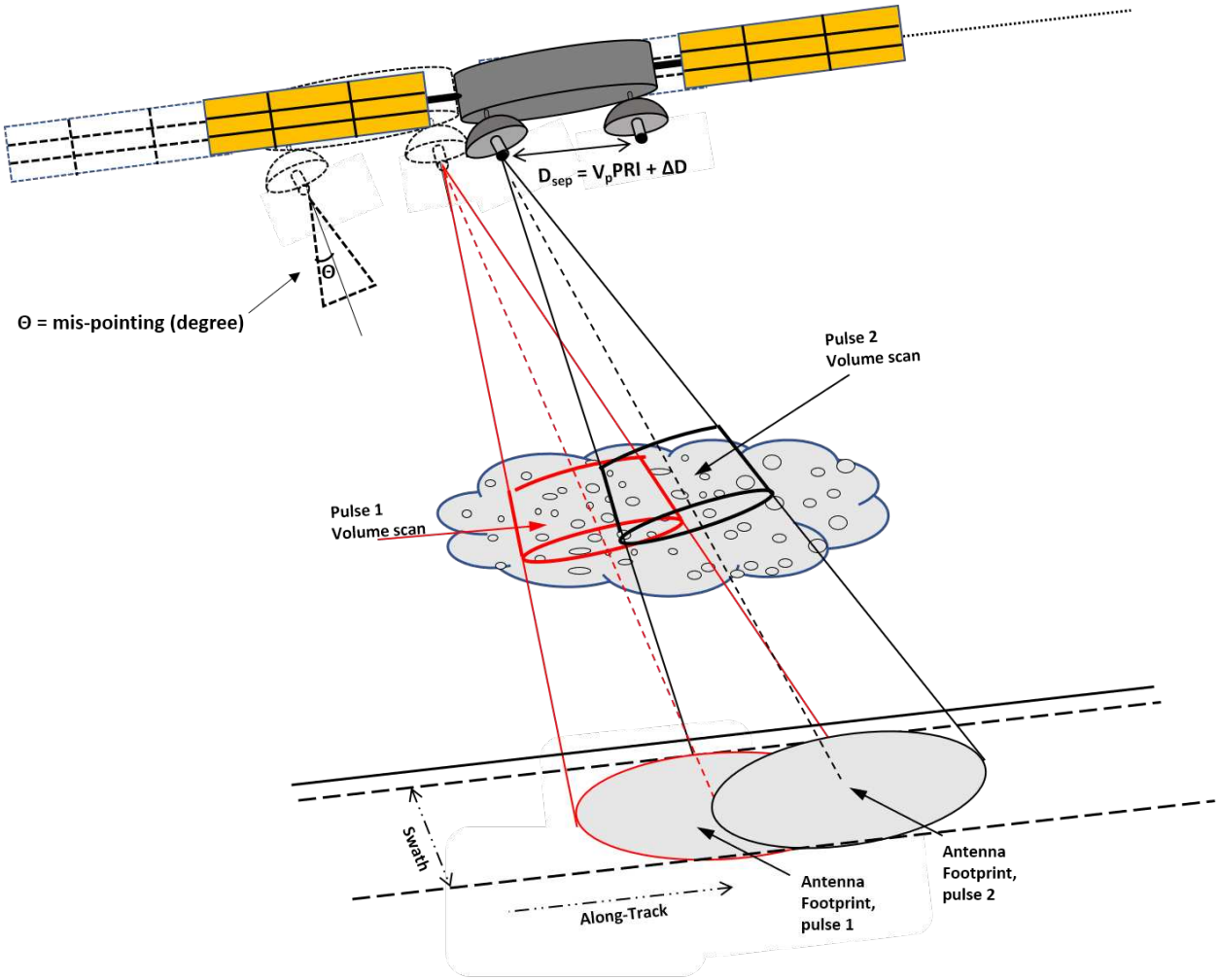

FIGURE 4.2. Diagram showing how mis-pointing between the antennas and a change in separation distance affects the volume scanned.

chapter will show the process used to model and simulate the sources of error in DPCA. We will characterize the uncertainty caused by the separation distance between antennas and the angle mis-pointing relative to the leading antenna. The chapter will first characterizing the two sources of errors independently (keeping one variable constant while changing the other) followed by characterizing the effects of deviations in both variables simultaneously. Once characterized, an analytical comparison between DPCA and a single antenna case will be shown.

4.1. Characterizing DPCA With An Ideal Notional Radar Configuration

Before showing how DPCA performs under various error sources, it is important to show the performance of DPCA in an ideal configuration. As mentioned previously, the largest contributor of Doppler velocity and spectrum broadening is the high platform velocity introduced as the radar orbits the Earth [2]. DPCA removes this velocity by configuring the two antennas to transmit and recieve at the same location in space. This is done by first transmitting pulse 1 using the forward antenna and then transmitting pulse 2 using the following antenna. To accurately do this, the antennas must be separated a distance which can be determined by the PRT and the platform velocity (V_p).

$$D_{sep} = V_p * PRT \tag{61}$$

To calculate the orbital velocity, we can use the equation for orbital velocity:

$$V_p = \frac{GM_e}{r_e + h}^{\frac{1}{2}} \tag{62}$$

where G is the gravitational force, M_e is the mass of the earth, r_e is the radius of the earth and h is the orbital height in relation to the earth [7]. In our simulation, the radar is in an LEO orbit, located 450km above the earths surface. Using this, we can calculate the orbital velocity to be approximately 7,640 m/s. The PRT is chosen to be 250 us for our simulation. By using (61), we calculate the ideal separation distance to be 1.9125m.

In our simulation, we are using a normalized static scatterer with weight equaling to 1, meaning that the other factors that affect velocity and spectrum width are gone. Using this logic, the resulting Doppler velocity and spectrum width should be equal to 0 m/s at an ideal configuration.

To show this, we simulate DPCA at its ideal configuration and compute our 3 key radar moments: return power, mean Doppler velocity and Doppler spectrum width. Return power is the first metric computed. As mentioned in Chapter 2, the mean return power can be estimated via the lag-0 autocorrelation estimate, or

$$Power = 10log_{10}(R(0)) \tag{63}$$

where R(0) is the lag-0 auto-correlation estimate from 100 pulses. For simplicity, the mean power (average of 100 pulses) will be referred to as power. The next radar moment computed is the mean Doppler velocity (referred to as Doppler velocity). Again, since we are using a static volume scatterer with a normalized weight, the only contribution of Doppler velocity can come from the platform. Since DPCA cancels out the platform velocity, the resulting velocity can be seen as 0 m/s. The last radar moment computed is the spectrum width, which shows the distribution of velocities. Since there is no velocity component, the Doppler spectrum can be seen as 0 m/s. To prove this, the range profile of power, velocity and spectrum width is plotted and shown in Figure 4.3.

To continue the characterization of DPCA, different configurations of static volume scatterers (realizations) are tested. A realization can be made in a way that can result favorably or unfavorably to DPCA, leading to an inaccurate representation of its performance. To characterize this, we use the law of large numbers, which states that the mean resulting from a large number of experiments should be close to the expected value of the performance. In our analysis, we calculate the mean by using 200 different realizations. The mean of power, mean velocity and mean spectrum width can be computed using the equation

$$\mu = \sum_{n=1}^{N} A_n \tag{64}$$

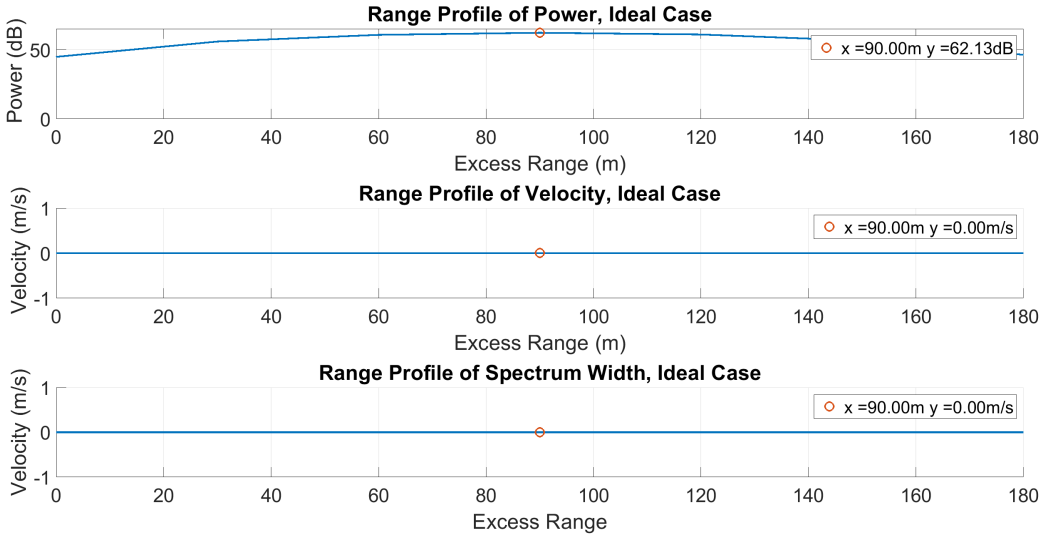

FIGURE 4.3. Diagram showing the power, velocity and spectrum width resulting from an ideal DPCA configuration. Since DPCA cancels out the apparent platform velocity and since the scatterer volumes are static, no velocity component is present. Leading to a velocity of 0 m/s and a spectrum width of 0 m/s.

where A is a placeholder for power, velocity and spectrum width and N is the number of the realizations. While the mean gives a reference or the expected performance of DPCA as the scatterer volume changes, it is also important to characterize the dispersion of values. To do this the standard deviation is computed. The standard deviation allows us to see the performance of DPCA under its worst cases scenarios. The equation can be computed as

$$\sigma_{std} = \sqrt{\frac{1}{N-1}\sum_{n=1}^{N}|A_n - \mu|^2} \tag{65}$$

where μ is the mean of the power, velocity or spectrum width. First we compute the mean of power. Since the location of the volume scatterer does not change, the max power should remain at 90m below the surface. To validate this, the mean power for the 200 realizations is computed using (59) and plotted on Figure 4.4 Next the standard deviation of the 200 realizations is computed using (60). As can be seen the power deviates by a maximum

of 1.6 dB. This meets expectation since if the scattererers are clustered in one location, the resulting power return would be larger. Finally a plot of the mean plus the standard deviation is shown to give a better visual representation of the tolerance in Figure 4.4. As can be seen, the max power remains at 90m below the surface and remains relatively consistent throughout each realizations.

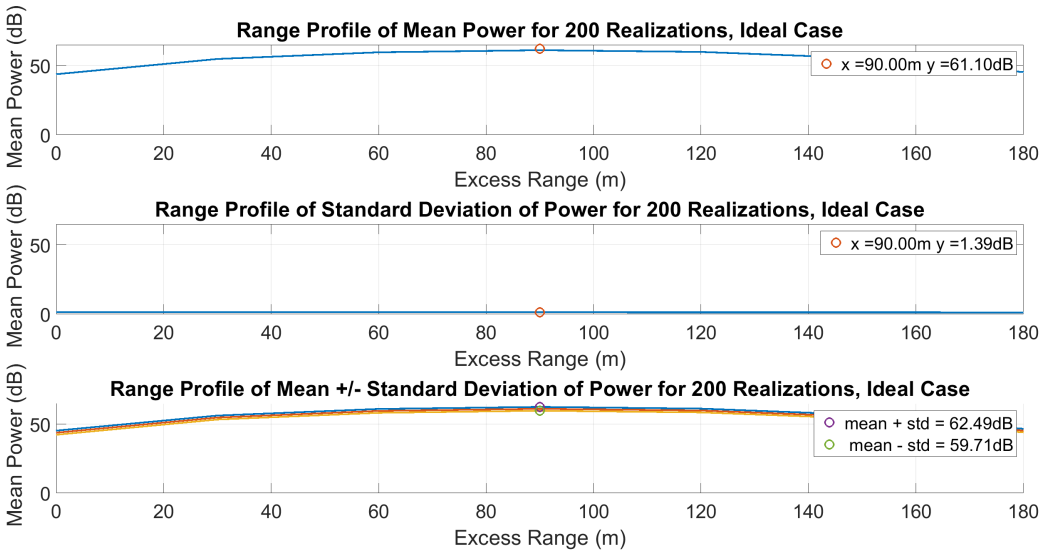

FIGURE 4.4. The figure shows the range profile of the statistical computations of mean power. The top plot shows the mean power for 200 realizations, the middle plot shows the standard deviation for power and the bottom one shows the mean +/- the standard deviation.

Next we compute the statistics for velocity. The characterization of velocity for 200 realizations follow the analysis of power. The mean of the velocity, the standard deviation and the mean +/- the standard deviation can be seen in Figure 4.5

As expected, since there is no apparent velocity component from the scatterer or the radar, the mean velocity component is 0 m/s for the mean and standard deviation. Regardless of the scatterer configuration, the samples between pulses are maintained at the same location. Additionally, the scatterers and the radar are seen as not moving, meaning that there should be no velocity component.

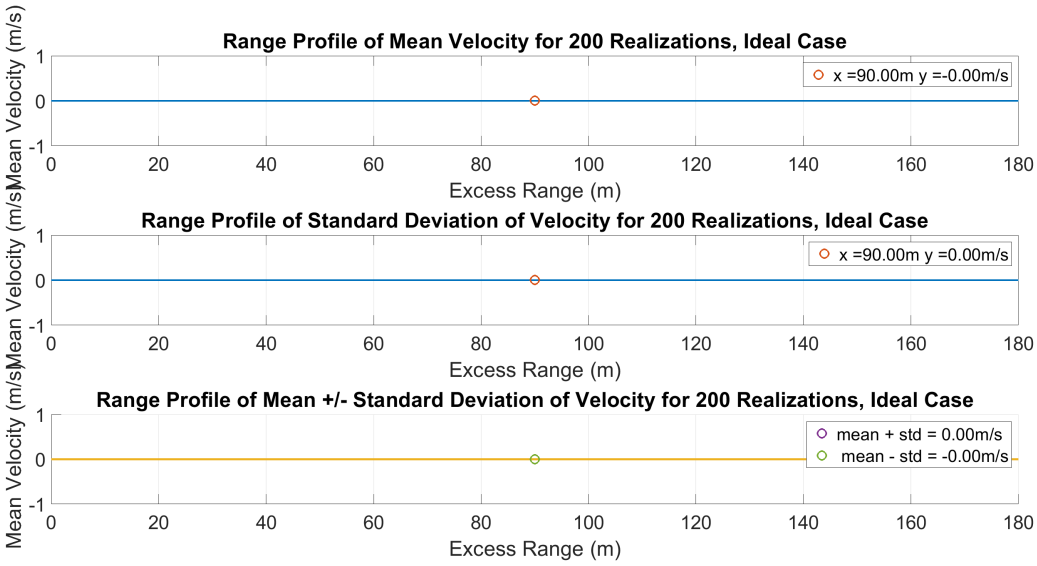

FIGURE 4.5. The figure shows the range profile of the statistical computations of mean velocity. The top plot shows the mean power for 200 realizations, the middle plot shows the standard deviation for power and the bottom one shows the mean +/- the standard deviation.

Next the spectrum width for 200 realizations is computed. Just as previous the mean, standard deviation and mean +/- standard deviation are computed and shown in Figure 4.6

As can be seen, the spectrum width results in a 0 m/s velocity, which follows the same logic as velocity. Since there are no moving parts, the correlation between pulse pairs should be perfect, resulting in no velocity contribution. Though the plots for power, velocity and spectrum width were shown over range, We must identify the range gate at which the maximum echo power from the volume is received. The reasoning for this is that the max power will be the point at which the full antenna beamwidth is encapsulating the volume. This can be visually represented byFigure 4.7 .

From Figure 4.3 and Figure 4.4, we see that the max power is located at 90 meters below the surface. Thus all of our analysis will be made at that point as it will provide the most accurate representation of how DPCA performs. In the case of the ideal configuration, the spectrum width and velocity at that range are 0 m/s.

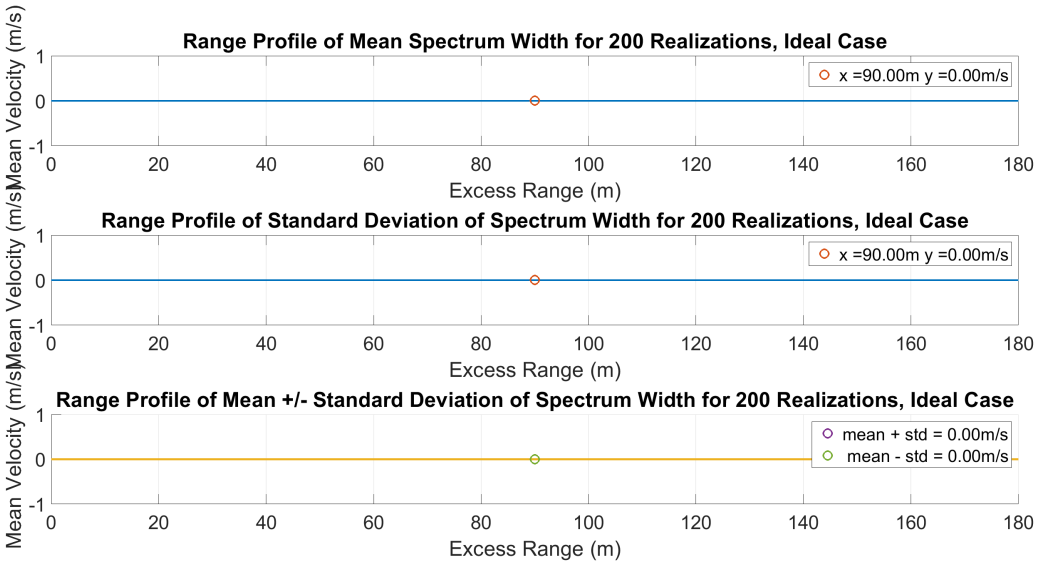

FIGURE 4.6. The figure shows the range profile of the statistical computations of mean spectrum width. The top plot shows the mean power for 200 realizations, the middle plot shows the standard deviation for power and the bottom one shows the mean +/- the standard deviation.

As can be seen by the analysis in this section, the simulator is functioning correctly according to theory. Since there is no apparent movement from the scatterer or the radar, there are no velocity components, resulting in a Doppler velocity and spectrum width of 0 m/s. This proves that at an ideal configuration, DPCA completely removes the difficulties encountered by single antenna systems. Additionally, this section provided a baseline to the performance of DPCA before accounting for any uncertainties in DPCA.

4.2. Characterizing Uncertainty Associated with the Separation Distance between Antennas

Now that the previous section calculated the performance of DPCA at its ideal case, we can begin analyzing the uncertainty associated with DPCA. As mentioned, the two variables we are going to vary is the mispointing and the separation distance of the antennas. To begin, the variables resulting in uncertainty within DPCA are characterize independent of

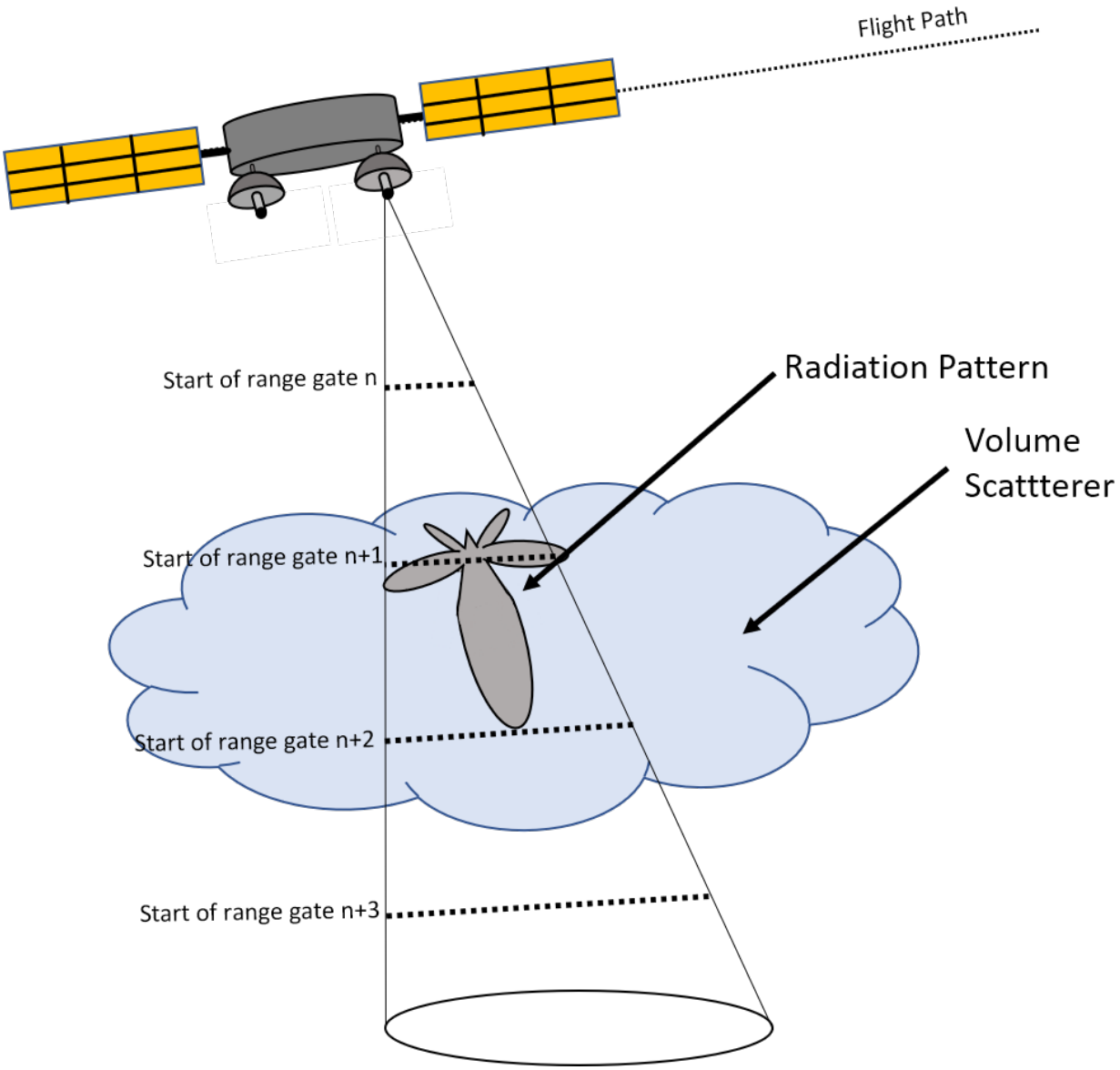

FIGURE 4.7. Diagram showing the point at which the full antenna beamwidth is encapsulating the volume scatterer

each other. While separation distance and mispointing are variables associated with the antennas, they can each effect DPCA in a different ways (i.e. one could produce a higher spectrum width, etc.). Additionally, by simulating each variable separately, we can use the information to identify any dependencies between the sources of error. With that being said, the effect of antennas separation distance on DPCA is simulated first.

The antenna separation is a function of the antennas PRI as well as the forward platform velocity of the radar. If the along track antennas are separated a distance that does not equal the chosen PRI or velocity (61), or if the separation distance is changed due to outside factors as mentioned previously, the transmit of pulse 1 and pulse 2 will happen at different locations in space as can be seen in Figure 4.8.

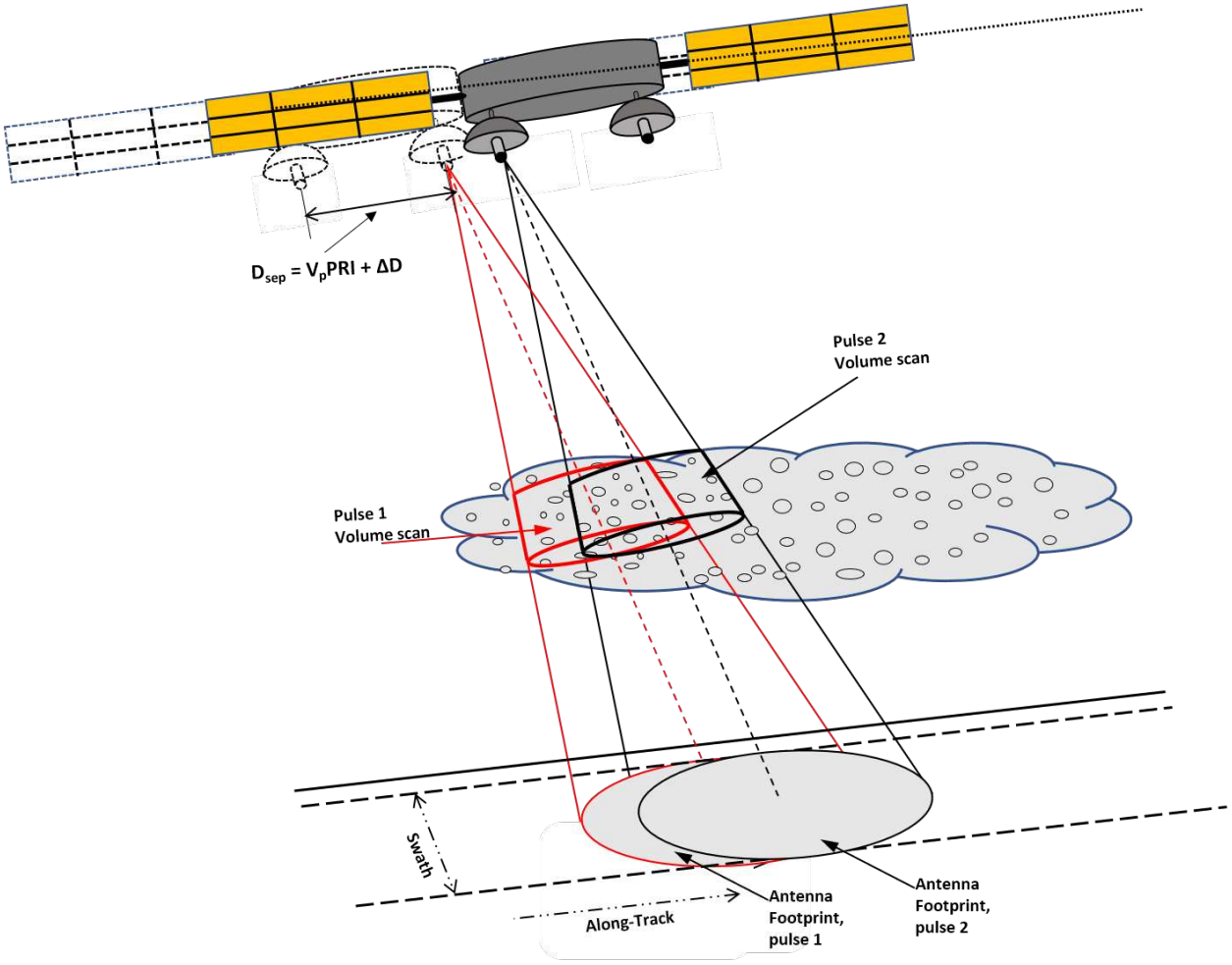

FIGURE 4.8. Diagram showing the transmit location of pulse 1 and pulse 2 when the separation distance between leading and following antenna are different from ideal. $\triangle D$ is the error in the separation distance which causes a shift in the location of transmit between pulses.

To obtain a realistic characterization of the effects separation distance has on DPCA, we varied the error by a max of 6.25% from the ideal case of 1.9125m. This results in a separation distance spanning between 1.8 and 2 meters.

The process for computing our radar moments follows the same logic as for the ideal case. First the power, velocity and spectrum width at each range gate is computed for each separation distances. To remove any variations between the ideal case and uncertainty, the same realizations were used throughout the analysis. Additionally, only the threshold separation distances are plotted as they use the most information about how DPCA performs.

The first metric compute was the power for 1 realization at the 15 different separation distances. Since the volume scatterer location and intensity remains the same, the power profile should not vary significantly as we change the separation distance as can be seen in the first figure in Figure 4.9. Additionally, as seen in the figure, the location of max power stays the same since the height of the scatterers relative to the radar does not change. With this, all of our analysis will be focused on 90 m below the surface.

Once we validated power, a velocity plot of a single realization is made to show how the threshold cases effect the performance of DPCA relative to the ideal. This can be seen in the second figure of Figure 4.9. Looking at the figure, for all separation distances tested, the velocity converges to approximately 0 m/s. This plot shows that while the separation distance is not exactly at nominal (or the ideal case of 1.9125 m), the decorrelation between pulse pairs at our threshold cases are low enough to where the resulting velocity is close to zero. While increasing or decreasing the separation distance may eventually result in larger velocity, at a systems level, the likelihood of having such high separation error is relatively low.

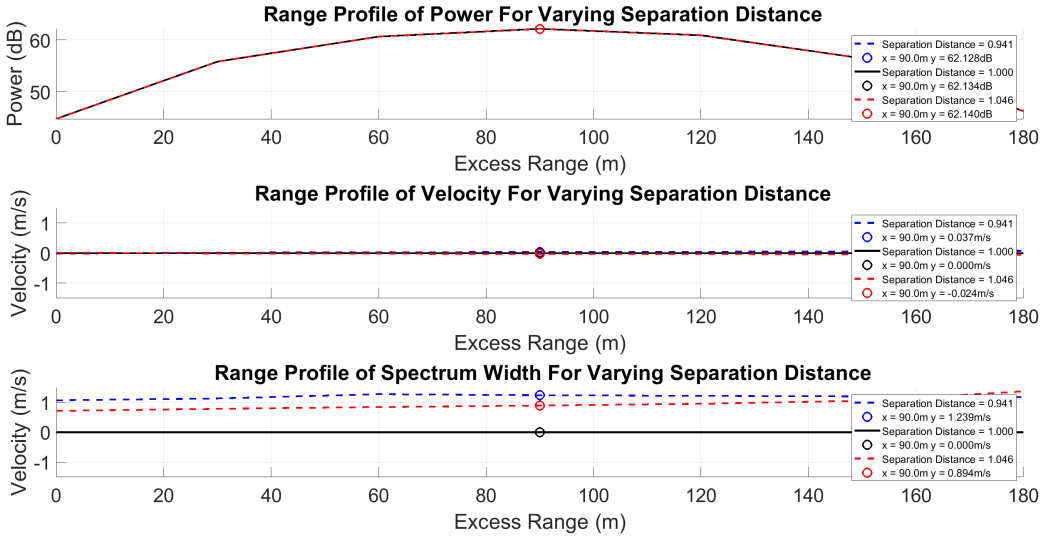

FIGURE 4.9. Range profile of power, velocity and spectrum width for different antenna separation distances. The resulting deviation in each of the radar moments follows a linear trend as the separation distance changes. Due to this, only the max, min and ideal case are plotted as they provide the most useful information when characterizing the effects of separation distance on DPCA.

The last moment computed is the spectrum width. The spectrum width can be seen as the standard deviation of the velocity distributions inside a volume, meaning that the value for spectrum width will always be positive. Since a change in separation distance decorrelates the pulse pairs, we expect to see a marginal increase of the spectrum width at its max and min as shown in Figure 4.9. As can be seen, the max spectrum width at 90m below the surface is approximately 1.3 m/s. Unlike velocity, the spectrum width increases quickly as the separation distance deviates from nominal. As the separation distance error increases, the correlation between pulses degradates, resulting in a larger distribution of velocities caused by white noise from the decorrelated portion of the signal.

Just like the ideal case, DPCA with varying separation distance will be simulated over 200 realizations. This will provide a more accurate characterization of its performance under different scatterer configurations. The analysis follows the same format, with the mean,

standard deviation, and the mean plus or minus the standard deviation being computed for power, velocity and spectrum width. The mean power and standard deviation is computed in the same fashion as previously and plotted in Figure 4.10

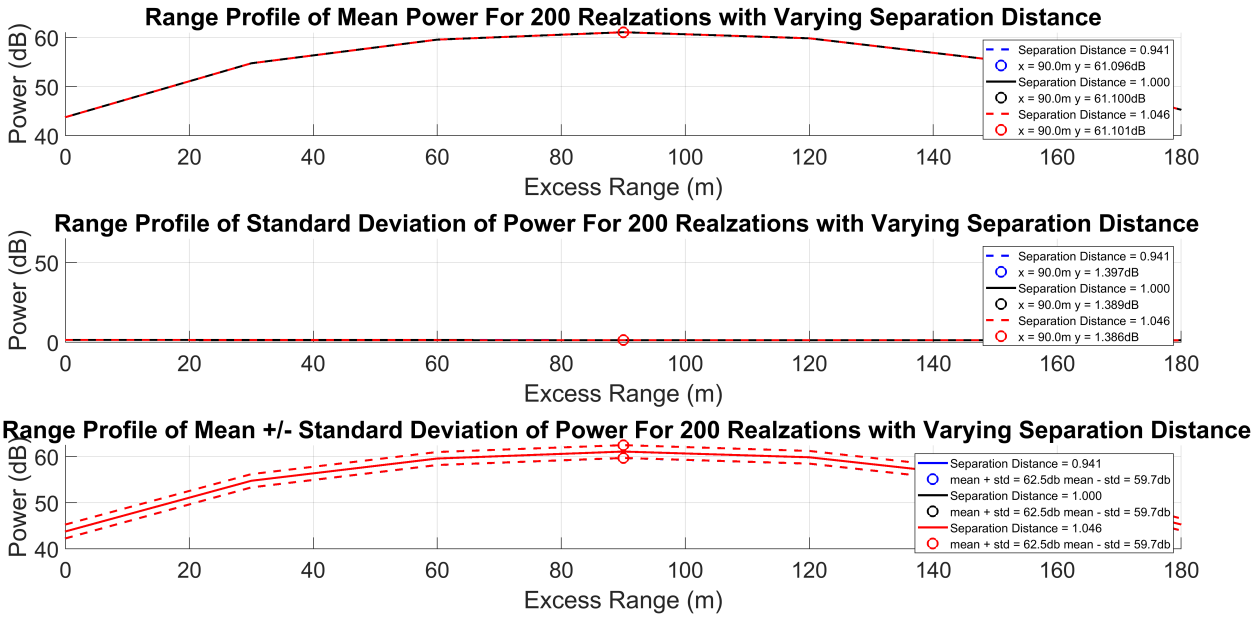

FIGURE 4.10. Diagram showing the mean, standard deviation and mean +/- the standard deviation of power for 200 realizations for varying separation distance and a mispointing at nominal.

As can be seen, the mean power for the threshold and ideal separation distances is approximately 61.1dB. Additionally, the standard deviation is approximately 1.4 dB for each separation distance, showing consistency in power returns. The mean +/- the standard deviation is plotted in Figure 4.10 The mean and standard deviation for all the separation distances tested were almost identical, leading to a plot that looks like only a single value.

The mean velocity and standard deviation is computed in the same way as for the ideal case and plotted in Figure 4.11. In the first plot in the figure, we can see that the mean of 200 realizations results in a velocity that approximately 0 m/s. While this does present good results, it only assumes the expected value of DPCAs performance over a large number of tries. To get a more accurate characterizations, we plot the standard deviation to show how

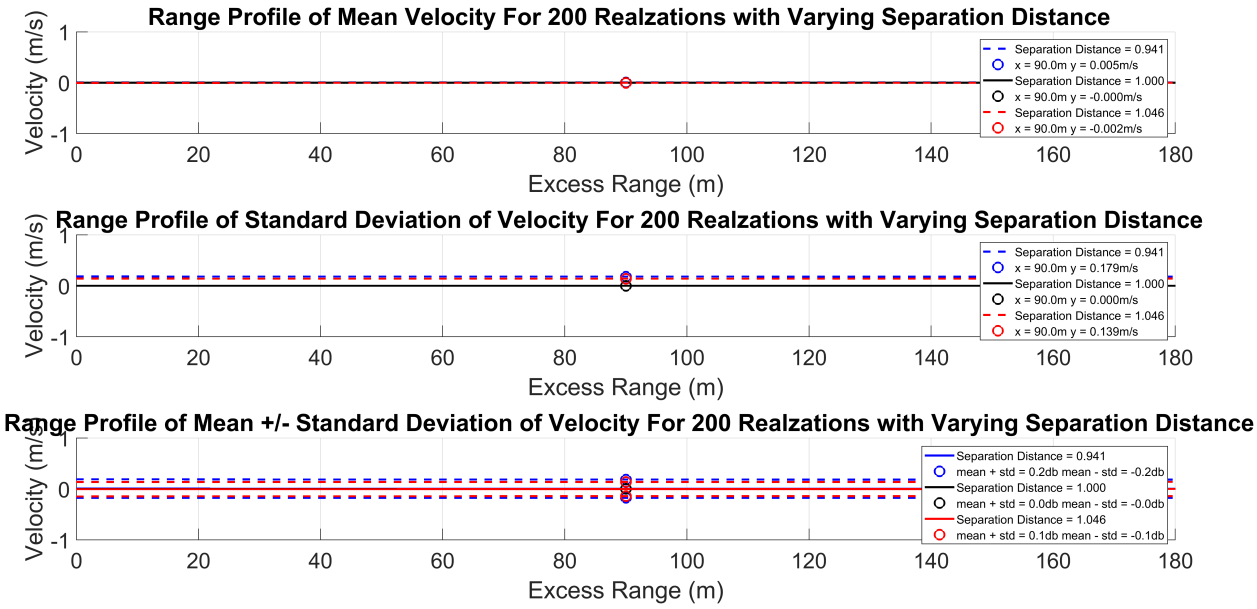

FIGURE 4.11. Diagram showing the mean, standard deviation and mean +/- the standard deviation of velocity for 200 realizations for varying separation distance and a mispointing at nominal.

separation distance can affect the return velocity in DPCA as can be seen in the second figure of Figure 4.11. The maximum deviation seen is actually 0.18m/s. The final characterization of its performance can be seen in Figure 4.11 As in the ideal case, the resulting velocity is exceptionally low, showing that the range in separation distance does not produce any substantial effects to the performance of DPCA.

Finally the mean spectrum width and standard deviation is computed in the same way as for the ideal case and plotted in Figure 4.12. The max of the mean spectrum width can be seen at around 1.28 m/s, which matches relatively closely to the spectrum width of 1 realization. Again, to further characterize, the standard deviation of the spectrum width is shown in the second figure of Figure 4.12. The max standard deviation can be seen as 0.34 m/s. To show the full effects of the variability of spectrum width, the mean +/- standard deviation is plotted in Figure 4.12 As mentioned before, the higher the spectrum width is,

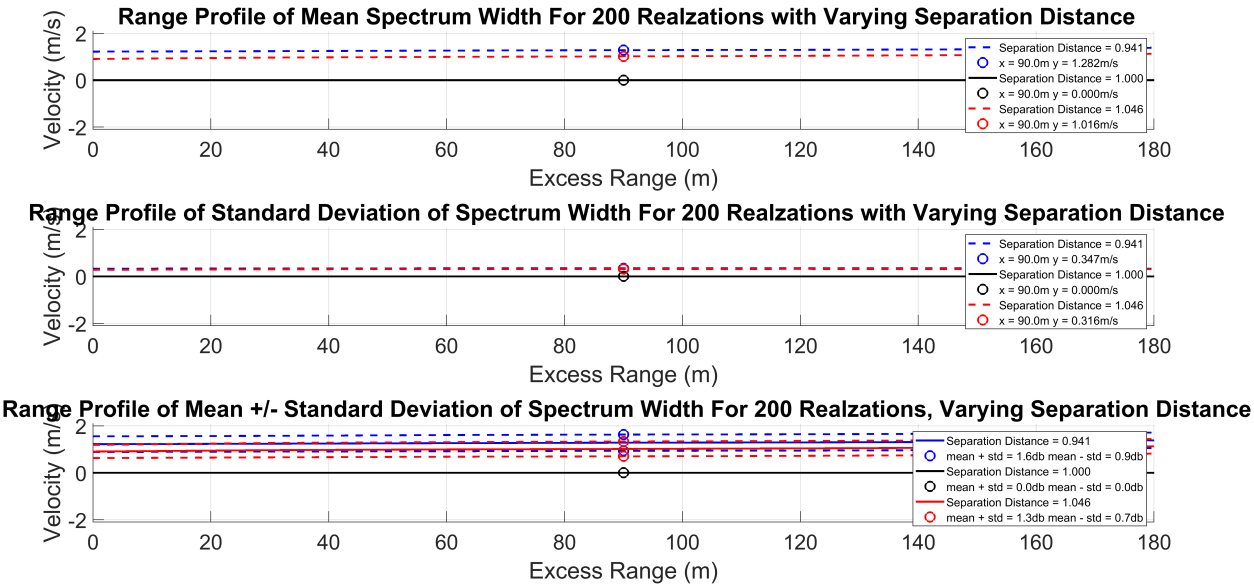

FIGURE 4.12. Diagram showing the mean and the standard deviation of spectrum width when only separation distance is varied over 200 realizations.

the larger the decorrelation between pulses is, resulting in a larger distribution of velocities. In this case, the max spectrum width is 1.629 m/s at 90m below the surface.

4.3. Characterizing Uncertainty Associated with Mispointing between Antennas

The next variable we characterize is the mis-pointing in the along track direction of the following antenna in relation to the leading antenna. When a mis-pointing happens, the transmit location between pulses is approximately in the same location, but the area being illuminated between pulses changes as shown in Figure 4.13.

To begin the analysis, we simulated the antenna at a pointing angle from -0.2 to 0.2 degrees from nadir or approximately half the beamwidth of the antenna. (the direction in which the leading antenna is pointing). This results in a maximum offset deviation of approximately 57% of the beamwidth for the notional radar configuration. Our first metric computed is power. The range profile of power should follow the same trend as the ideal case

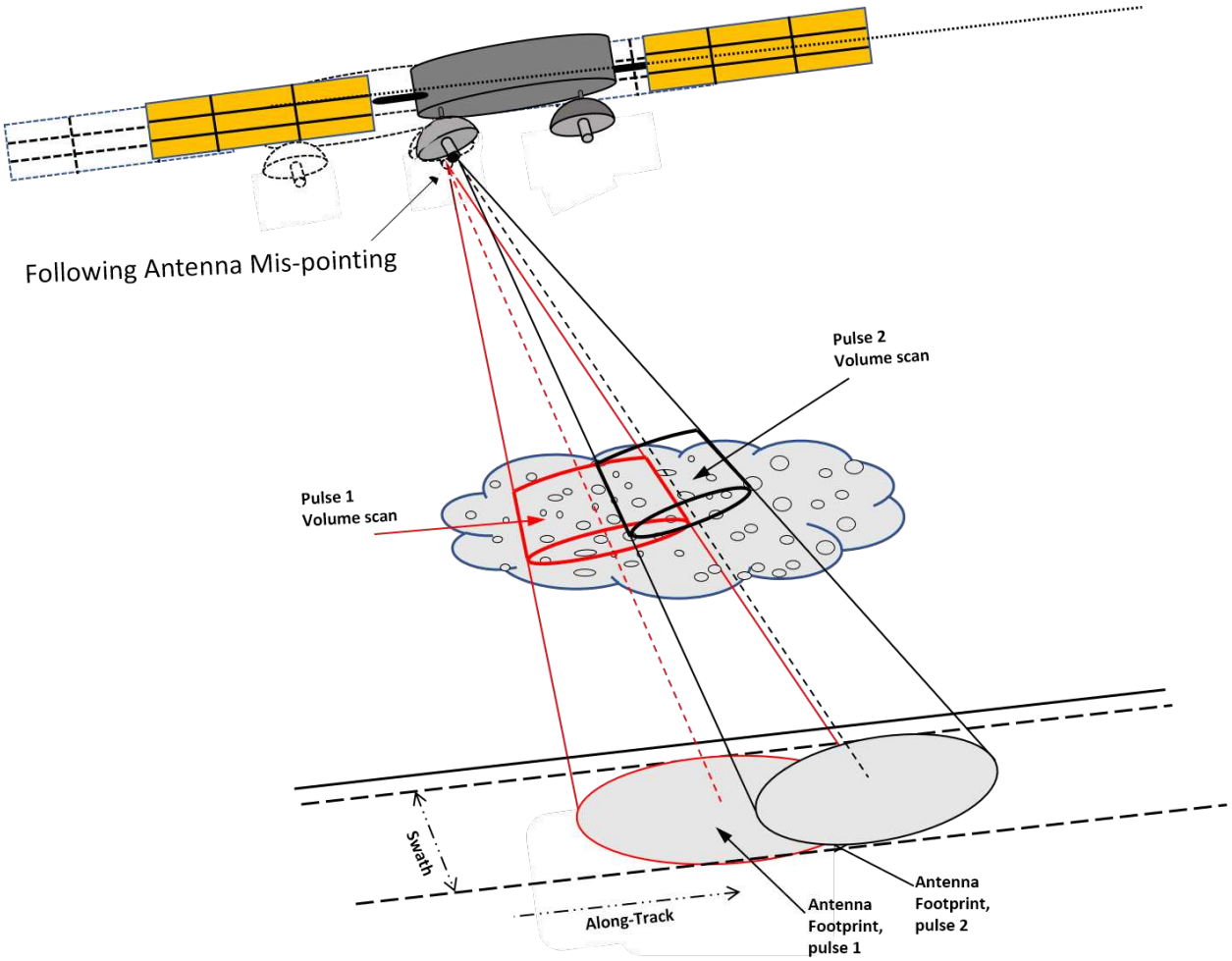

FIGURE 4.13. Diagram showing how mis-pointing between the antennas affects the volume scanned.

and for varying separation distance since the location of the scatterer has not changed. This mean that the max power should remain consistently at 90m below the closest distance to the surface for the duration of the simulation. To validate this, a range profile of power for the max, min and ideal case for mispointing are computed and plotted in Figure 4.14. As predicted, the power follows the same bell curve from previous analysis with a max power located at the 90m range gate. The Doppler velocity is plotted next. Looking at the second plot in Figure 4.14 90m below the surface, the effects can be seen as negligible, resulting in a max velocity of -0.055 m/s.

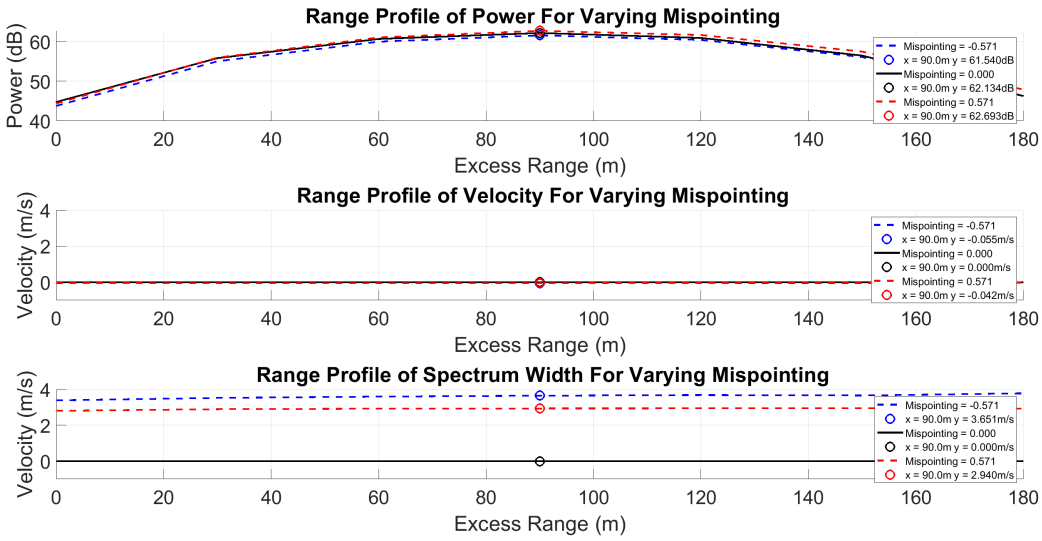

FIGURE 4.14. Diagram showing the power, velocity and spectrum width when mispointing is varied.

Next the spectrum width is plotted. Since a mispointing decorrelates the pulse pairs, we expect to see a marginal increase of the spectrum width at its max and min just like in the separation distance. This can be seen in the third figure of Figure 4.14.

As in separation distance, the spectrum width can be seen to increase as the mipointing angle error increases. Since the correlation between pulses is larger in the mispointing, the seen spectrum width is higher. Looking at the max and min values at 90m below the surface, the spectrum width can be seen at a max of 3.651 m/s.

Just like in the ideal case, different volume scatterers have the potential to change the performance of DPCA when varying the separation distance. To accommodate for this, DPCA was again simulated with varying separation for 200 realizations. The analysis follows the same as for the ideal case, with the mean, standard deviation, and the mean plus or minus the standard deviation being computed. While the location of max power should remain at 90m below the surface through each realization, we compute the mean and standard deviation to provide additional validation as shown in Figure 4.15 The mean power remains

consistent throughout the mispointing angles. The standard deviation shows a relatively consistent change, with a standard deviation of approximately 1.4 dB at 90m below the surfaceas shown in Figure 4.15.

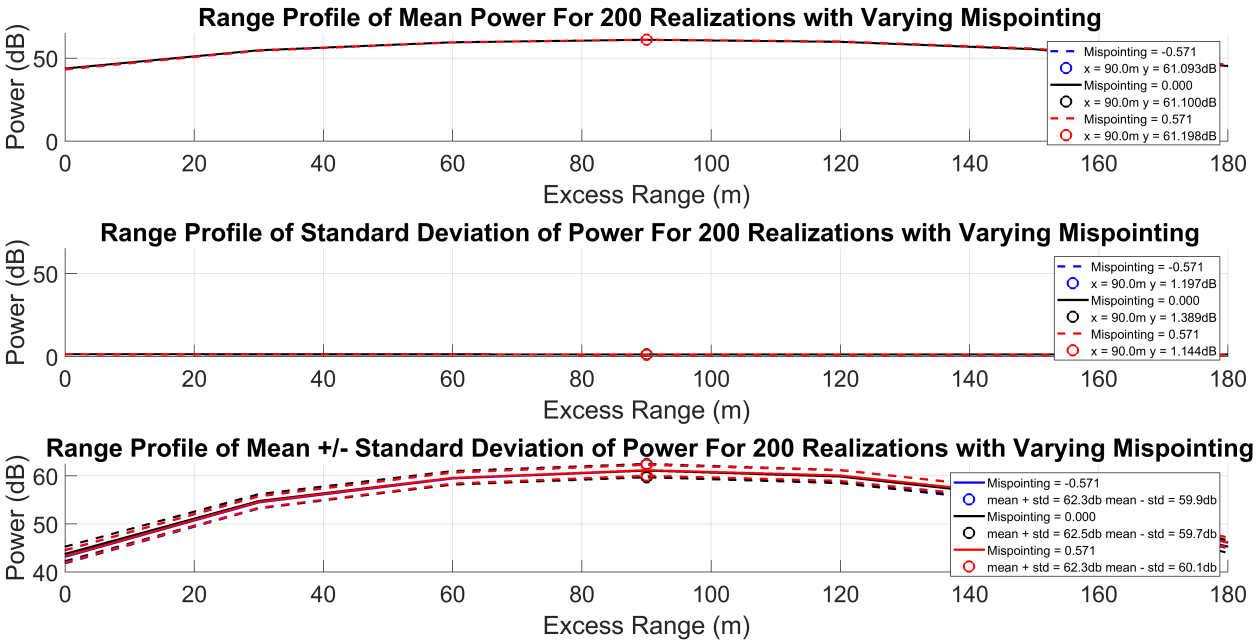

FIGURE 4.15. Diagram showing the standard deviation of power when only mispointing is varied over 200 realizations.

This follows logic since the scatterers can be more dense in certain areas leading to changes in the max power seen at 90m below the surface. Finally the mean plus or minus the standard deviation is shown in Figure 4.15 The mean and standard deviation for all the mispointing were almost identical.

The mean velocity is computed and plotted in the first figure in Figure 4.16. The max mean velocity can be seen as approximately 0 m/s while the standard deviation shows a variation of 0.157 m/s. As can be seen, the maximum deviation seen is actually 0.18m/s, leading to a maximum velocity of 0.18 m/s as seen in the figure.

Finally the mean and the standard deviation of spectrum width is compute and plotted as shown in Figure 4.17

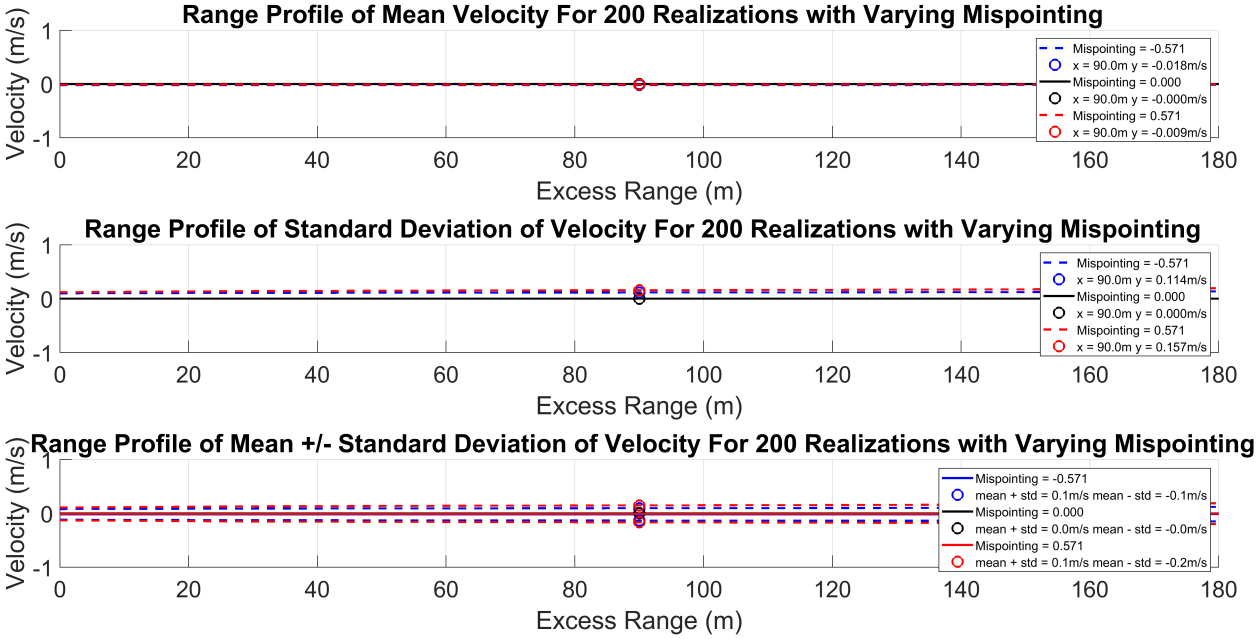

FIGURE 4.16. Diagram showing the mean velocity and the standard deviation of velocity when only mispointing angle is varied over 200 realizations.

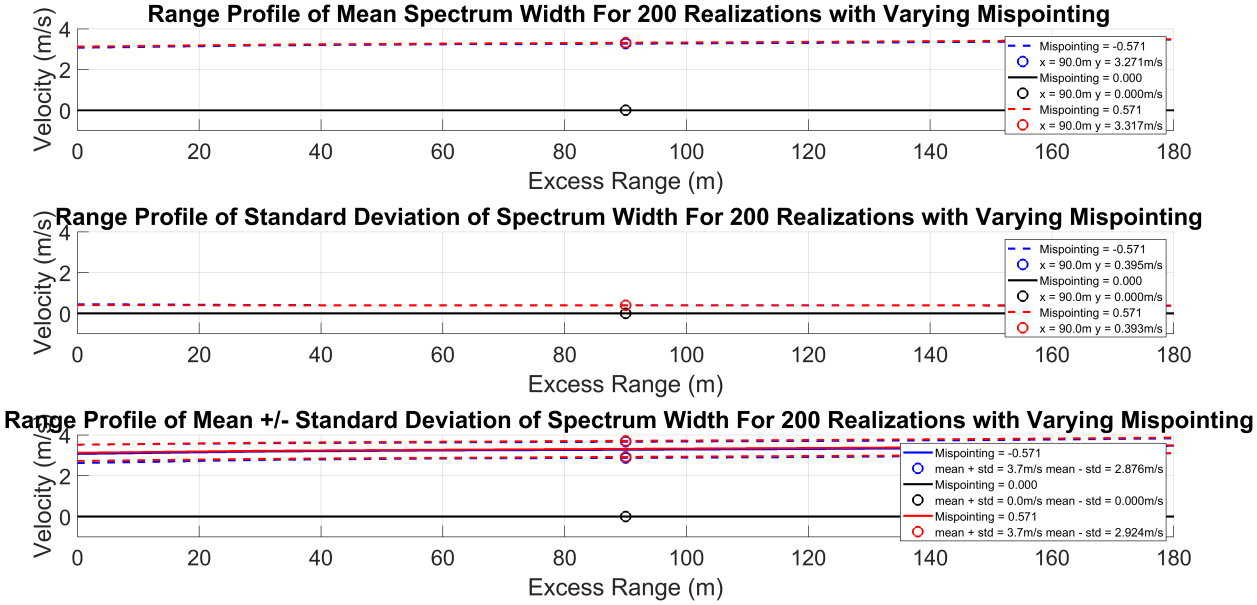

FIGURE 4.17. Diagram showing the mean and standard deviation of spectrum width when only mispointing is varied over 200 realizations.

The mean of the spectrum width show a lower velocity value then for a single realization. To see if this is accurate, the standard deviation is computed and plotted as shown in the second plot. As seen, the standard deviation of spectrum width is at approximately 0.4 m/s.

This results in a max spectrum width of 3.7 m/s. In a real implementation, the pointing angle would more than likely not have such a high degree of error after manufacturing, calibration, etc. Regardless, the characterization is still performed at a mispointing angle approximately half the size of the beamwidth.

4.4. Characterizing Uncertainty of Separation Distance and Mispointing Simultaneously

In a real life implementation of DPCA, there is a high likelihood that more than one sources of error will present itself at a given time. Due to this, it is necessary to characterize how a combination of separation error and mispointing error can affect the performance of DPCA. To do this, we simulate every combination of the 15 mispointing and 15 separation distance errors. In total, this resulted in 225 simulations per realization, or 45000 simulations for the 200 realizations.

To provide a more detailed and focused characterization of uncertainty on DPCA, the analysis will focus on computing the mean and standard deviations for each of the radar moments at the location of max power. As previously determined, the location of the max of the mean power for each of the realization can be observed at 90m below the surface as shown in Figure 4.18. Additionally, the changes in mean power as separation distances and mispointing varies remains relatively the same, with a value of approximately 61 dB as seen in (a) of Figure 4.19. The standard deviation for power follows a relatively consistent change of around 1 dB, varying by a small margin as the rear antenna offset error increases as show in (b). Therefore, all of our analysis will be obtained using the returns at 90m below the surface.

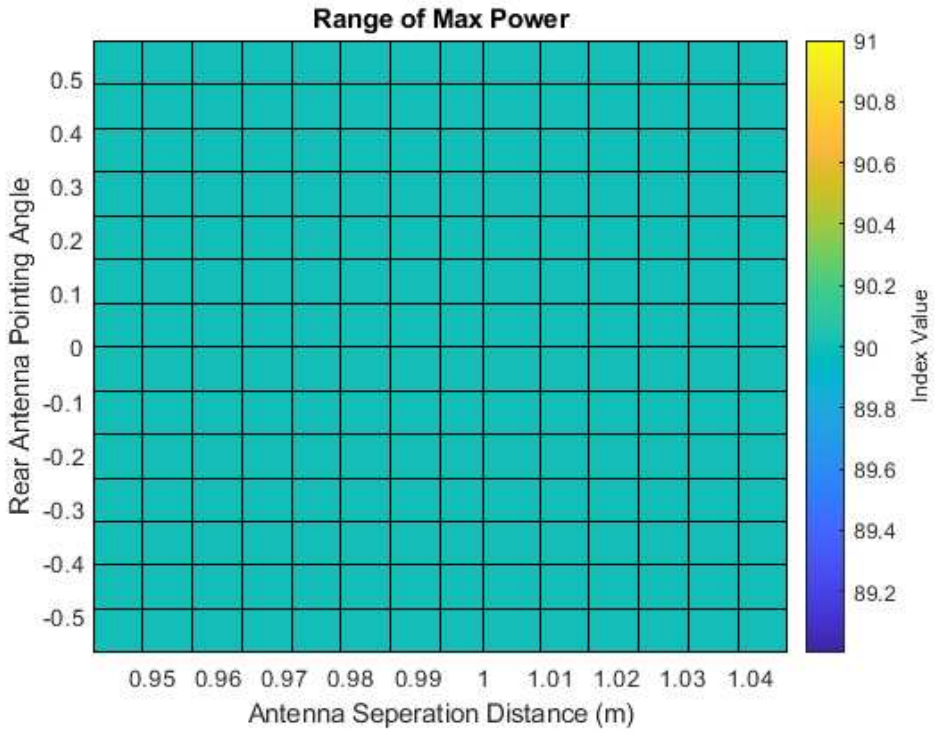

FIGURE 4.18. Diagram showing the location of max power for all the different separation distances and mispointings. As can be seen by the plot, all of the realizations are 90m below the surface (0m being the surface of the surface scatterer).

Figure 4.20 A shows a 3-D plot characterizing the mean velocity estimates from the 200 surfaces at the different antenna mispointings. At the ideal case we see a near zero velocity which aligns with expectations- the platform velocity is canceled using the DPCA technique. As the separation distance and antenna mis-alignment moves away from the ideal conditions, a bias in the mean velocity is observed. With these offsets, the vertical velocity profile begins to see some degradation in performance due to increased velocity uncertainties from the surface returns. But as can be seen, at the threshold cases of a separation distance deviation of approximately 1.05 from the nominal and rear antenna pointing offset of 0.5 of the beamwidth, the effect introduced result in a relatively low degradation of the velocities with a maximum vertical velocity bias of 0.8 m/s.

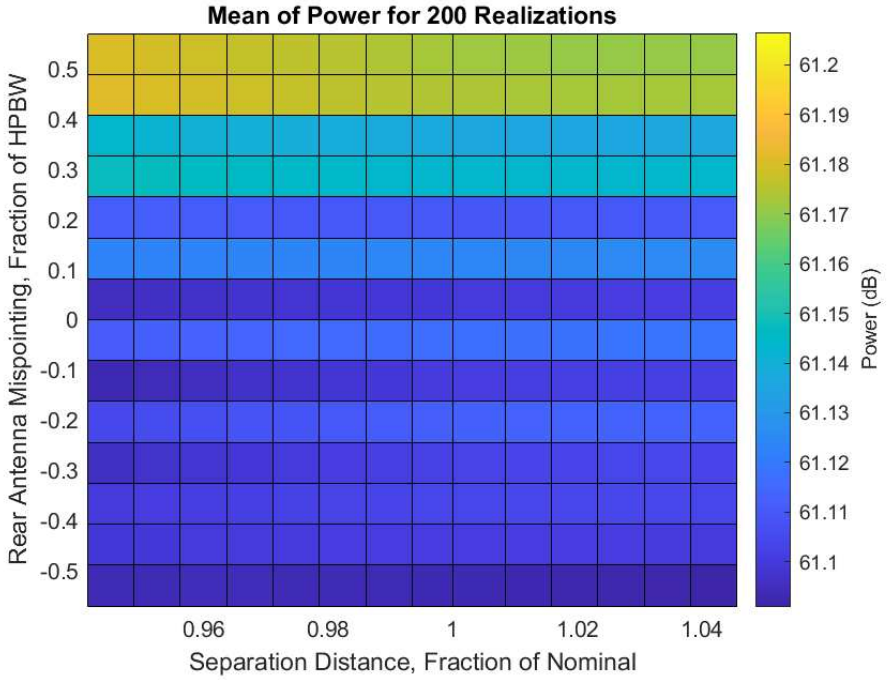

(A)

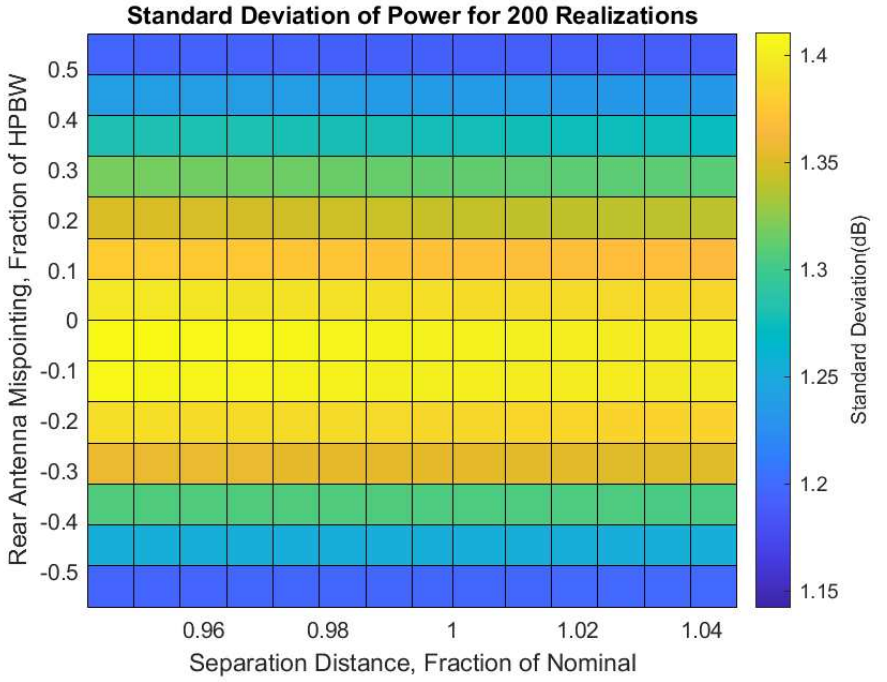

(B)

FIGURE 4.19. (A) Plot of the mean power for 200 Realizations with varying separation distance and mispointing.
(B) Plot of the standard deviation of mean power for 200 Realizations with varying separation distance and mispointing

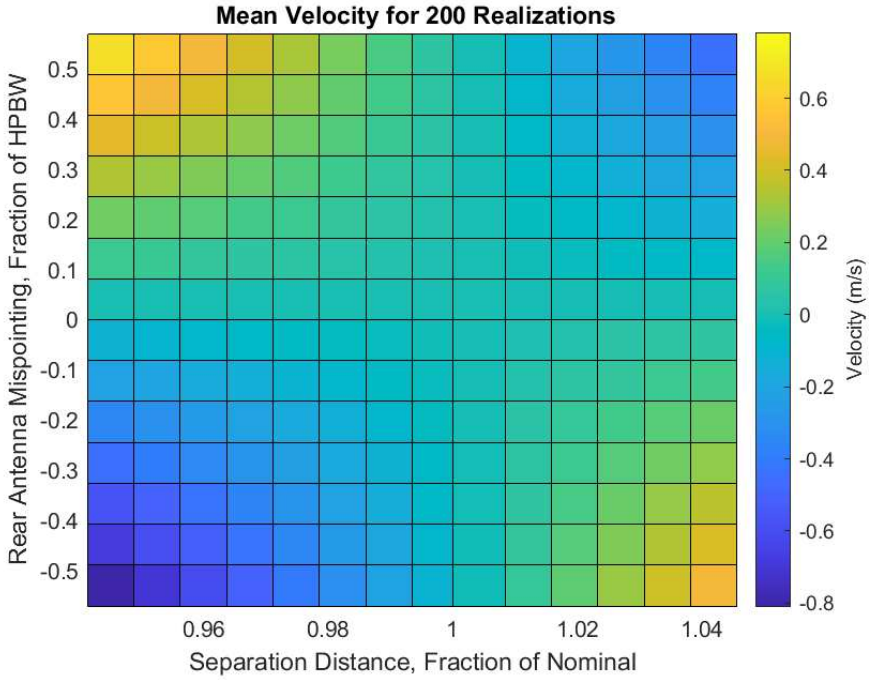

(A)

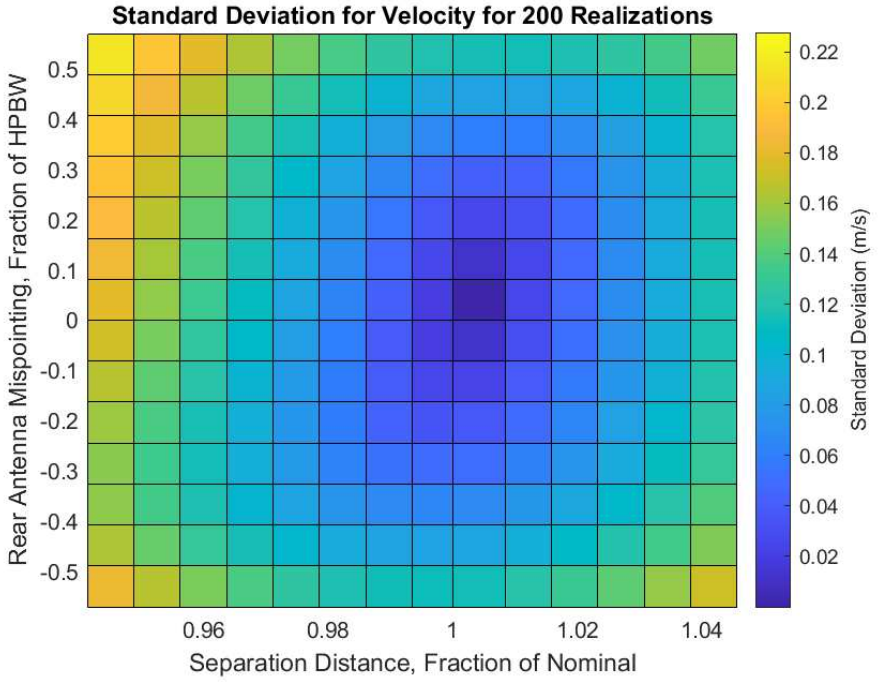

(B)

FIGURE 4.20. (A) Plot of the mean velocity for 200 Realizations with varying separation distance and mispointing.
(B) Plot of the standard deviation of velocity for 200 Realizations with varying separation distance and mispointing

To further evaluate the velocity estimator performance with DPCA, consider the standard deviation of the velocity estimate from the 200 surface realizations. The standard deviation measures the variation in the estimates among the realizations. From the plot of standard deviation for DPCA on Figure 4.20 B, the variance is the smallest at ideal conditions. As the misalignment between antennas diverges from the ideal case, there is an increase in the velocity estimate's standard deviation because the areas illuminated by the two antenna are increasingly different, resulting in higher levels of decorrelation between pulse pairs. If the antenna separation is also varied from the nominal, an extra velocity component due to spacecraft motion presents itself. Both of these effects lead to additional velocity estimation uncertainty which is consistent with a higher standard deviation of the velocity estimates. Even so, the standard deviations of the velocity estimates are relatively low, with the threshold cases resulting is a max standard deviation of 0.22 m/s.

By adding the standard deviation to the mean, we can characterize the expected range of velocity estimates. Consider the ideal and threshold cases for antenna separation distance and pointing misalignments to visualize the velocity estimate uncertainty in Figure 4.21. From these plots, our maximum velocities error is approximately 1 m/s for the worst case scenario.

The same analysis can be performed on the resulting spectrum width. Figure 4.22 A shows a 3-d plot characterizing the mean spectrum width for 200 surfaces as we vary the antenna from the nominal case. As the separation distance and mispointing deviate from the ideal case, we can see an increase of the spectrum width as the correlation between pulse pairs dwindles. At the threshold cases of a separation distance deviation of approximately 1.05 from the nominal and rear antenna mispointing of 0.5 of the beamwidth, the uncertainty results in a max mean spectrum width of around 3.9 m/s.

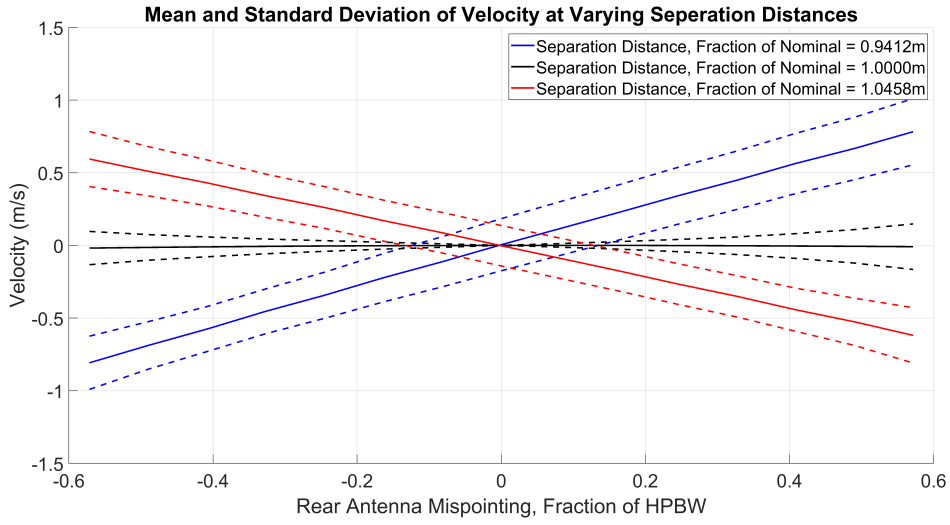

(A)

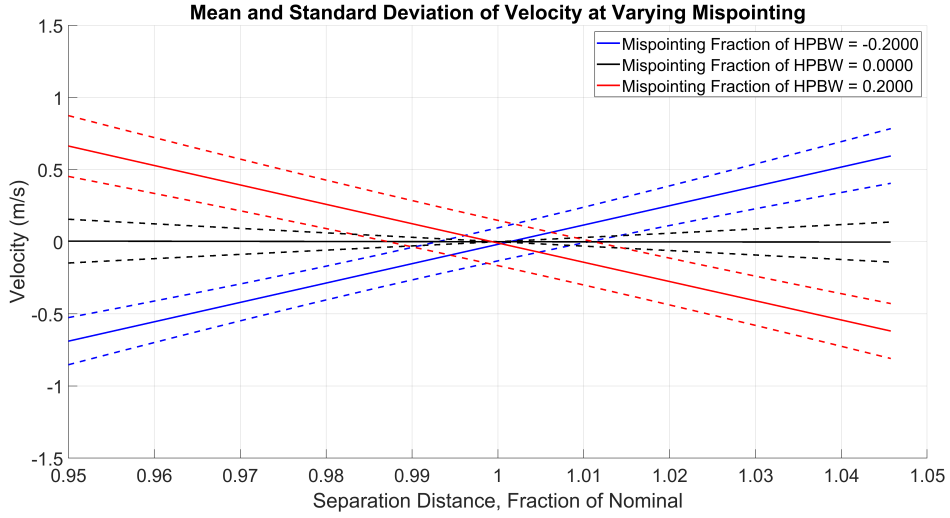

(B)

FIGURE 4.21. (A) Plot of the mean spectrum width for 200 Realizations with varying separation distance and mispointing.
(B) Plot of the standard deviation of spectrum width for 200 Realizations with varying separation distance and mispointing

To further calculate the uncertainty, the standard deviation is computed to measure the variance between realizations. From Figure 4.23 B, we can see that the standard deviation increases in the same pattern as the distribution of the mean spectrum width. From the plot of standard deviation for DPCA on Figure 4.23 B, the standard deviation is close to zero at ideal conditions. When the mispointing is held constantly at ideal and the separation

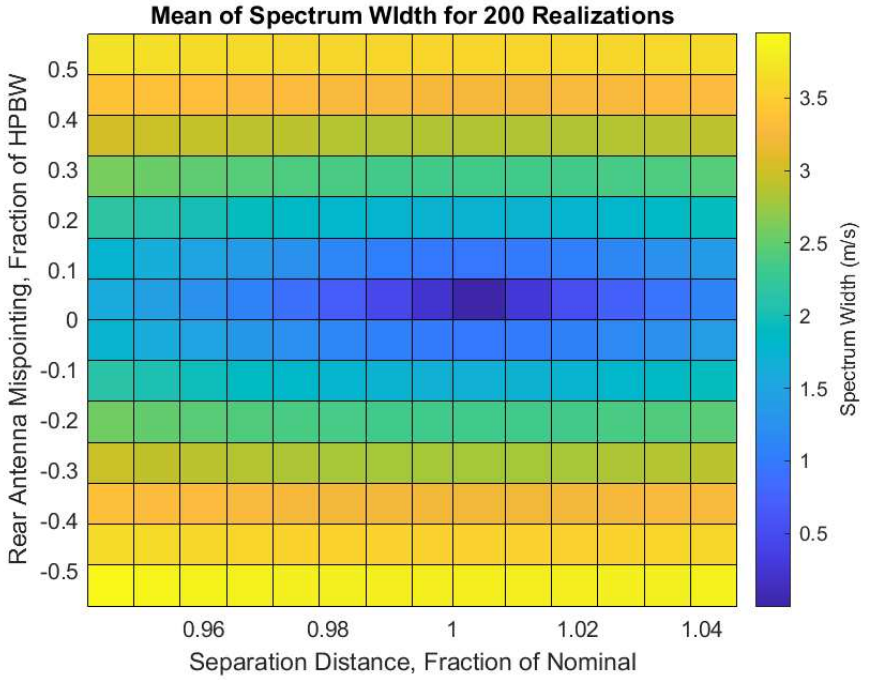

(A)

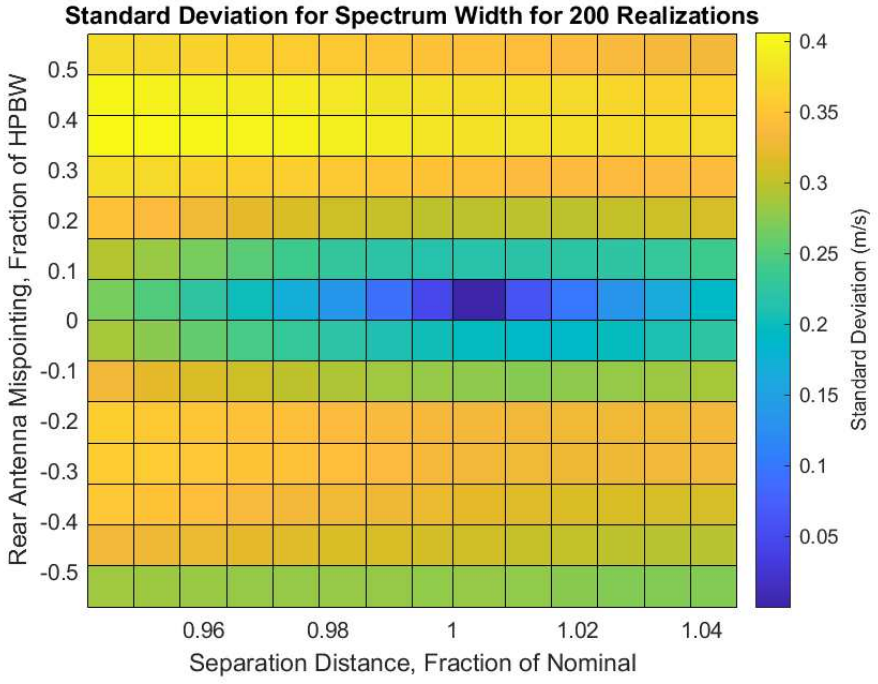

(B)

FIGURE 4.22. (A) Plot of the mean spectrum width for 200 Realizations with varying separation distance and mispointing.
(B) Plot of the standard deviation of spectrum width for 200 Realizations with varying separation distance and mispointing

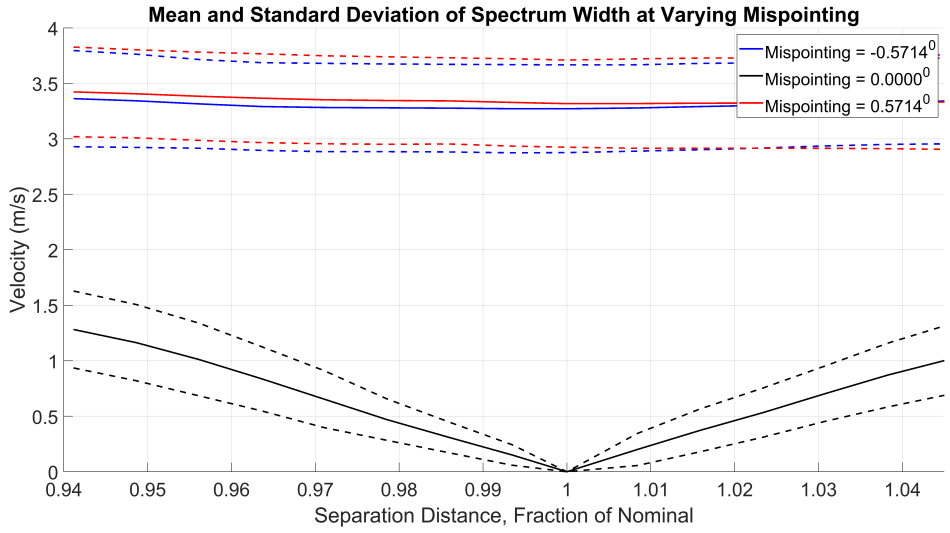

(A)

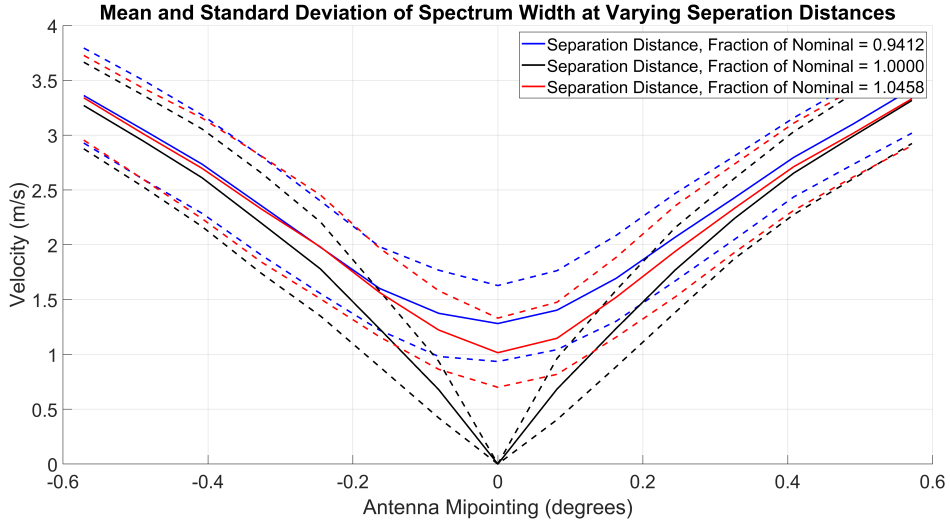

(B)

FIGURE 4.23. (A) Plot of the mean spectrum width for 200 Realizations with varying separation distance and mispointing.
(B) Plot of the standard deviation of spectrum width for 200 Realizations with varying separation distance and mispointing

distance is varied, we can see a less rapid change in the variance of the spectrum width as compared to a mispointing. This makes sense since the maximum mispointing error produces a larger decorrelation than the separation distance. For separation distance, when it is varied, an additional velocity component due to the spacecrafts forward motion resulting in more uncertainty in the distribution of velocities, leading to a broader spectrum. Even so,

the standard deviation is low, resulting in a max of 0.4 m/s. Adding the standard deviation to the mean gives us a more accurate characterization of DPCA when uncertainty from separation distance and a mispointing are introduced.

Just as in velocity, consider the ideal and threshold cases for antenna separation distance and pointing misalignments to visualize the spectrum width as shown in Figure 4.21. Looking at the ideal and threshold cases for antenna separation and mispointing, we can see that there is a maximum spectrum width of 3.8 m/s.

4.5. DPCA vs Single Antenna Case

Once the sources of error in a DCPA configuration are characterized, the next step is to compare it with a single antenna (used here a plausible best-case reference standard for single antenna Doppler measurements). The simulation for the single antenna case follows the same principle as for DPCA. We generate a surface with scatterers, calculate the returns at the receiver due to each scatter, and coherently sum the received signals. To remove any biases when comparing the two configurations, we simulated the models under the same conditions as DPCA, i.e. same PRF, frequency, orbital altitude, waveform, scatterer, etc, with the only difference being the antennas.

In DPCA, we are using an 1.6m long antenna at a beamwidth of 0.35deg at a frequency of 35.75GHz. For a single antenna, we chose an antenna that is around 5m in size, which is plausible for a spaceborne weather radar at LEO operating at 35.75 GHz. Since we are using the same frequency, the resulting beamwidth can be calculated at 0.112deg, or approximately a scaling of 3x the beamwidth of the antennas used for DPCA. With this, the simulation is ran using the same 200 volume scatterers that were used for DPCA.

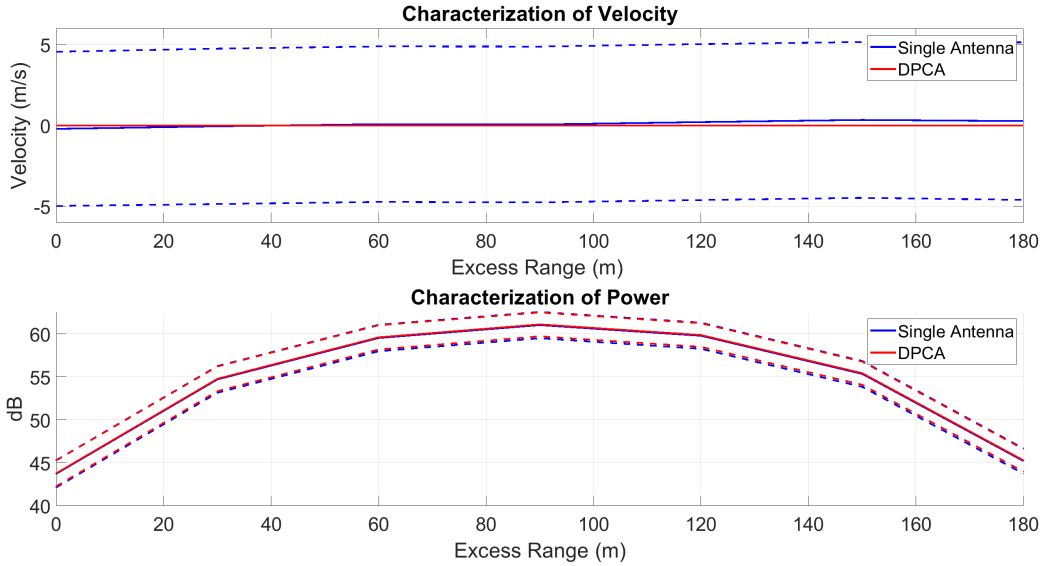

FIGURE 4.24. Doppler velocity of single Antenna vs DPCA performance at ideal DPCA configuration

In Figure 4.24, we show the velocity profile between both configurations using the ideal DPCA conditions. The plots for both single antenna and DPCA show the mean velocity with the standard deviation for 200 surface realizations. As can be seen by Figure 4.24, DPCA with ideal conditions, significantly outperforms the single antenna, with a Doppler velocity of 0 m/s. This Follows logic, since DPCA has a 0 m/s velocity when perfectly configured. In the case of a single antenna, the Doppler returns can be seen to deteriorate due to the forward velocity decorrelatinng the signal between pulse pairs. The max velocity can be seen at 2.5 m/s.

For a more realistic comparison between the two scenarios, the worst case scenario for a DPCA configuration is used (dual 1.6m antennas are separated by a deviation of 4.6% from the nominal case and antenna pointing mis-pointing at 40% of the beamwidth). Since a single antenna does not have to deal with the uncertainty introduced by DPCA, we will be comparing the worst case scenario of DPCA, with the same returns used when comparing to an ideal case. As can be seen in Figure 4.25 though, DPCA still outperforms the single

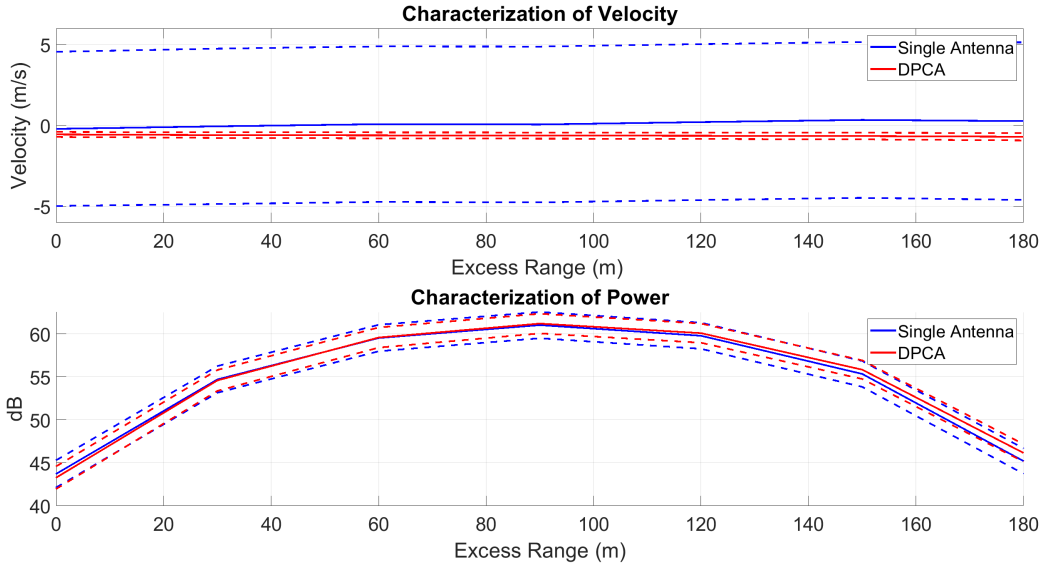

FIGURE 4.25. Doppler velocity of single antenna vs DPCA performance at worst case DPCA configuration

antenna case by a large margin. For the single antenna, a maximum velocity uncertainty of 2.5 m/s is estimated, while for DCPA, the maximum uncertainty is 0.8 m/s. Using the ACCP SATM Rev. E as a guideline [23] [24], it can be seen that a single antenna configuration does not meet vertical velocity uncertainty requirement of less than 2 m/s, while the DPCA configuration does by a large margin.

To continue with the anaylsis for DPCA and a single antenna system, the spectrum width for each are compared. High platform velocity is the predominant source or spectrum broadening in single antenna spaceborne weather radars. While single antennas greatly suffer from it, DPCA has the advantage of removing the apparent velocity (or substantially reduces it). Using the same analysis as before, the corresponding figures show the results of spectrum width for DPCA and a single antenna. Figure 4.26 shows the spectrum width of the 5m antenna and DPCA at its idea configuration. As mentioned previously, the pulse pairs in DPCA are correlated perfectly, resulting in a spectrum width of 0 m/s. As for a single

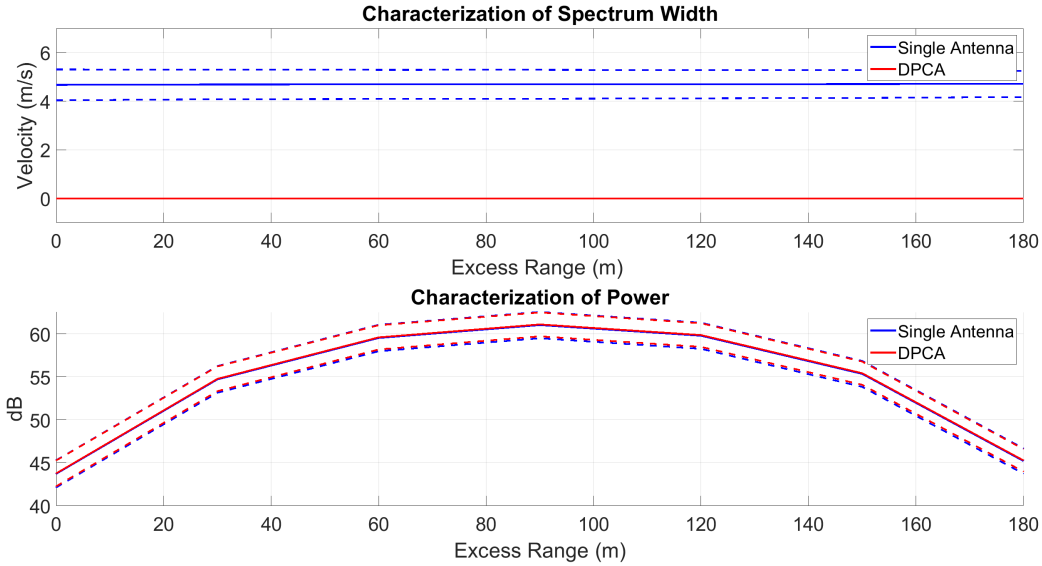

FIGURE 4.26. Spectrum width of Single Antenna vs DPCA at best case DPCA configuration

antenna systems, the spectrum width is shown to suffer greatly in performance, resulting in a max spectrum width of 5.6 m/s. This can be seen Figure 4.27

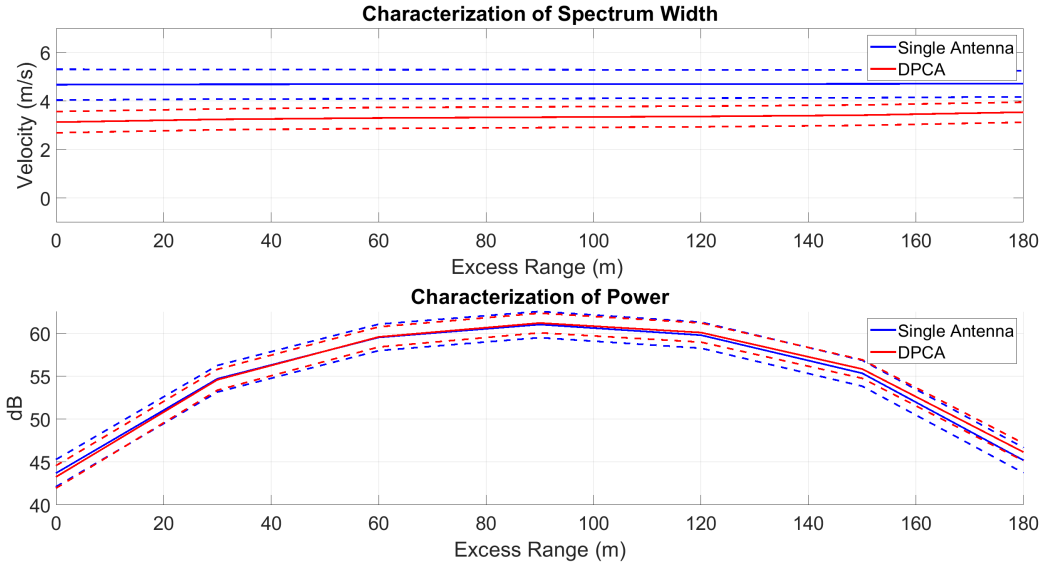

FIGURE 4.27. Spectrum width of Single Antenna vs DPCA at worst case DPCA configuration

To show a more accurate representation of DPCA, the spectrum width at its least ideal is computed and plotted as can be seen in Figure 4.27 While the spectrum width does seem to increase, the resulting value for spectrum width can be seen at around 3.8 m/s. As for the single antenna case, a spectrum width of 5.7 m/s, which is significantly higher

Though DPCA does have added uncertainty due to the antennas, it still seems to outperform a single antenna configuration. For the single antenna case to produce better results, it would be neccessary to increase the size of the antenna, but, this again, would never resolve the main issue resulting in spectrum broadening, which is the high platform velocity while in orbit in space.

4.6. Summary

In this section, we characterized the uncertainty of DPCA resulting from the antennas. As opposed to a single antenna, DPCA has two antennas, resulting in possible error coming from the spacing and mispointing between the antennas. If the antennas are properly configured the radar will appear to not be moving between transmit pulses. Since we are using a static scatterer, this means the resulting Doppler velocity will converge to 0 m/s. But, in a real life scenario, there is always some amount of error that presents itself. By varying the mispointing and separation distance between the antennas, we can characterize the two largest sources of error, to better see how DPCA performs at the worst possible case. From the analysis, we were able to show that DPCA performs significantly better than a single antenna system and fall well under the ACCP requirement of a velocity less than 2 m/s.

CHAPTER 5

Effects of Non-Uniform Beam-Filling

To simplify the analysis of rainfall cases, it is assumed that the distribution of scatterers will be uniform inside a resolution value. This is referred to as uniform beamfilling. As such, the previous chapter focused its analysis on discussing and characterizing the effects that antenna misalignment has on the performance of DPCA when using a uniformly distributed scatterer volume. In this instance, we constructed a scatterer volume that was horizontally uniform over a range of approximately 4km to encapsulate the entirety of the antennas footprint. While this analysis is representative of a homogeneous rain event, it will not hold for convective rain events where the distribution of rain is not homogeneous [25]. In these cases, gradients in the radars reflectivity are presented in the radar footprint as can be seen in the diagram on Figure 5.1. This phenomenon is known as Non-uniform beamfill ($NUBF$).

In Doppler spaceborne weather radars, the non-uniformity within the scatterer volume will weigh the frequency shift differently due to the high platform velocity, resulting in a distorted Doppler spectrum. This will then lead to a reduction in accuracy when computing the vertical Doppler velocity of the scatterer volume [25]. While NUBF presents a challenge to accuracy of Doppler velocity estimates for single antenna spaceborne weather radars, DPCA presents a a solution to minimize or even eliminate velocity estimation bias due to its two antenna system. Since DCPA results in an apparent cancellation of the platform velocity due to the high correlation between pulses, the performance of DPCA should not degrade when NUBF is present.

In this chapter we will show how non-uniform beamfilling affects the performance of DPCA. Like the previous chapter, we will characterize the effects uncertainty has on DPCA

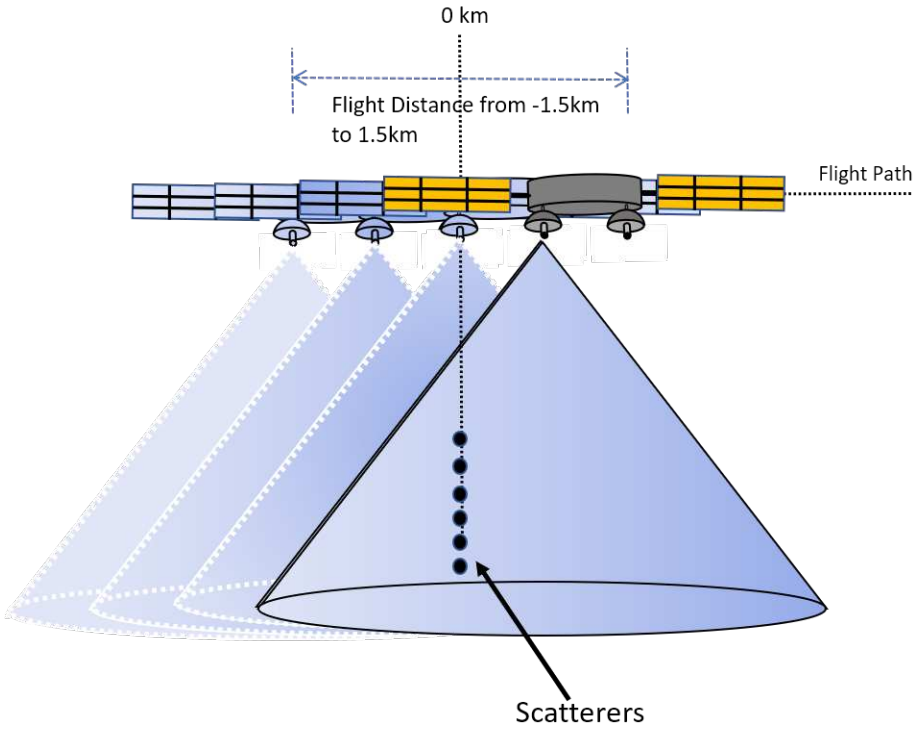

FIGURE 5.1. Example diagram of NUBF while scanning using DPCA.

under inhomogeneous distributions of scatterers within the radar's observation volume. Additionally, to provide a baseline comparison, we will simulate NUBF on a single antenna system and provide a comprehensive comparison between the performance of the two configurations.

5.1. Simulating Non-Uniform Beamfilling

Simulating NUBF can be achieved by a volume of scatterers that is distributed non-uniformly in the along track direction. In the case of our simulation, the radar footprint is approximately 3km for DPCA (1.9m antenna) and 880m for a single antenna (5m antenna), meaning that we needed a to create a scatterer volume that was smaller than 880m in the along track. To accomplish this, we created two different volumes: a single point scatterer

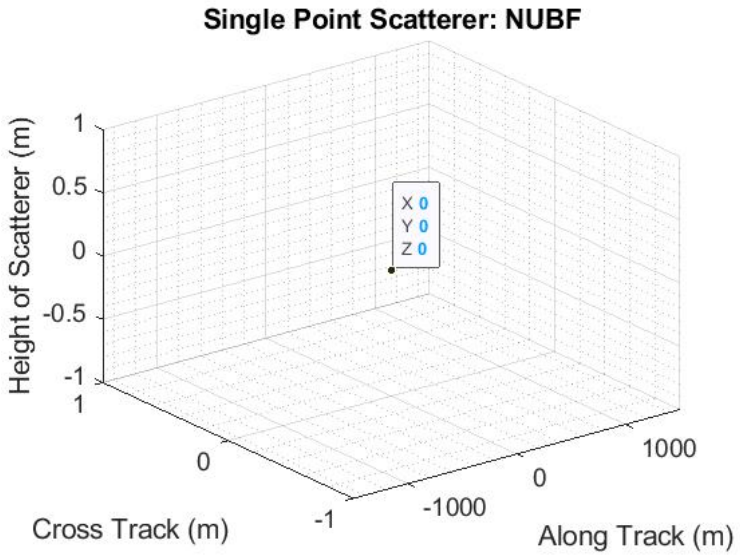

(A)

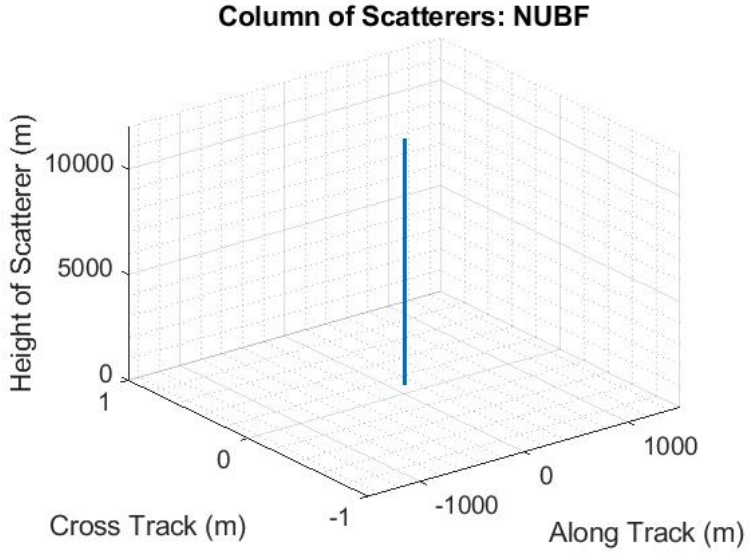

(B)

FIGURE 5.2. (A) Plot of the single point scatterer used to simulate NUBF. (B) Plot of the column of scatterers used to simulate NUBF

and a vertical column of scatterers, both with a size of 1m in the along track and cross track direction and with a velocity of 0 m/s as can be seen in Figure 5.2.

After creating the scatterer plane, the simulation was set up to have the same radar parameters as in Chapter 4 to remain consistent throughout the experiments (100 pulses, PRT of 250us, platform velocity of 7650 m/s, etc). We then ran the simulation and flew the

platform from -1.5km to 1.5km in the along-track direction, with 0 m being the center point, where the point scatterer and column of scatterers are located. By having the scatterer in the middle of the simulation, we can see the effects of NUBF as we move the radar towards and away from the volume. In total, this resulted in about 32 simulated along-track positions for both DPCA and a single antenna.

After completing the simulation, the return voltages are used to calculate the radar moments of interest to characterize its performance.. Just as in Chapter 4, we compute power, Doppler velocity and spectrum width as our metrics for characterizing DPCA under NUBF. For this analysis, the velocity and spectrum width will refer to the mean of the 100 pulses per scan.

The next section focuses on showing the performance of DPCA with NUBF. Here we will show how DPCA performs in comparison to a single antenna case by using a single point scatterer and a column of scatterers as our volume. Additionally, this chapter will show how DPCA performs under uncertainty from the antennas, similar to the analysis done in Chapter 4.

5.2. Non-Uniform Beamfilling results: Single Point Scatterer

The first test case in simulating NUBF for DPCA and a single antenna is a volume that consists of single point scatterer. A single point scatterer is the best non-homogeneous field to use for initial testing of the performance of DPCA due to its simplicity. Since there is only one scatterer, there will only be its contribution to the measured. While the spectrum width cannot be computed since there is only 1 scatterer with a velocity contribution in the volume, we can still see how the Doppler velocity is affected.

To begin we simulate the single antenna case to provide us our baseline. As before, we compute the power and velocity using the equations described in Chapter 2 and 4. Since a single antenna has a large forward velocity contribution, the correlation between pulse pairs is low. As shown in the previous chapter, this resulted in a large degradation of accuracy in our Doppler estimates. In the case of NUBF, the forward velocity even further degrades the performance as the weighting of the frequency shift for the point scattterer differs as can be seen in the first plot in Figure 5.3. The velocity profile can be seen to vary between the

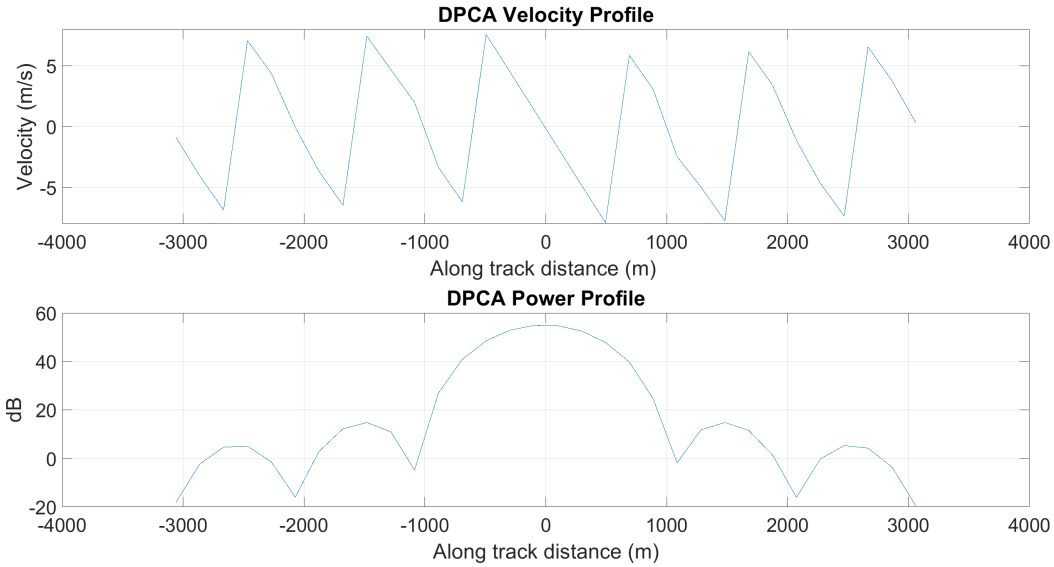

FIGURE 5.3. The figure shows the results from a single antenna system simulated using 1 point scatterer located at 0m. The top plot shows the mean Doppler velocity profile while the bottom plot shows the mean power.

unambiguous velocity of the radar between -7 m/s and 7m/s with a 0 m/s velocity as the spacecraft flies directly above the scatterer. The power as shown in the second plot increases as we move towards the scatterer and decreases in the same fashion as it flies away from it. As shown by the plot, the single antenna case performs quite poorly under NUBF conditions as compared to the uniform beamfilling. With this, we have our baseline to compare DPCA with.

Next DPCA is simulated at ideal conditions (A separation of 1.9125m between the leading and following antenna, and both antennas pointing at nadir). The largest contribution of error in measured scatterer velocity, as can be seen by the single antenna case, is the platform velocity. Since DPCA removes the apparent spacecraft velocity due to its high correlation between pulses, the effects of NUBF should be minimal. This means that for the duration of the flight, we should see a near 0 m/s Doppler velocity. Additionally, we should see a steady increase in power as we approach the scatterer and a steady decrease as we move away from it. The peak power should also be seen at the point in which the spacecraft is right above the scatterer. To demonstrate this, we simulate DPCA at ideal antenna conditions, and calculate the power and velocity as can be seen in Figure 5.3. As expected, the Doppler

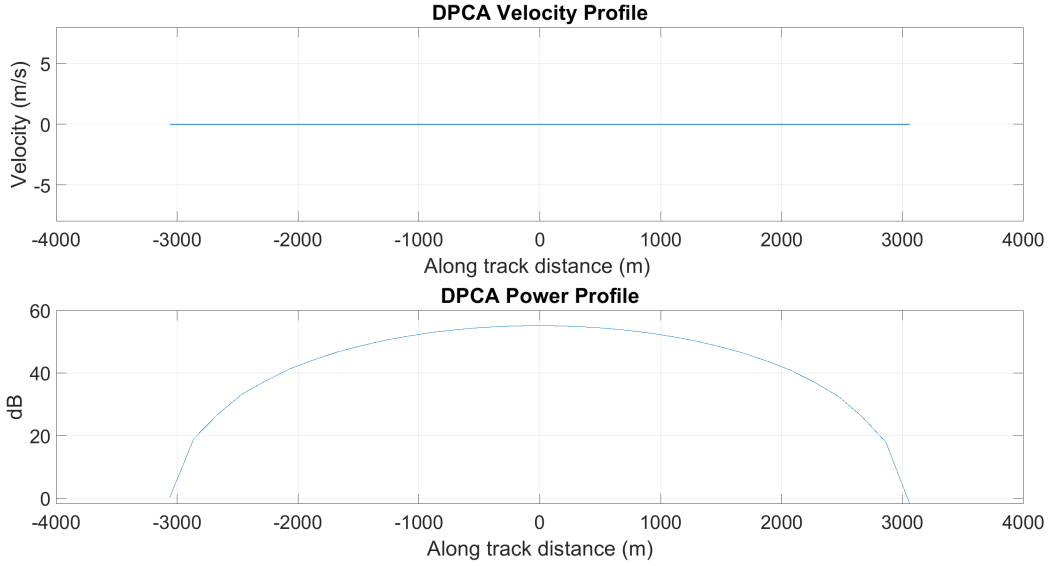

FIGURE 5.4. The figure shows the results from DPCA simulated using 1 point scatterer located at 0m. The top plot shows the mean Doppler velocity profile while the bottom plot shows the mean power.

velocity for DPCA remained consistently at 0 m/s for the duration of the flight. The power, as shown by the second plot in Figure 5.4, also follows expectation resulting in a symmetrical increase and decrease of power as we fly across the scatterer.

To further our proof of DPCAs advantage over a single antenna case, we simulate DPCA with uncertainty. As in Chapter 4, we vary our separation distance between 93% to 1.045% of the nominal and our rear antenna mispointing angle by about half a fraction of the the HPBW. As expected, the Doppler velocity estimates reduce in accuracy as we vary the separation distance towards its corner case as can be seen from the first plots in Figure 5.5 For a separation distance of 1.045 of the nominal, and a mispointing of +/- 57% of the

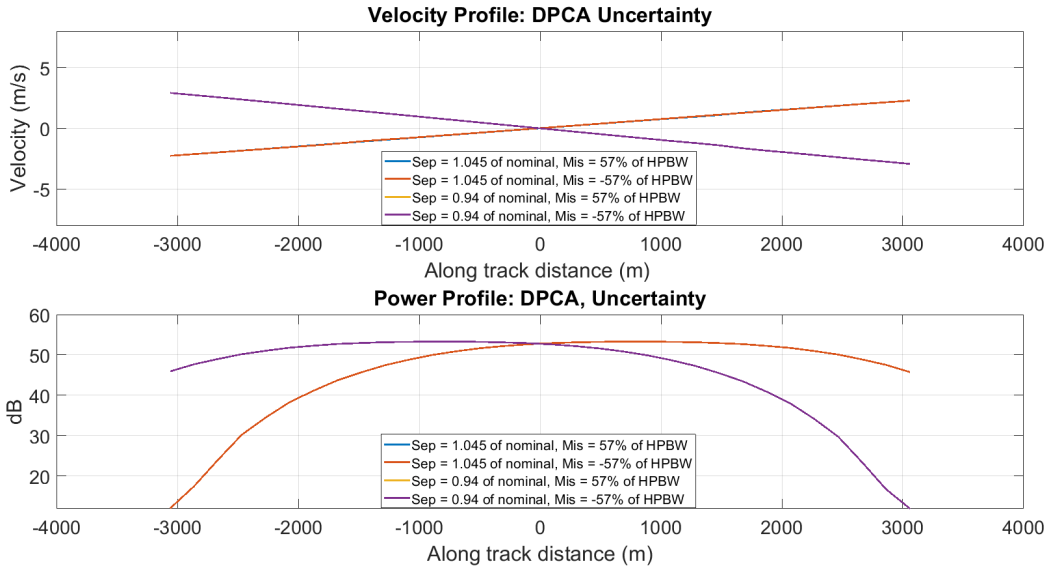

FIGURE 5.5. The figure shows the results of DPCA with uncertainty using 1 point scatterer located at 0m. The top plot shows the mean Doppler velocity profile while the bottom plot shows the mean power. The separation distance is expressed as a ration of the nominal while the antenna mispointing is represented as a fraction of the HPBW.

HPBW, we can see a linear increase in the velocity through the duration of the flight. For a separation distance of 0.94 of the nominal, and a mispointing of +/- 57% of the HPBW, we can see a linear decrease through the duration of the flight. This follows reason since as we increase the separation distance from nominal, the location at which antenna 2 transmits happens before the location at which antenna 1 transmits. In other words, the velocity change of the scatterer as seen between pulses should be negative before we fly over the

scatterer and positive as we fly past the scatterer. The inverse logic can be applied to the separation distance that is 0.94 of the nominal. The contribution of the mispointing can be seen as much smaller than the effects of separation distance. This makes sense since the effects of platform velocity impact the Doppler estimates significantly more in NUBF as can be seen by comparing the Doppler velocity of a single antenna scanning a uniform volume vs a non-uniform volume. If the antenna separation is off from nominal, than an apparent platform velocity will be introduced into DPCA. It will not be as significant as for a single antenna, but enough to reduce the accuracy of the Doppler measurements. With that being said though, the Doppler estimates for DPCA still greatly outperform a single antenna system.

The power on the other hand, can be seen to change as we mispoint the following antenna. As we point the antenna forward, the power is higher at the start of the flight as compared to the end as seen in the second plot in Figure 5.5. This makes sense since to the positive angle results in the antenna illuminating the scatterer closer to its boresight before being directly over the scatterer. As it passes it though, it illuminates less of the scatterer as would a nadir pointing antenna. The inverse logic can be applied to a mispointing of -57% of the HPBW.

As mentioned above, DPCA greatly outperforms a single antenna when computing our Doppler estimates. In a single antenna, we are seeing Doppler velocities of up to 7 m/s, while in DPCA at its worst, we are seeing a max Doppler velocity of 3 m/s. The next section expands on NUBF and shows how DPCA and a single antenna perform when a column of scatterers are used to simulate NUBF.

5.3. Non-Uniform Beamfilling results: Column of Scatterer

To further show the performance of DPCA when NUBF is present, we simulated DPCA and a single antenna with a column of static scatterers located at 0m in the along track and cross track direction, and spanning from 500m to 10km in the horizontal direction. The volume can be seen in plot B of Figure 5.2. Since there is more than one scatterer present in the volume, we are able to show how NUBF affects the Doppler velocity and the velocity spectrum.

As before, we simulated the single antenna case using a column of scatterers to provide a baseline comparison. Again, since the platform velocity is so high in the single antenna case, we expect to see a high Doppler velocity as well as a large spectrum as can be seen in Figure 5.6. As can be seen, the resulting radar moments are noisy, producing unreliable

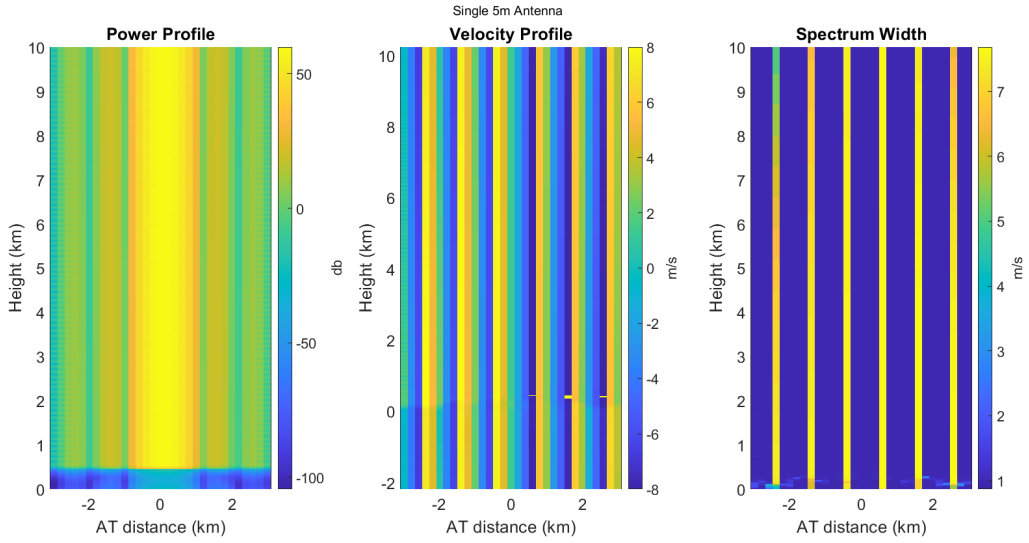

Figure 5.6. The figure shows the results of a single antenna using a column of scatterer located at 0m in the along track direction. The left plot shows the power, the middle plot shows Doppler velocity while the right most plot shows the spectrum width.

returns for the power, velocity and spectrum width.

Next DPCA is simulated at ideal conditions. As mentioned before, DPCA at its ideal configuration result in a near perfect correlation between pulses. This in turn removes the platform velocity contribution, which should result in a Doppler velocity and spectrum of 0 m/s. To test this out, we computed the power, Doppler velocity and Spectrum width using the return voltages after simulating DPCA. As can be seen by Figure 5.7, the velocity and spectrum width converge to 0 m/s. To further prove the viability of DPCA to providing

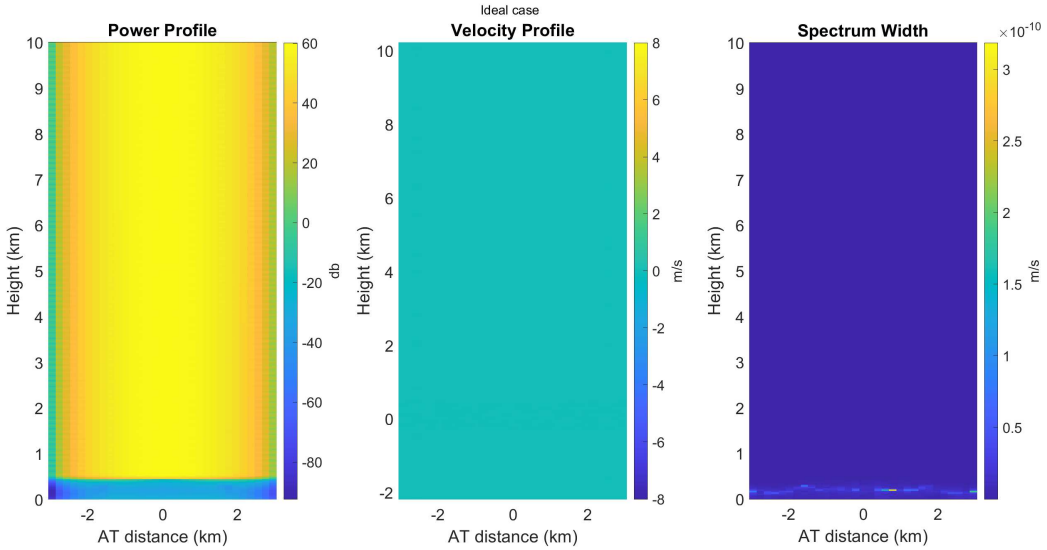

FIGURE 5.7. The figure shows the results of DPCA at ideal using a column of scatterer located at 0m in the along track direction. The left plot shows the power, the middle plot shows Doppler velocity while the right most plot shows the spectrum width.

accurate Doppler measurements under NUBF, we added the possible uncertainty from the antennas. Just as in the single scatterer simulation, we are varying the antenna separation distance and mispointing. To provide a better visual representation of the results, only the corner cases are shown as they provide the worst possible performance of DPCA. To begin, Figure 5.8 shows how DPCA performs when the separation distances is 1.04 of the nominal and the mispointing is +/-57% of the HPBW. As can be seen, the velocity seems to degrade in a similar manner as seen in the single point scatterer case. Since the separation distance

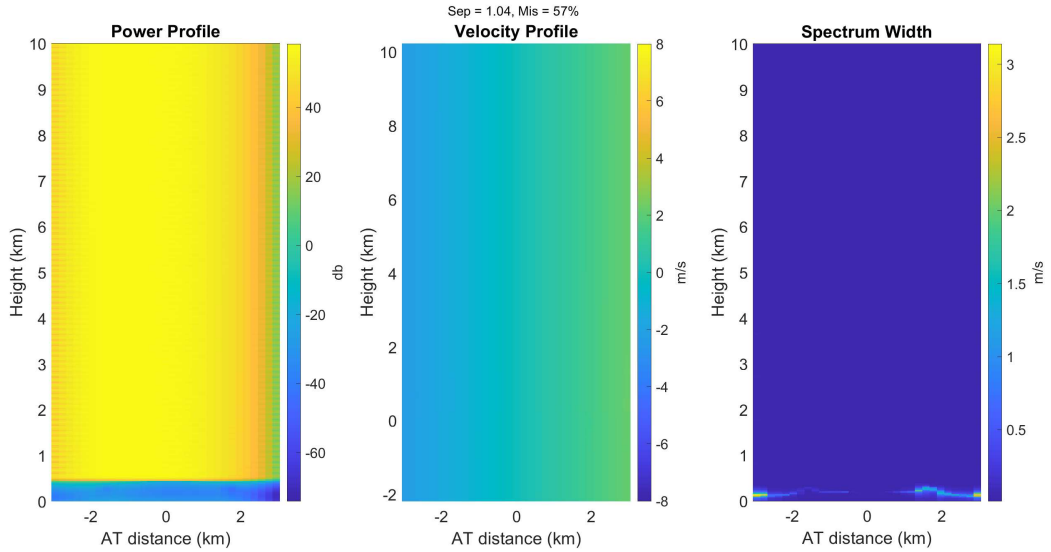

(A)

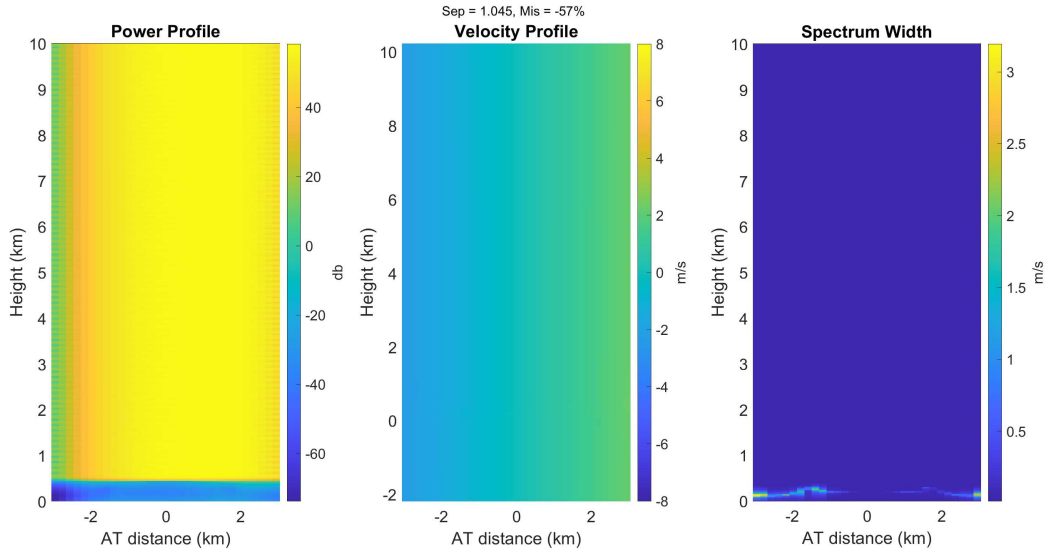

(B)

FIGURE 5.8. (A) Shows the power, velocity and spectrum width when DPCA is at a separation distance of 1.04 of the nominal and a mispointing of 57% of the HPBW.
(B) Shows the power, velocity and spectrum width when DPCA is at a separation distance of 1.04 of the nominal and a mispointing of -57% of the HPBW.

is greater than the ideal, the velocity should increase as it flies towards and away from the column of scatter. The spectrum width converges to 0 m/s.

Figure 5.9 shows how DPCA performs when the separation distances is 0.94 of the nominal and the mispointing is +/-57% of the HPBW. As can be seen, the velocity also seems to follow a similar trend to that of the single point scatterer. Since the separation distance is less than the ideal, the velocity should decrease as it flies towards and away from the column of scatter. The spectrum width converges to 0 m/s.

As can be seen by the analysis presented in this section, DPCA outperforms the single antenna case by a large margin. In the single antenna, we are seeing a max velocity of 8 m/s, while in DPCA we are seeing a max velocity of 3 m/s using its most unideal antenna configuration of a mispointing of 57% of the HPBW and a separation distance of 0.94 or 1.04 of the ideal. Overall, DPCA show promise for accurately measuring Doppler estimates under the conditions of NUBF.

5.4. Summary

In this section, we showed how DPCA performed when NUBF was present. By using a single point scatterer and a column of scatterer points, we were able to simulate the effects on Doppler estimates for both a single antenna and DPCA. To further our analysis, we also showed how DPCA performed under high levels of uncertainty, that could present itself in a real implementation. From the analysis, we were able to see that DPCA outperformed a single antenna system by a large margin even under worst case conditions. The max velocity that we saw using DPCA was around 3 m/s, while the max velocity seen in the single antenna case was around 8 m/s. Overall, DPCA seems like a viable to prevent the effects of NUBF when taking measurements from a spaceborne weather radar.

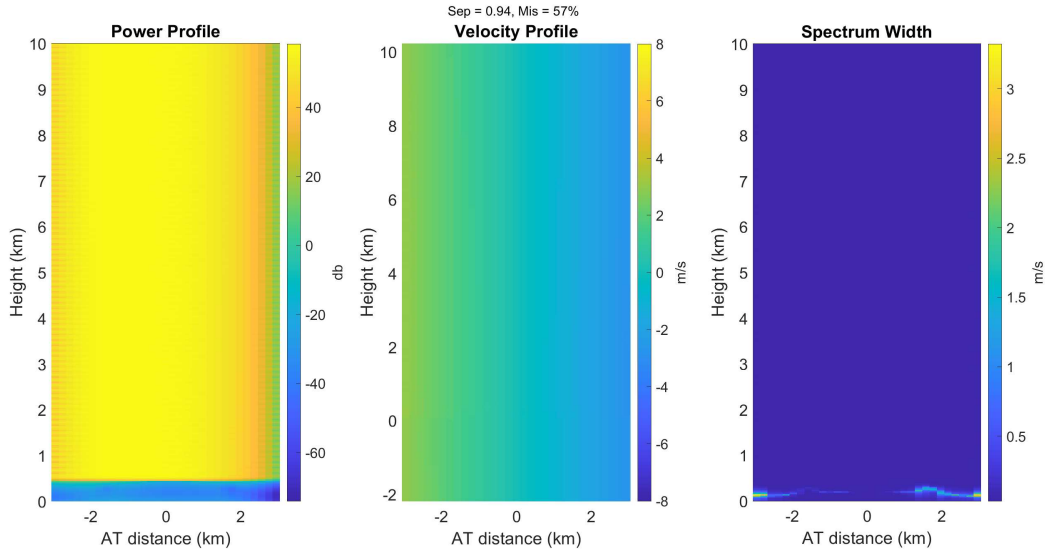

(A)

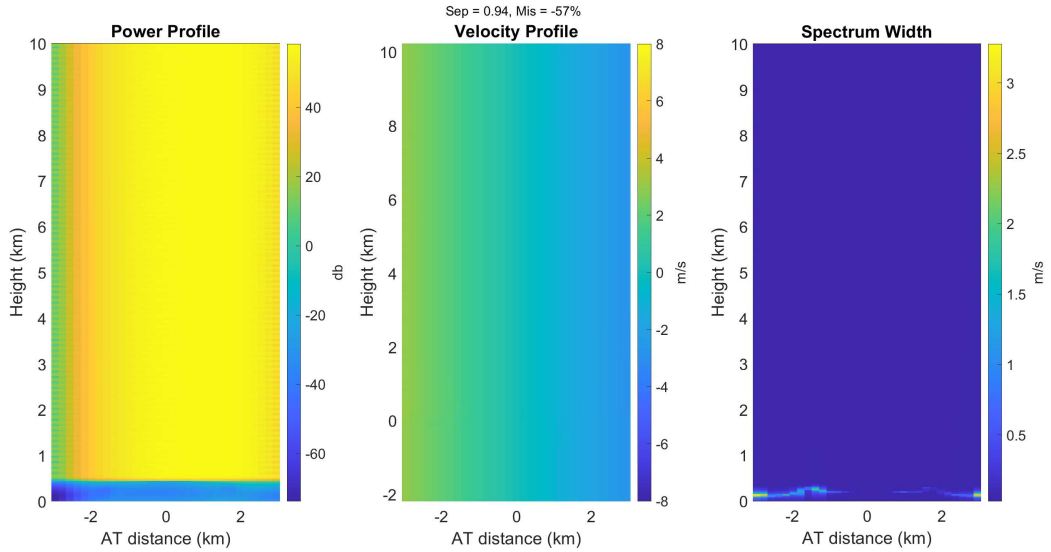

(B)

FIGURE 5.9. (A) Shows the power, velocity and spectrum width when DPCA is at a separation distance of 0.94 of the nominal and a mispointing of 57% of the HPBW.
(B) Shows the power, velocity and spectrum width when DPCA is at a separation distance of 0.94 of the nominal and a mispointing of -57% of the HPBW.

CHAPTER 6

Summary and Future Work

6.1. Summary

Taking accurate Doppler measurements of the atmosphere from space is an ongoing issue of extreme importance. Extremely high levels of fidelity are required to allow the scientific community to produce accurate predictions of weather events. While ground and airborne radars have been refined to provide accurate measurements of the atmosphere, spaceborne weather radars are limited in their abilities due to high platform velocities introduced by the orbit of the spacecraft around Earth. If the antenna is not made large enough, successive pulses are not well correlated, resulting in a degradation in the accuracy of Doppler measurements. While techniques have been used in an attempt to reduce the effects of high platform velocities, the inherent problem of uncorrelated pulses still remains a big issue. With this, a displaced phase center antenna configuration has been proposed to remove these biases introduced by the high platform velocities.

The objective of this thesis was to show the effectiveness of using a displaced phase center antenna configuration for taking Doppler measurements from space over current implementations. First the concept of DPCA was described and translated over for use in spaceborne weather radars. To demonstrate the effectiveness of DPCA for taking Doppler estimates from space, simulations were ran using both uniform and non-uniform volumes. In an attempt to provide a more accurate representation of how DPCA would perform in a real life situation, this work focuses on characterizing the uncertainty associated with DPCA in a real life implementation. DPCA relies on 2 antennas to remove the apparent platform velocity causing the bottleneck in current spaceborne Doppler estimates. Due to this, it

is necessary to understand how changes in the antennas position could affect the Doppler measurements taken using DPCA. By varying the separation distance of the antennas, and varying the mispointing of the following antenna in relation to the leading antenna, we were able to provide a full characterization of the uncertainty brought upon by DPCA. Finally, an analytical comparison between the accuracy of taking Doppler measurements using a single antenna system and DPCA is shown. As can be seen in the research, DPCA outperforms current spaceborne weather radar implementations by a significant margin. This is made especially clear when showing the effects NUBF has on the accuracy of Doppler estimates using a single antenna vs DPCA.

6.2. Future Work

Future work on DPCA that are outside of the scope of this thesis are suggested in this section. This includes additional characterizations, more robust scatterer volumes which simulate real weather events and further implementations to the radar hardware.

DPCA's mains sources of error come from the antennas. This work focused on characterizing two of the most significant sources of error, the separation distance and mispointing of the following antenna in relation to the forward. Additionally, DPCA can obtain additional sources of uncertainty from the attitude of the spacecraft as it orbits the Earth. This can most significantly be seen in deviations from the Yaw of the spacecraft. It is possible that the contributions from this could reduce the accuracy of DPCA by a small margin.

The tested volumes in this work consisted of static scatterers distributed uniformly and nonuniformly. A more robost approach would be to generate a moving scatterer to emulate the dynamic process of the atmosphere. By doing so, it would be possible to get a more accurate understanding of how DPCA could perform under convective and stratiform rain.

Pulse compression techniques could be added to future simulations to quantify its uses in spaceborne weather radars using DPCA. Pulse compression is a widely used technique in ground based radars that could potentially be used in DPCA to improve the range resolution.

Bibliography

[1] S. Durden, P. S. Luc, and S. Tanelli, "On the use of multiantenna radars for spcaeborne doppler precipitation measurements," *IEEE Geoscience and Remote Sensing*, vol. 4, no. 1, pp. 181–183, 2017.

[2] S. Tanelli, S. Durden, and M. Johnson, "Airborne demonstration of dpca for velocity measurements of distributed targets," *IEEE Geoscience and Remote Sensing*, vol. 12, no. 10, pp. 1415–1419, 2016.

[3] S. Tanelli, E. Im, S. L. Durden, and L. Facheris, "Analyses of spaceborne doppler radar system performance on measuring vertical rainfall velocity," in *Seventh Symposium on Integrated Observing Systems: the Water Cycle Long Beach, CA, USA*, 2003.

[4] R. Meneghini and T. Kozu, *Spaceborne Weather Radar*. Artech House Publishers, 1 ed., 1990.

[5] P. Amayenc, J. Testud, and M. Mazoug, "Proposal for a spaceborne dual-beam rain radar with doppler capability," *Journal of Atmospheric and Oceanic Technology*, vol. 10, pp. 262–276, 1992.

[6] R. Doviak and D. Zrnic, *Doppler radar and weather observations*. Dover Publications, 2 ed., 2006.

[7] T. Pratt, C. W. Bostian, and J. E. Allnutt, *Satellite Communications 2nd Edition*. Wiley, 2 ed., 2002.

[8] A. J. Illingworth, H. W. Barker, A. Beljaars, M. Ceccaldi, H. Chepfer, N. Clerbaux, and J. C. et al., "The earthcare satellite: The next step forward in global measurements of clouds, aerosols, precipitation, and radiation," *Bulletin of the American Meteorological Society*, vol. 96, no. 9, 2015.

[9] S. Bolen, V. Chandrasekar, and A. Benjamin, "Estimation of spaceborne radar signals from polarimetric ground radar observations," in *En Preprints 29th International Conference on Radar Meteorology, Montreal, Canada*, 2001.

[10] S. Kobayashi, H. Kumagai, and H. Kuroiwa, "A proposal of pulse-pair doppler operation on a spaceborne cloud-profiling radar in the w band," *Journal of Atmospheric and Oceanic Technology*, vol. 18, no. 9, pp. 1294–1306, 2002.

[11] R. Klemm, "Introduction to space-time adaptive processing," in *IEE Colloquium on Space-Time Adaptive Processing (Ref. No. 1998/241)*, pp. 1/1–111, 1998.

[12] W. Melvin, "A stap overview," *IEEE Aerospace and Electronic Systems Magazine*, vol. 19, no. 1, pp. 19–35, 2004.

[13] A. Battaglia, P. Kollias, R. Dhillon, R. Roy, S. Tanelli, and et al., "Spaceborne cloud and precipitation radars: Status, challenges, and ways forward," *Reviews of Geophysics*, vol. 58, pp. 1–59, 2020.

[14] R. E. Rinehart, *RADAR for Meteorologists*.

[15] V. N. Bringi and V. Chandrasekar, *Polarimetric Doppler weather radar: principles and applications*. Cambridge university press, 2001.

[16] J. F. I. VENTURA, "Design of a high resolution x-band doppler polarimetric weather radar," 2009.

[17] P. Amayenc, J. Testud, and M. Mazoug, "Displaced phase center antenna technique," *Lincoln Laboratory Journal*, vol. 12, pp. 281–296, 2000.

[18] C. Capsoni and M. D'Amico, "A physically based radar simulator," *Journal of Atmospheric and Oceanic Technology*, vol. 15, no. 2, p. 593–598, 1998.

[19] A. D. B. et al., "A weather radar simulator for the evaluation of polarimetric phased array performance," *IEEE Transactions on Geoscience and Remote Sensing*, vol. 54, no. 7, pp. 4178–4189, 2016.

[20] V. Santalla del Rio and M. Vera-Isasa, "A unified formulation of polarimetric weather radar with application to iq data simulation," *IEEE Transactions on Geoscience and Remote Sensing*, vol. 57, pp. 5098–5107, 2019.

[21] R. M. Beauchamp, S. Tanelli, E. Peral, and V. Chandrasekar, "Pulse compression waveform and filter optimization for spaceborne cloud and precipitation radar," *IEEE Transactions on Geoscience and Remote Sensing*, vol. 55, pp. 915–931, 2017.

[22] A. V. Oppenheim, *Discrete-Time Signal Processing*. Prentice Hall, 2 ed.

[23] A. Aerosols and Clouds-Convection-Precipitation, "Science and applications traceability matrix," 2020.

[24] NASA, "Accp aerosols and clouds-convection-precipitation," 2021.

[25] S. Tanelli, E. Im, S. L. Durden, L. Facheris, and D. Giuli, "The effects of nonuniform beam filling on vertical rainfall velocity measurements with a spaceborne doppler radar," *Journal of Atmospheric and Oceanic Technology*, vol. 19, no. 7, pp. 1019–1034, 2002.